

# pH-Triggered Membrane Insertion of Proteins

*by*

*Mauricio Vargas-Uribe*

Submitted to the graduate degree program in Biochemistry and Molecular Biology and the Graduate Faculty of the University of Kansas in partial fulfillment of the requirements for the degree of Doctor of Philosophy

---

Aron W. Fenton, Chairperson

---

Alexey S. Ladokhin

---

Mark T. Fisher

---

Kenneth Peterson

---

Jed N. Lampe

---

04/28/2015

Date defended

The Dissertation Committee for Mauricio Vargas-Urbe certifies that this is the approved  
version of the following dissertation:

pH-triggered membrane insertion of proteins

---

Aron W. Fenton, Chairperson

04/28/2015  
Date approved

## ABSTRACT

Several classes of membrane proteins refold from their original soluble conformations in response to acidification and insert into lipid bilayers. Despite the recent advances in unraveling the molecular mechanisms of pH-triggered insertion of membrane proteins, many aspects of this process remain unknown. In this study we used two proteins that share structural similarities as model systems: the diphtheria toxin translocation domain (T domain) and the anti-apoptotic regulator Bcl-xL. We addressed the following specific questions: (1) Do structurally similar T domain and Bcl-xL share common mechanisms of membrane insertion? (2) What is the role of titratable histidine residues on the late stages of transmembrane insertion of the T domain? (3) How do the physicochemical properties of the lipid bilayer modulate the pH-triggered membrane insertion of Bcl-xL? First, we characterized the main features of the pH-triggered membrane insertion pathway of Bcl-xL using circular dichroism (CD) and a battery of fluorescence-based methods and compared them to those previously determined for the T domain. We demonstrate that both proteins follow distinct membrane insertion pathways despite of the structural similarities of the initial solution and putative final transmembrane folds. Second, we used site-directed mutagenesis and functional and spectroscopic assays to characterize the membrane interactions of the C-terminal histidines of the T domain. We determine that H322 is critical for proper refolding of the N-terminal helices within the membrane, which is critical for the formation of the Open-Channel State of the T domain within the lipid bilayer. Finally, we determined the role of various lipids on the membrane interactions of Bcl-xL using several fluorescence-based techniques. We demonstrate that the initial

membrane association of Bcl-xL is modulated by the membrane surface potential, while the transmembrane insertion is regulated by additional properties, e.g. mechanical stress. We conclude that the pH-triggered membrane insertion of proteins can be modulated at multiple levels, including protonation of specific titratable residues and changes in the membrane lipid composition. These differences in the mechanisms of regulation are relevant to the physiological function of the corresponding membrane proteins (e.g., T domain and Bcl-xL).

## ACKNOWLEDGEMENTS

I am thankful to my research advisor, Dr. Alexey S. Ladokhin, who is not only a great scientist but also a great mentor. During these years he taught me to think, discuss and write as a scientist; and importantly, how to stand still against challenging and stressful scientific situations. As his first graduate student, I will be forever indebted to all the patience and dedication he put on my training.

I am thankful to the members of my dissertation committee - Dr. Aron W. Fenton, Dr. Mark T. Fisher, Dr. Kenneth Peterson and Dr. Jed N. Lampe - who supported me during my training. They always gave me a third point of view and constructive feedback, along with advices and challenges that helped me build. They advised me and challenge me when required.

I am also thankful to the members and past members of the lab of the Ladokhin lab. I am especially thankful to Dr. Alexander Kyrychenko and Dr. Mykola V. Rodnin, two great scientists from whom I learned the experimental and theoretical basis of techniques used during my training.

I thank my fellow grad students (or past) - Mary Ashley, Eephie, Allen, Victor, Rushi, Jackie, Zhen, Dan and Subhash - who always extended friendly help when needed. They made sure I always had a smile in my face.

Finally, I am thankful to my parents Jose Soto Aguilar and Maria Angelica Uribe, and to my grandparents Aldo Uribe Altamirano and Gloria Barahona Oyarzun. The geographical distance did not allow me to see them as often as I would like, but they were always on the phone when I needed them. Although none of them is a scientist, and only my mother went to college, they taught me and encouraged me to dream big and fight adversity.

## TABLE OF CONTENTS

ABSTRACT	iii
ACKNOWLEDGEMENTS	v
TABLE OF CONTENTS	vi
LIST OF FIGURES	ix
LIST OF TABLES	xii
CHAPTER 1 INTRODUCTION	1
BIOLOGICAL MEMBRANES	1
Chemical composition	2
MEMBRANE PROTEINS	5
Structural and thermodynamic features of membrane proteins	5
Membrane insertion of proteins	7
DIPHThERIA TOXIN TRANSLOCATION DOMAIN	10
BCL-2 FAMILY OF PROTEINS AND APOPTOSIS	15
Apoptotic pathways and MOMP	15
Bcl-2 proteins	16
Bcl-xL	19
COMPARISON OF BCL-XL TO THE DIPHThERIA TOXIN TRANSLOCATION DOMAIN	21
MEMBRANE LIPIDS AND APOPTOSIS	24
SUMMARY, HYPOTHESES AND SPECIFIC AIMS	25
Summary	25
Hypotheses	26
Specific aims	26

CHAPTER 2. COMPARING pH-DEPENDENT MEMBRANE INSERTION PATHWAYS OF BCL-XL AND DIPHTHERIA TOXIN T DOMAIN	27
INTRODUCTION	27
RESULTS	32
Folding and stability of Bcl-xL in solution: truncation of TM helix	32
Folding and pH-dependent stability in solution: comparison to T domain	34
Membrane association	37
Membrane insertion of the hydrophobic helical hairpin	41
DISCUSSION	45
MATERIALS AND METHODS	48
CHAPTER 3 ROLE OF C-TERMINAL HISTIDINES IN THE MEMBRANE INSERTION OF THE DIPHTHERIA TOXIN T DOMAIN	52
INTRODUCTION	52
RESULTS	56
DISCUSSION	64
MATERIALS AND METHODS	68
CHAPTER 4 REGULATION OF THE MEMBRANE INTERACTIONS OF BCL-XL BY LIPIDS	72
INTRODUCTION	72
RESULTS	76
Effect of anionic lipids on membrane binding	76
Effect of anionic lipids on membrane insertion/refolding	81
Kinetic regulation of the membrane insertion/refolding	83
DISCUSSION	87
MATERIALS AND METHODS	91

CHAPTER 5 CONCLUSIONS AND FUTURE DIRECTIONS	95
BCL-XL VERSUS T DOMAIN	95
HISTIDINES AND FOLDING OF T DOMAIN IN THE MEMBRANE	98
LIPID REGULATION OF MEMBRANE INTERACTIONS OF BCL-XL	100
CHAPTER 6 REFERENCES	103

## LIST OF FIGURES

FIGURE 1.1	Structure of lipid bilayer.....	5
FIGURE 1.2	Examples of the thermodynamically permitted folds of membrane proteins.....	7
FIGURE 1.3	Mechanisms of membrane protein insertion.....	9
FIGURE 1.4	Entry of the diphtheria toxin into cells.....	11
FIGURE 1.5	Structural features of the diphtheria toxin T domain.....	12
FIGURE 1.6	Kinetics and thermodynamics of the pH-triggered membrane insertion of the T domain.....	13
FIGURE 1.7	Location of histidines within the structure of the T domain.....	14
FIGURE 1.8	Apoptotic pathways, MOMP and Bcl-2 family of proteins.....	17
FIGURE 1.9	The Embedded Together Model of apoptosis regulation.....	19
FIGURE 1.10	High resolution structure of Bcl-xL.....	20
FIGURE 1.11	Structural comparison between Bcl-xL and diphtheria toxin translocation domain.....	22
FIGURE 2.12	Similarities between the membrane insertion models of Bcl-xL, Bax and the T domain as suggested in the literature.....	23
FIGURE 2.1	High resolution structures of the T domain and Bcl-xL.....	29
FIGURE 2.2	Schematic representation of the mode of attachment of the diphtheria toxin and Bcl-xL to their target membranes.....	30
FIGURE 2.3	Thermal unfolding of the full-length and truncated Bcl-xL in solution at pH 8.....	33
FIGURE 2.4	pH-dependent variation in secondary structure of Bcl-xL and the T domain in solution.....	35
FIGURE 2.5	pH-dependent variation in thermostability of Bcl-xL and the T domain in solution.....	36

FIGURE 2.6	Reversibility of pH-dependent membrane association of Bcl-xL examined by the FRET measurements between donor-labeled protein and acceptor-labeled LUV .....	38
FIGURE 2.7	Effect of acidification and labeling position on spectral features of the probe Alexa488 attached to Bcl-xL .....	39
FIGURE 2.8	Comparison of pH-dependent binding of Bcl-xL and the T domain to LUV composed of different mixtures of POPC and POPG.....	40
FIGURE 2.9	Membrane insertion of Bcl-xL monitored by fluorescence of the environment-sensitive probe NBD attached to the residue N175C .....	42
FIGURE 2.10	Effect of pH on spectral features of probe NBD selectively attached to Bcl-xL .....	43
FIGURE 2.11	Comparison of pH-dependent membrane insertion of the hydrophobic helical hairpins of the T domain and Bcl-xL .....	44
FIGURE 2.12	Schematic representations of the pH-triggered membrane insertion pathways of the diphtheria toxin T domain and apoptotic regulator Bcl-xL .....	47
FIGURE 3.1	Crystal structure of the T domain showing the consensus insertion unit TH8-TH9 and the C-terminal histidines .....	54
FIGURE 3.2	Thermal stability of mutants H322Q, H323Q and H372Q at pH 8 and pH 6.....	58
FIGURE 3.3	Tryptophan spectra of WT and H322Q mutant in the presence of LUV at pH 8 and pH 5.3 .....	60
FIGURE 3.4	Membrane-induced misfolding of T domain's mutants of H322 followed by tryptophan fluorescence.....	61
FIGURE 3.5	Membrane-induced misfolding of C-terminal histidine mutants correlates with loss of function.....	63
FIGURE 3.6	Model of the role of the C-terminal histidines in the refolding process of the T domain within the bilayer.....	66

FIGURE 4.1	pH-triggered membrane insertion pathway of Bcl-xL.....	73
FIGURE 4.2	Structure and properties of membrane lipids used in this study .....	75
FIGURE 4.3	pH-dependence of binding of Bcl-xL to LUV composed of various mole fractions of cardiolipin (TOCL) and phosphatidylcholine (POPC).....	77
FIGURE 4.4	Regulation of membrane binding of Bcl-xL by membrane surface potential.....	79
FIGURE 4.5	Thermodynamics of membrane binding of Bcl-xL to LUV .....	80
FIGURE 4.6	Effect of anionic lipids on the insertion/refolding of helices $\alpha 5$ - $\alpha 6$ into the bilayer monitored through changes in the fluorescence intensity of NBD-labeled Bcl-xL.....	82
FIGURE 4.7	Effect of different anionic lipids in the kinetics of insertion/refolding of Bcl-xL into LUV .....	84
FIGURE 4.8	Effect of POPE and LysoPC in the insertion of Bcl-xL into the lipid bilayer at pH 4.5.....	86

## LIST OF TABLES

TABLE 2.1	Thermodynamic parameters for the thermal unfolding of the T domain and Bcl-xL in solution at the indicated pH .....	36
TABLE 3.1	Relative activities of the C-terminal histidine mutants of the diphtheria toxin T domain .....	57
TABLE 3.2	Thermodynamic parameters derived from the fitting of thermal unfolding data of mutants of T domain.....	59
TABLE 4.1	pH-dependent binding parameters of Bcl-xL to LUV of various lipid compositions .....	78
TABLE 4.2	Parameters of pH titrations of insertion/refolding of Bcl-xL into LUV of various lipid compositions.....	83
TABLE 4.3	Quantitative analysis of the kinetics of insertion of Bcl-xL into LUV of various lipid compositions.....	85

## CHAPTER 1 INTRODUCTION

Membrane proteins (MPs) are critical for proper cellular function. They control the selective crossing of molecules through biological membranes and energy production, serve as support for the cytoskeleton, regulate apoptosis, and are involved in cell signaling, among other tasks. It is predicted that MPs constitute about 25-35% of the human proteome [1, 2], and they are the target of almost 60% of the pharmaceutical drugs [3, 4]. However, despite their biological and pharmaceutical significance, much less is known regarding the structure and assembly of MPs in their native environment in comparison to their soluble counterparts (only 535 unique MPs of known high resolution structure up to April of 2015, <http://blanco.biomol.uci.edu/mpstruc/>). The technical difficulties and the intrinsic complexity of the lipid bilayer hinder the understanding of fundamental principles behind membrane protein folding [5-7]. Because some membrane proteins are initially synthesized in the relatively isotropic environment of the cytosol or extracellular fluid (e.g. bacterial toxins), they serve as model proteins to understand membrane protein folding. In this chapter, we first discuss the structure and physical properties of the membrane and the physical principles involved in membrane protein folding. Then, we introduce the pH-triggered membrane insertion and refolding of proteins as a model system to study membrane protein folding, with emphasis in the diphtheria toxin translocation domain and the apoptotic regulator Bcl-xL.

### *BIOLOGICAL MEMBRANES*

Membrane proteins reside in a lipid environment and the structure and dynamics of membrane proteins depend on the molecular structure and physicochemical properties of the lipid milieu. Therefore, we will first discuss the physical and chemical organization of biological membranes.

### *Chemical composition*

Biological membranes function as selective permeability barriers that separate different compartments in the cell. They are composed of amphiphilic molecules (i.e. they are both hydrophobic and hydrophilic), called membrane lipids, arranged in a continuous double layer structure with the hydrophobic regions facing each other and the hydrophilic heads facing the aqueous phase [8]. Biological membranes are formed by several types of lipids, including glycerophospholipids, sphingolipids and sterols [9, 10]. Glycerophospholipids (usually referred simply as phospholipids) are formed by two acyl chains attached to a glycerol moiety, with a phosphate group linking a hydrophilic headgroup to the third carbon of the glycerol (e.g. phosphatidylcholine, Fig. 1.1B). In sphingolipids, however, the glycerol group and one of the acyl chains are substituted by a sphingosine moiety. Some sphingolipids also contain a phosphate group (e.g. sphingomyelin), while others have complex oligosaccharides attached (gangliosides). Finally, sterols are moieties with multiple aromatic rings and a single hydrophilic functional group (e.g. cholesterol).

The variety in the lipid composition of membranes goes beyond the mere replacement of glycerol with sphingosine. Several natural functional groups are known to be attached to the phosphate moiety, including glycerol, choline, serine and inositol, among others. The aliphatic chains of these lipids have lengths ranging from 4 to >30 carbons, and different levels of saturation. Unsaturated acyl chains can be mono- or polyunsaturated fatty acids and have a *cis* or *trans* configurations at the double bond. Thus, only counting the length, saturation and configuration of acyl chains, and the functional group attached to the phosphate, cells synthesize thousands of different lipids with different chemical and physical properties. A comprehensive

review on the synthesis and location of these lipids can be found in reference [8], while structures and physicochemical properties of them can be found in the LIPID MAPS database (<http://www.lipidmaps.org/data/structure/>) [10]. In this dissertation, we focus on the most common glycerophospholipids with a single configuration at the acyl chains (See Table 4.1 for structures and properties). For simplicity, we referred as them simply as phospholipids or lipids.

### *Structure and physical properties of the lipid bilayer*

Given the complex composition of the lipid bilayer, it is challenging to visualize the structure of the membrane at a high resolution level. Fig. 1.1A shows a snapshot of a lipid bilayer composed of phosphatidylcholine created by computational molecular modelling [11]. Although this membrane is made of only one type of lipid, it is clear that there is enormous thermal disorder that complicates even more the creation of a resolution model of the membrane. In the picture, however, it is possible to visualize the general structure of the membrane, with lipids arranged in a double layer, the hydrophobic tails (sticks) facing each other, and the functional groups of the lipid headgroups (balls) in contact with the water molecules (light blue).

A more accurate representation of the membrane is determined by time averaging the position of functional groups along the normal axis  $z$  of the membrane using X-ray and neutron scattering of oriented multilamellar membranes [12] (Fig 1.1B). The structure of a DOPC membrane is presented in Fig. 1.1C, where the spatial distribution of each functional group along the bilayer normal axis  $z$  is shown as a histogram. Three features of this membrane are immediately evident. First, the hydrocarbon core is flanked by two interfacial regions whose combined width ( $\sim 15\text{\AA}$  each) equals that of hydrocarbon core ( $\sim 30\text{\AA}$ ). Second, the membrane interface is chemically complex and contains the functional groups of the lipid headgroups and water of

hydration. The hydrocarbon core, on the other hand, contains the lipid acyl chains. Third, there is a gradient of polarity that decreases from the aqueous phase to the hydrocarbon core (Fig. 1.1D), passing through the interfacial region. The width of the distributions is consistent with the thermal disorder. This type of arrangement holds true for membranes composed of other lipid systems [13-16]; however, combination of different lipids are expected to create a more complex picture, possibly with lipid domains of different structures and physicochemical properties [6, 17].

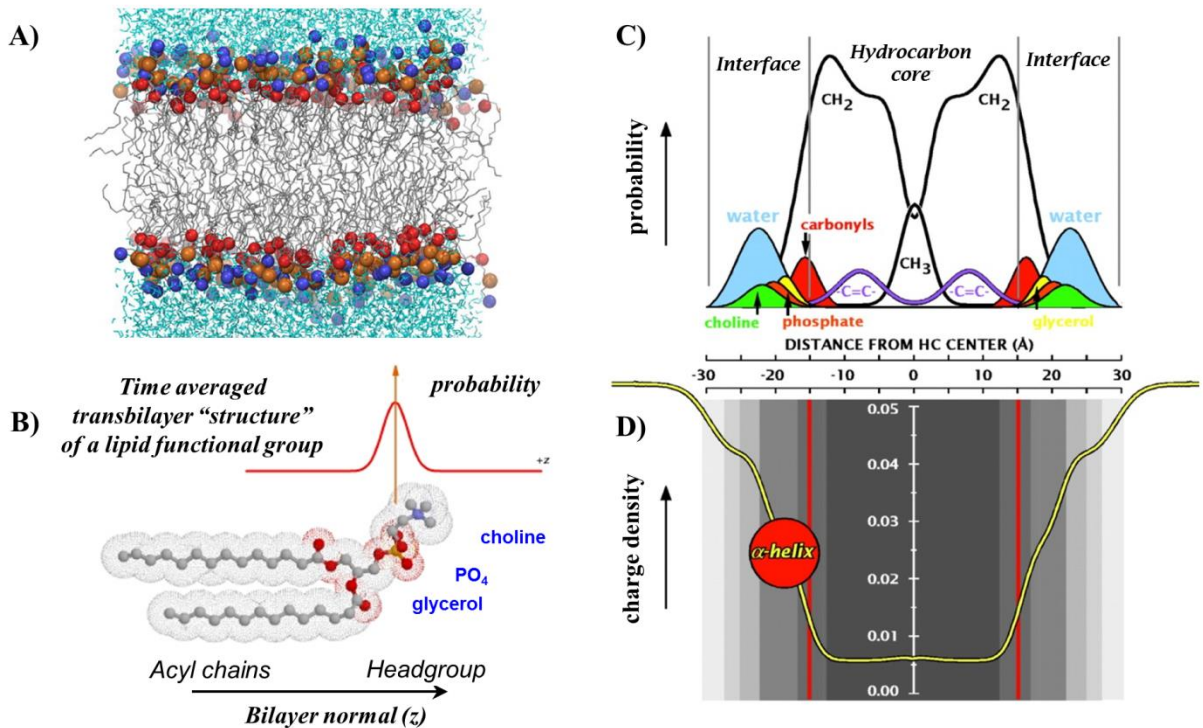


**FIGURE 1.1 Structure of lipid bilayer.** **A)** DOPC lipid bilayer modeled through computational methods illustrating the substantial thermal disorder [11]. **B)** Schematic representation of the structure of a phosphatidylcholine molecule. While acyl chains are hydrophobic, the headgroup is hydrophilic. The estimation of the time averaged probability of functional groups across the bilayer normal axis  $z$  determines the structure of the bilayer. **C)** Structure of a DOPC bilayer determined by X-ray and neutron diffraction as illustrated in panel B [12]. Notice the presence of a 30Å wide hydrocarbon core flanked by two interfacial regions of 15Å each (width accommodates  $\alpha$ -helix). Interface is chemically complex and includes functional groups of lipid headgroups and water of hydration. **D)** Charge density along the bilayer normal axis shows a gradual decrease of charges from the interface towards the hydrocarbon core. Panels B-D are taken from website of Dr. Stephen White Lab at University of California, Irvine ([http://blanco.biomol.uci.edu/Bilayer\\_Struct.html](http://blanco.biomol.uci.edu/Bilayer_Struct.html)).

## MEMBRANE PROTEINS

### *Structural and thermodynamic features of membrane proteins*

Membrane proteins (MPs) are embedded in the lipid bilayer, either *via* a transmembrane or interfacially moiety. Regardless of the mode of attachment, they share some features with soluble proteins, while others are unique to membrane proteins. A comparison with soluble proteins reveals that membrane proteins are not inside-out structures [18]. In fact, one of the first solved structures of the photoreactive center bacteriorhodopsin revealed that the majority of amino acids in the interior of the protein were non-polar [19]. The exceptions are the pore-forming proteins (e.g. porins, bacterial toxins), whose interiors are water-filled [20, 21]. Other

common elements between the interior of soluble proteins and membrane proteins are the presence of salt bridges and formation of hydrogen bonds. Thus, packing and general principles of folding of membrane proteins are not as different as those of soluble proteins [18, 22]. However, some features are more specific to MPs. For example, the exterior of membrane proteins is more hydrophobic than that of soluble proteins [23]. Finally,  $\alpha$ -helices are usually longer in MPs because they must span the entire hydrophobic core of the lipid bilayer ( $\sim 30\text{\AA}$ ) to be thermodynamically stable (see below) [18].

Membrane proteins adopt a limited number of folds within the membrane [18, 24]: transmembrane  $\alpha$ -helical bundles and  $\beta$ -barrels (Fig. 1.2A-B). Because membrane proteins exist in thermodynamic equilibrium with their environment, they fold in agreement with the laws of thermodynamics [18, 25, 26]. Hydrogen bond formation (H-bond) within the protein backbone, resulting in secondary structure formation, reduces the large energetic cost of bringing the backbone into the hydrophobic core of the bilayer [18]. According to computational calculations, this reduction is about 4.2 kcal/mol per residue [27, 28], which in a 20 residue-long peptide (average length of a transmembrane helix) adds to more than 80 kcal/mol. Thus, the most stable motifs within the membrane are those where the protein backbone is fully H-bonded:  $\alpha$ -helices and  $\beta$ -barrels. There is a third type of topology generally found in membrane proteins: interfacial  $\alpha$ -helices (Fig. 1.2C). In this case, H-bond formation stabilizes the protein backbone in about 0.37 kcal/mol per residue [29]. This number does not appear as large as that achieved by H-bond formation in the hydrocarbon core, but it is large enough to drive the formation of  $\alpha$ -helices in the membrane interface (a 15-residue helix is about 5.5 kcal/mol more stable than the unfolded peptide).

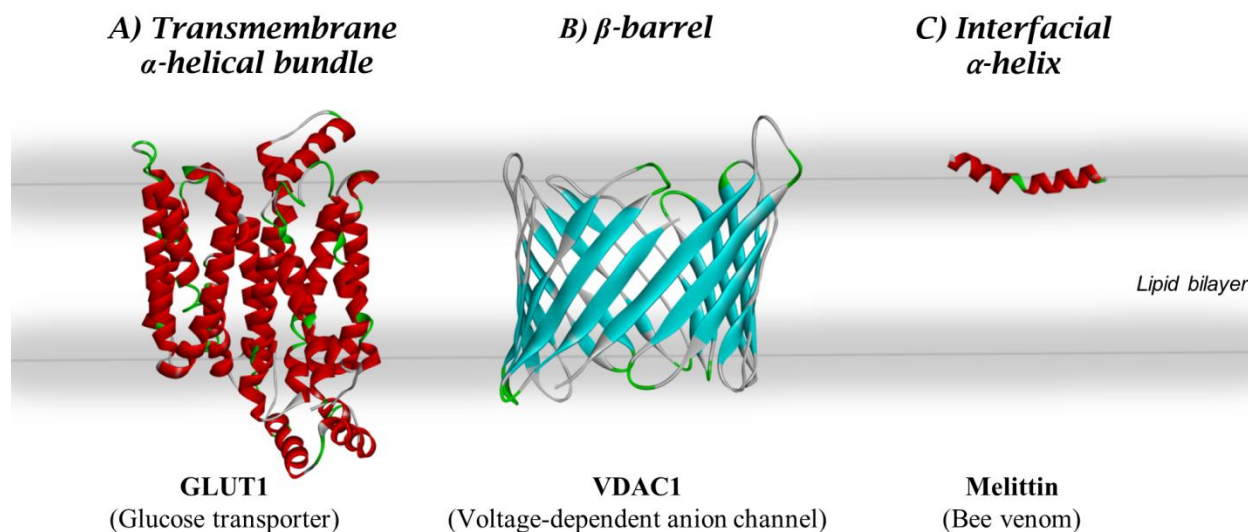


**FIGURE 1.2** Examples of the thermodynamically permitted folds of membrane proteins.

**A)** Transmembrane  $\alpha$ -helical bundles, **B)**  $\beta$ -barrels, **C)** and interfacial  $\alpha$ -helices. Structures correspond to the glucose transporter GLUT1 (4PYP) [30], voltage-dependent anion channel VDAC1 (2JK4) [31], and the bee venom melittin (2MLT) [32]. H-bond formation at the protein backbone drives the thermodynamic equilibrium of these structures within the lipid bilayer (see text for details). For simplicity, the membrane is shown as two parallel lines with the shadowed areas representing the interfacial region.

### *Membrane insertion of proteins*

According to their mode of membrane insertion, MPs can be classified into two groups: those that require the help of another protein, i.e. translocons; and those that insert spontaneously without the help of other proteins. Because this dissertation addresses the second type of membrane protein insertion, the protein-assisted membrane protein folding will be merely mentioned. The protein-assisted membrane insertion requires the action of complex machineries to assist the integration of transmembrane segments into the bilayer. The machinery is different

depending on the organism and the MP fold. For example, the Sec complex assists on the membrane insertion of  $\alpha$ -helical proteins [33, 34], where the ribosome is attached to the translocon to ensure the co-translational insertion of MPs (Fig. 1.3A). The Sec61 complex is the eukaryotic variant and is found in the membrane of the endoplasmic reticulum, while the SecYEG is the bacterial homolog and is found in the bacterial inner membrane. Membrane proteins with  $\beta$ -barrel topology use a different type of assembly machineries [35, 36], where SAM (sorting and assembly machinery) and TOC (translocon of the outer membrane of chloroplasts) complexes chaperone the insertion and folding of  $\beta$ -barrel proteins in mitochondria and chloroplast, respectively. BAM ( $\beta$ -barrel assembly machinery) is the bacterial homolog. Although the molecular details of the membrane action of these assembly machineries are only partially understood [37-41], it is clear that their action is critical for the proper folding of MPs.

Several classes of membrane proteins adopt their transmembrane topology after being synthesized as water-soluble structures. Examples include bacterial toxins [42-44] and colicins [45], which are secreted to the extracellular space; and certain annexins [46] and members of the Bcl-2 proteins [47], which are synthesized as cytosolic proteins. The unique characteristic of these proteins is their ability to move from the polar environment of the aqueous medium to the non-polar milieu of the lipid bilayer without the help of translocons or assembly machineries (Fig. 1.3B). This process occurs in response to a given cellular signal (e.g. change in pH, proteolytic cleavage) and involves a massive refolding of the solution structure of the protein. The exact molecular mechanism of this refolding/insertion process is not fully understood, and some open questions will be addressed during this dissertation. In the following sections, we will introduce two proteins that insert into the membrane under acidic conditions, the diphtheria

toxin T domain and the apoptotic repressor Bcl-xL, and three open questions that will be addressed in the following chapters.

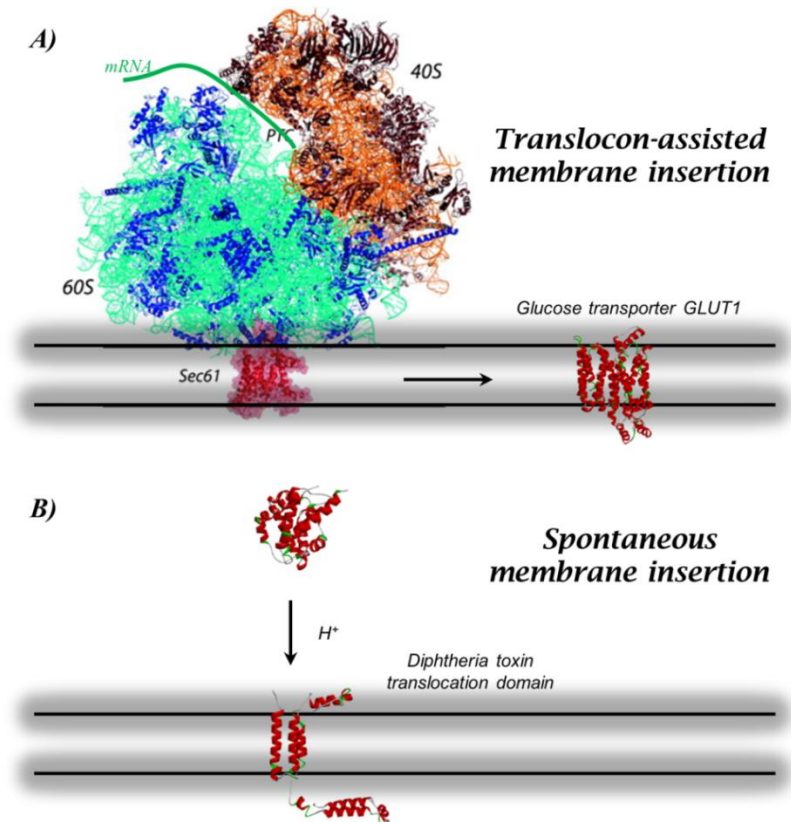


**FIGURE 1.3 Mechanisms of membrane protein insertion.** **A)** Schematic representation of the insertion of a membrane protein assisted by Sec61 [37]. In the example, the glucose transporter GLUT1 [30] is inserted into the lipid bilayer assisted by the Sec61 translocon [48]. The mechanism involves the passage of the nascent chain from the ribosome through a channel in the Sec61 protein before entering the lipid bilayer. **B)** Schematic representation on the spontaneous membrane insertion of proteins. In the example, the diphtheria toxin translocation domain inserts into the membrane in response to acidification without the help of other proteins [43]. For diphtheria toxin T domain, models correspond to the crystal structure in solution at neutral pH [49] and a membrane-inserted model based on spectroscopic and functional assays [50-53].

## DIPHTHERIA TOXIN TRANSLOCATION DOMAIN

The diphtheria toxin is a protein synthesized and released by the bacterium *Corynebacterium diphtheriae*. The toxin is composed of three domains (Fig. 1.4A) [49]: the catalytic domain (C-domain), the translocation domain (T domain), and the receptor-binding domain (R domain). The toxin enters the target cell *via* the endosomal pathway of internalization [42], which is initiated by the attachment of the R domain to its receptor in the target membrane (Fig. 1.4B). Upon endosomal internalization and acidification (endosomes can reach pH values as low as 5 [54-56]), the T domain undergoes a series of pH-triggered conformational changes that lead to its membrane binding and insertion [43]. As a result of T domain's membrane insertion, the N-terminus and the attached C domain are translocated across the endosomal membrane. The C domain, now in the cytosol, inhibits protein synthesis by ADP-ribosylating the translation factor EF-2. Thus, the T domain plays a key role in the entry of the C domain, which ultimately causes cell death.

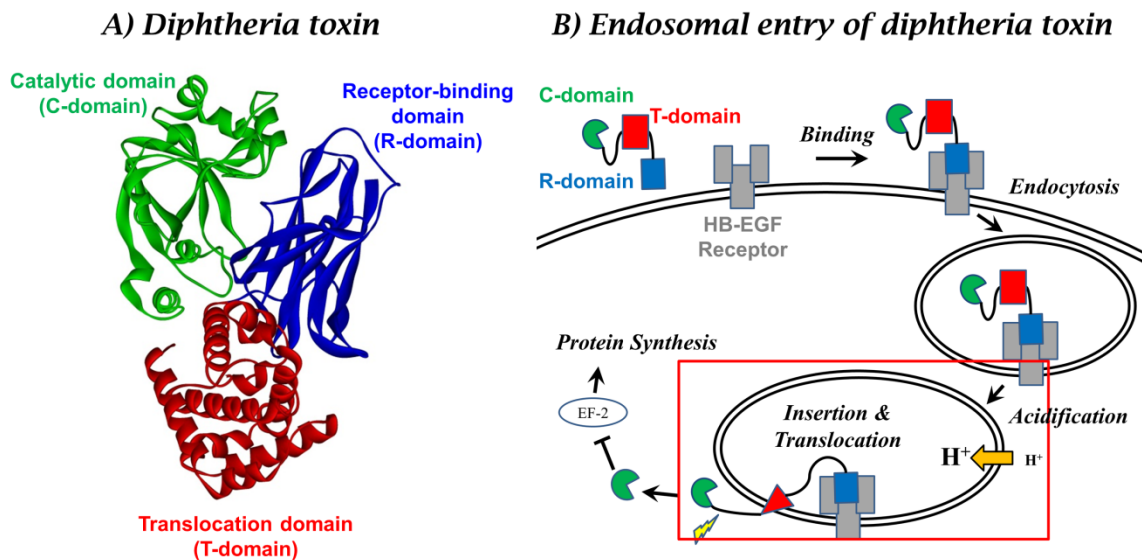


**FIGURE 1.4 Entry of the diphtheria toxin into cells.** **A)** Crystal structure of the diphtheria toxin [49] showing its three domains as ribbons of different colors. **B)** Schematic representation of the endosomal entry of the diphtheria toxin into the cell [42]. The red box highlights the step under discussion in this chapter.

The crystal structure of the T domain in solution at neutral pH shows 9  $\alpha$ -helices [49], named TH1 to TH9, arranged in a globular fold (Fig. 1.5). Two of these helices, TH8 and TH9 (purple helices), form the hydrophobic core of the protein in solution. The remaining helices are amphipathic helices that surround the core of the protein and keep it soluble in an aqueous environment. There is no high resolution structure available for the membrane-inserted state. However, multiple evidence indicates that helices TH8-TH9 insert as a transmembrane hairpin, with the loop connecting both helices on the *trans* side of the bilayer, while the rest of the structure adopts multiple conformations [51, 53, 57-61]. Since the N-terminus of the T domain is translocated across the membrane, it is argued that TH5 also takes a transmembrane topology [51, 59, 61, 62].

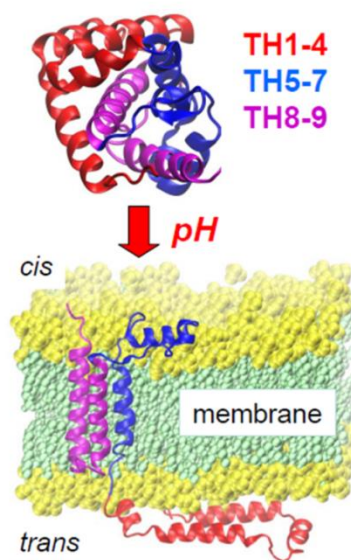


**FIGURE 1.5 Structural features of the diphtheria toxin T domain. Top)** Crystal structure of the T domain in solution at neutral pH [49]. **Bottom)** Structural model of the T domain in the membrane inserted state based on spectroscopic and functional assays [51, 53, 57-60] .

The refolding and membrane insertion pathway of the T domain occurs in multiple steps [43], where the kinetic and thermodynamic features have been described [53, 63]. The kinetic pathway (Fig. 1.6A) starts with a conformational change in solution in response to acidification, where the membrane-incompetent W state is converted into the membrane-competent  $W^+$  state. The process continues with the partitioning of the  $W^+$  state to the membrane interface to form the interfacial I state. Finally the T domain adopts a transmembrane T state after a series of conformational changes within the membrane (this state is also known as open-channel state or OCS). T domain can be kinetically trapped in the I state by modulating the pH and the lipid composition. The folding landscape of the T domain is shown in Fig. 1.6B, where the bulk of free energy of stabilization of the membrane inserted state comes from the membrane binding event ( $W^+$  to I state). Based on structural similarities, it has been hypothesized that other proteins (e.g. members of the Bcl-2 family of proteins) follow a similar membrane insertion pathway [64-66]. In Chapter 2, we test this hypothesis by comparing the membrane insertion pathway of Bcl-xL and that the T domain (more details in section of Bcl-2 family of proteins).

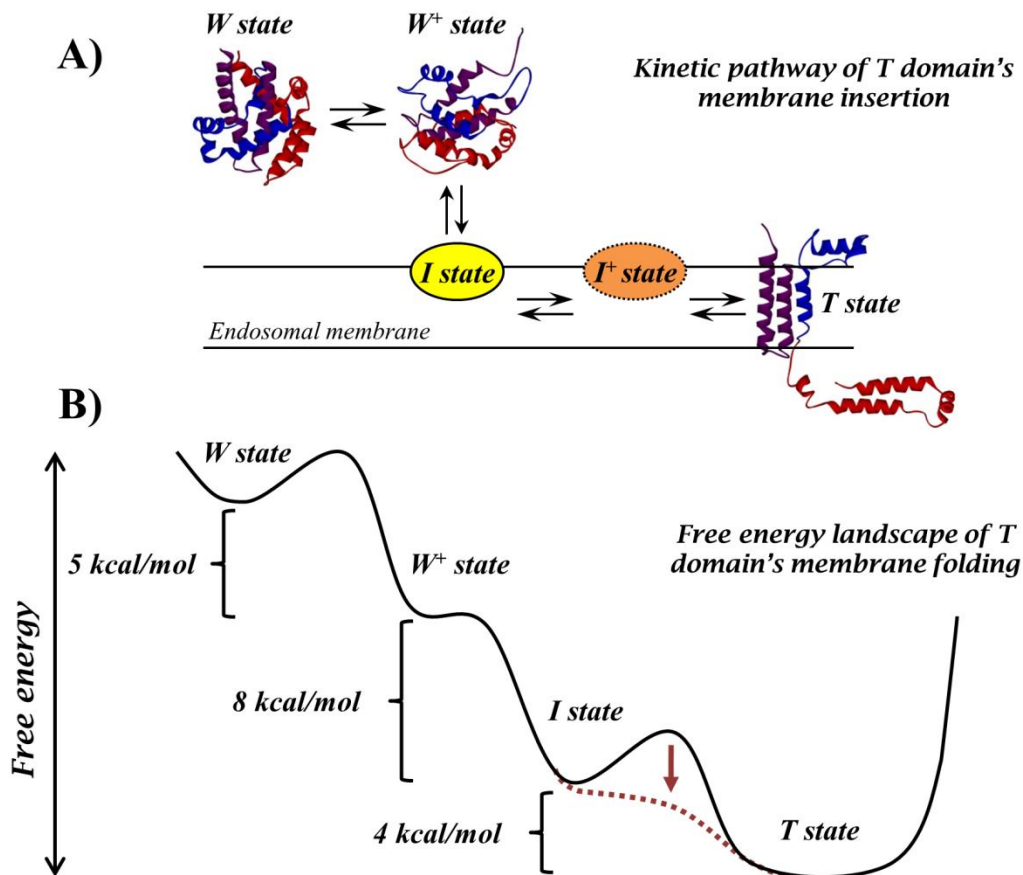


**FIGURE 1.6 Kinetics and thermodynamics of the pH-triggered membrane insertion of the T domain.** **A)** Kinetic pathway of membrane insertion of the T domain [53]. Intermediates states are formed in solution and in the membrane (See text). **B)** Free energy landscape for the folding of T domain into the membrane [63]. Bulk of free energy stabilizing the final T state comes from the binding step. The arrow indicates modulation of the pathway by anionic lipids, which lowers the kinetic barrier of transmembrane insertion.

It is suggested that the conformational changes of the T domain are driven by the protonation of histidine residues [43, 67]. There are six histidine residues in the T domain, which in the structure of the T domain are arranged into two clusters (Fig. 1.7): the N-terminal cluster of histidines and the C-terminal cluster of histidines. The N-terminal histidines have been shown to

be involved in the solution refolding of the T domain (W to W<sup>+</sup> state in Fig. 1.6). Mutagenesis of these histidines followed by spectroscopic and functional characterization of the mutants revealed that protonation of H257 triggers the initial conformational changes [52]. Extended molecular dynamic simulations suggested that electrostatic repulsion between H257 and H223 upon protonation initiates the initial conformational change [50], with H223 acting as a safety latch to prevent the refolding of the T domain at neutral pH.

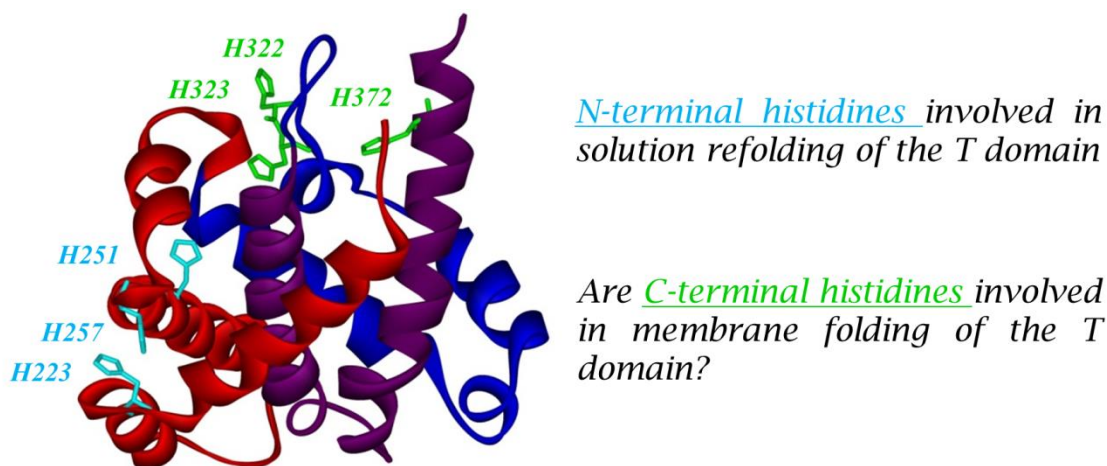


**FIGURE 1.7 Location of histidines within the structure of the T domain.** Histidines are arranged into the N-terminal (light blue) and the C-terminal cluster of histidines (green). While it has been demonstrated that the N-terminal histidines trigger the refolding of the T domain in solution, it is hypothesized that the C-terminal histidines are involved in the folding of the T domain within the membrane.

The role of the C-terminal histidines is less clear, but their location on top of the membrane insertion unit TH8-TH9 (purple helices) suggest their involvement in the folding of the protein in the membrane. Indeed, a recent study found that the triple mutation of the C-terminal histidines leads to a non-functional T domain in the membrane [68]. The fact that the T domain was

unable to form the open-channel state initially suggested its inability to insert into the membrane. However, the membrane insertion of helices TH8-TH9 and the translocation of the N-terminus were unaffected by these mutations. Thus, it is unclear why the T domain does not reach its final folding state while still having an apparently normal interaction with the membrane. Likewise, it is not clear if the three C-terminal histidines are involved in the final folding of the T domain into the OCS, or any of the histidines are more important. We hypothesize that the C-terminal histidines are involved in the folding of the N-terminal helices despite being located on top of the helical hairpin, and that histidines connecting to the N-terminal helices will be especially important. In chapter 3 this hypothesis will be tested and individual mutants of the C-terminal cluster of T domain will be characterized functionally and spectroscopically.

## *BCL-2 FAMILY OF PROTEINS AND APOPTOSIS*

### *Apoptotic pathways and MOMP*

Apoptosis is a cell death program used by multicellular organisms to eliminate unwanted cells [69]. Apoptosis is of critical importance, as malfunction is often associated with neurodegenerative diseases and cancer [70, 71]. There are two known pathways of apoptosis: the extrinsic and the intrinsic pathway (Fig. 1.8) [47, 72]. The extrinsic route responds to certain external signals (e.g. tumor necrosis factor) that trigger a cascade of events in the cell upon binding of a signaling ligand to its receptor. The intrinsic route takes action when internal cellular damage is irreversible (e.g. extensive viral damage). A common hallmark of both pathways is the activation of a cascade of proteases called caspases (cysteine-aspartic proteases), whose function is to cleave cellular proteins, leading to cell death. Importantly, the activation of

these caspases depends on a prior event known as mitochondrial outer membrane permeabilization (MOMP) [71-73].

The mitochondrial outer membrane permeabilization causes the release of the mitochondrial content into the cytosol (Fig. 1.8) [73]. This irreversibly redistribution of mitochondrial proteins initiates the execution of apoptosis through caspase activation. For example, cytochrome C forms the apoptosome upon binding to a protein complex called Apaf-1. The apoptosome directly activates caspase-3, which digests cellular proteins. Another group of mitochondrial proteins known as SMACs (small mitochondrial-derived activator of caspases) indirectly activate apoptosis by sequestering and preventing the action of inhibitors of caspases. Because MOMP is irreversible, and it causes a dual activation of caspases, it is considered to be the point of no return towards cell death. MOMP is controlled by the action of a group of proteins known as the Bcl-2 family of proteins.

### *Bcl-2 proteins*

The mitochondrial outer membrane permeabilization is tightly controlled by the action of the Bcl-2 family of proteins. The Bcl-2 family of proteins is subdivided into three groups based on their apoptotic action and sequence homology [74]. The proapoptotic members (e.g. Bax, Bak) contain three homology domains, BH1-3 (Bcl-2 homology domain), and promote MOMP. The antiapoptotic or prosurvival members (e.g. Bcl-xL, Bcl-2) share four homology domains, BH1-4, and prevent MOMP. The BH3-only members (e.g. Bid, Bim) contain only the BH3 domain and have been reported to sensitize apoptotic signals, activate proapoptotic members, and inhibit antiapoptotic members. The molecular mechanism of action of the Bcl-2 family of proteins remains unclear despite active research [75, 76]. Importantly, some members of the Bcl-2 family

of proteins reside in both the cytosol and the mitochondrial outer membrane, and its dynamic exchange is suggested to be part of their molecular mechanism [77-81].

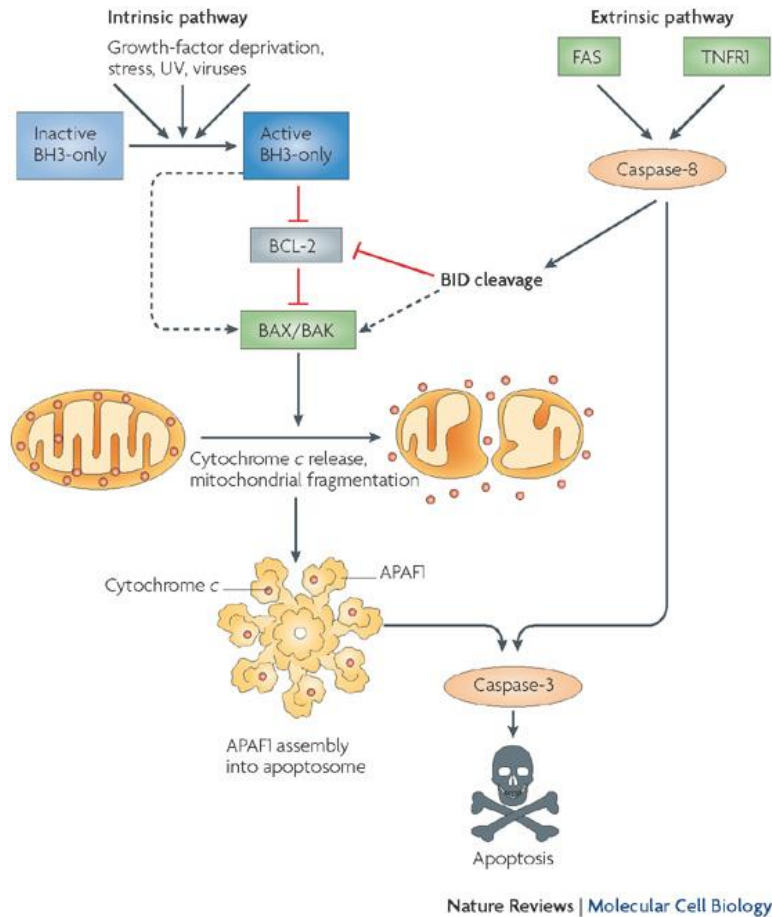


**FIGURE 1.8 Apoptotic pathways, MOMP and Bcl-2 family of proteins.** There are two pathways leading to apoptosis depending on the origin of the cell death signal: intrinsic and extrinsic routes. Bcl-2 proteins control the release of cytochrome C and other mitochondrial proteins into the cytosol, leading to the activation of a cascade of caspases. Caspases then digest the cellular proteins and activate DNases, causing the demolition of the cell. (Figure taken from reference [47]).

The most accepted model for the mechanism of action of the Bcl-2 family of proteins is the embedded together model (Fig. 1.9) [82]. According to this model, there are multiple interactions between pro- and anti-apoptotic members of the Bcl-2 family of proteins. In the absence of anti-apoptotic members, pro-apoptotic members are recruited from the cytosol into the lipid bilayer, where they oligomerize and form a pore that permeabilizes the mitochondrial outer membrane. In the presence of anti-apoptotic members, this oligomerization is inhibited. For instance, in the scheme shown in Fig. 1.9, pro-apoptotic Bid (blue) is activated by proteolytic cleavage, promoting its own partitioning and that of the pro-apoptotic Bax to the mitochondrial membrane. Bax oligomerizes, which causes pore formation and release of apoptotic factors into the cytosol [83] and cell death. It is not clear how Bcl-xL (purple) prevents cell death, but it is suggested that Bcl-xL either competes with Bax for binding sites in tBid or sequesters Bax molecules to prevent its oligomerization, or both. In either case, Bcl-xL plays a critical role on apoptotic regulation since it is the last line of defense to prevent cell death. From this point, we will focus on the membrane action of Bcl-xL.

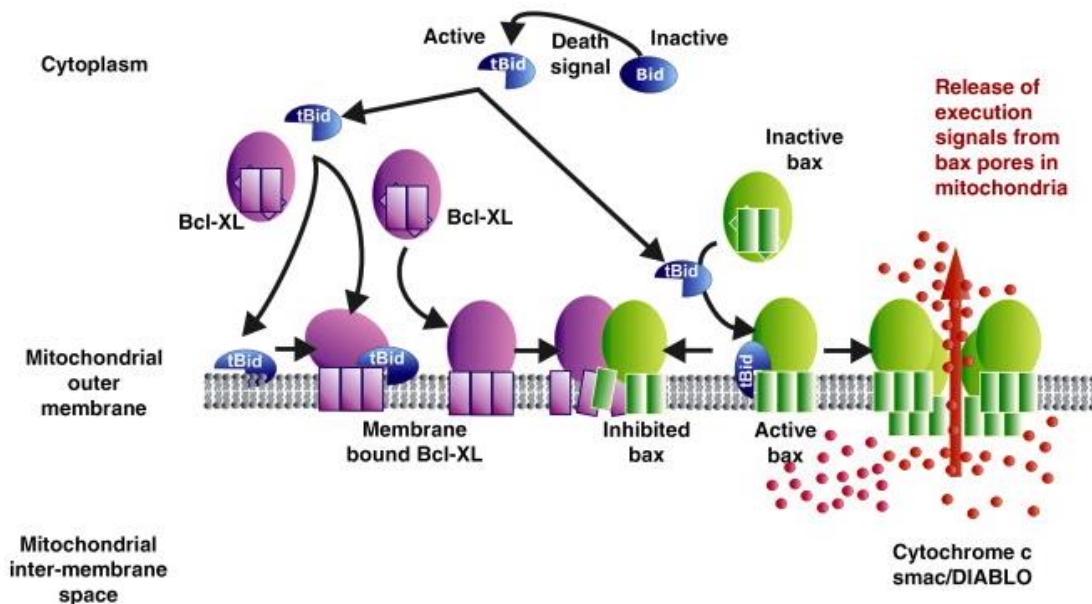


**FIGURE 1.9 The Embedded Together Model of apoptosis regulation** [82]. Multiple interactions between Bcl-2 family members occur in solution and in the mitochondrial membrane to either promote or prevent the formation of a pore that permeabilizes the mitochondrial outer membrane. For example, cleavage of Bid (blue, BH3-only) upon a death signal forms tBid, which can induce membrane partitioning of both Bcl-xL (purple, anti-apoptotic) and Bax (green, pro-apoptotic). Bax oligomerizes in the membrane and forms the apoptotic pore. Bcl-xL sequesters tBid and Bax to prevent their pro-apoptotic action. Apoptosis occurs when Bcl-xL is unable to prevent the apoptotic function of tBid and/or Bax. The membrane not only acts as platform, but also regulates the dissociation constants of these protein-protein interactions [84].

### *Bcl-xL*

Bcl-xL was the first member of the Bcl-2 family of proteins with known high resolution structure [66]. The NMR (Fig 1.10A) and X-ray structure of Bcl-xL shows 7  $\alpha$ -helices ( $\alpha$ 1 to  $\alpha$ 7) arranged in a globular fold. Helices  $\alpha$ 5 and  $\alpha$ 6 form the hydrophobic core of the protein, which is surrounded by the remaining helices. Bcl-xL has an additional helix, TM helix, which was truncated to crystallize the protein because it reduces the solubility of the protein [66]. Because of its hydrophobicity, it was suggested that the TM helix anchors Bcl-xL to the membrane (Fig. 1.10B, TM helix is modeled in blue). Experimental evidence indicates that the isolated TM helix indeed adopts a transmembrane topology [85]. A recent NMR study reports that the TM helix anchors Bcl-xL to lipid nanodiscs [86], supporting the role of this helix as the initial attachment of Bcl-xL to the mitochondrial membrane. Thus, Bcl-xL is composed of two domains: the soluble or N-terminal domain, and the TM helix. Although the TM helix has been suggested to be important for the interactions with Bax [87], it is not clear if it is necessary for

membrane partitioning of the soluble domain. In fact, Bcl-xL can interact with the membrane at low pH in the absence of the TM helix [65, 84, 88-90]. For the purposes of this dissertation, where we study the membrane insertion of the soluble domain, the TM helix is truncated.

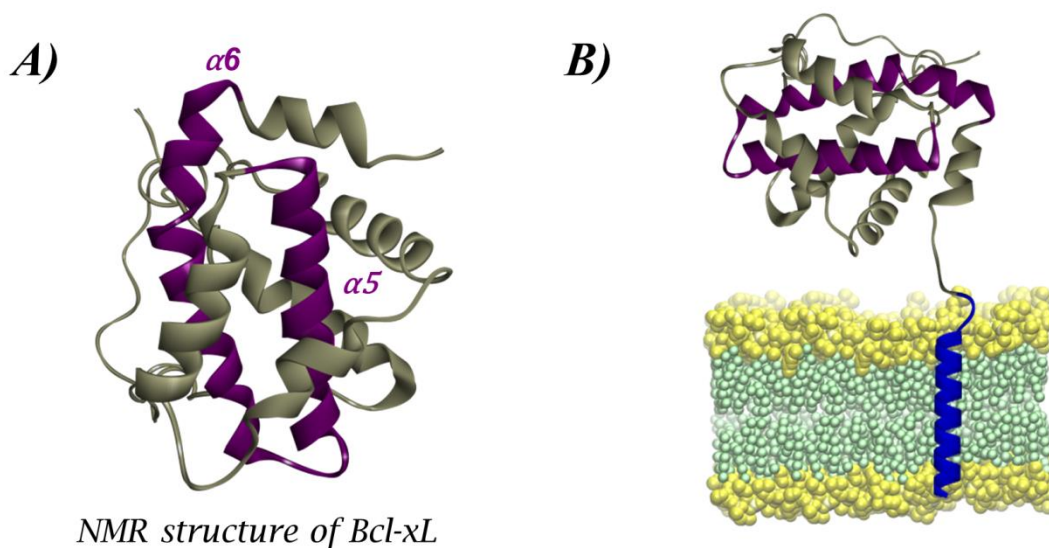


**FIGURE 1.10 High resolution structure of Bcl-xL (PDB 1LXL) [66]. A)** NMR structure of Bcl-xL lacking the TM helix. Helices  $\alpha 5$  and  $\alpha 6$  (purple) form the hydrophobic core of the protein. **B)** Putative model of Bcl-xL attached to the membrane through the TM helix as suggested in references [85, 86]. In this dissertation we study the membrane insertion of the soluble domain, so the TM helix is truncated.

Several mechanisms have been proposed for the inhibitory role of Bcl-xL. For example, Bcl-xL sequesters Bax in the membrane, which prevents the oligomerization of Bax [83]. Similarly, Bcl-xL sequesters tBid in the membrane, hence reducing the chances of tBid recruiting and activating Bax [76]. Finally, Bcl-xL exists in a dynamic equilibrium between its cytosolic and its membrane-bound form, where it can pull Bax out of the membrane during its dissociation [80,

81]. Whatever the case, Bcl-xL must partition from the cytosol into the mitochondrial membrane to execute its pro-survival action.

#### *COMPARISON OF BCL-XL TO THE DIPHTHERIA TOXIN TRANSLOCATION DOMAIN*

The initial characterization of Bcl-xL revealed that its high resolution structure resembled that of the diphtheria toxin T domain. Fig. 1.11 shows the crystal structures of both proteins as initially reported [66]. Both proteins share a similar globular fold in solution under neutral conditions, with helices arranged in a similar fashion: two central hydrophobic helices (colored in red in Fig. 1.11) surrounded by amphipathic helices. Although the structural similarities end there, this comparison was crucial for apoptosis research. When the structure of Bcl-xL was initially published, the role of the Bcl-2 proteins (only a few Bcl-2 proteins were known to exist) in apoptosis regulation was unknown. On the other hand, the function of the diphtheria toxin T domain was well known [91, 92]. The similarities between the structure of Bcl-xL and that of the T domain led to test the Bcl-2 proteins as pore-forming proteins [65, 93-95], which ultimately led to propose them as regulators of MOMP and apoptosis. Interestingly, while testing them as pore-forming proteins, researchers showed that low pH triggers the membrane interactions of Bcl-2 protein. Since then, *in vitro* studies on the membrane interactions of Bcl-xL are triggered by low pH [65, 84, 88, 90], although it is not clear if this is a prevailing signal that triggers insertion in the cell.

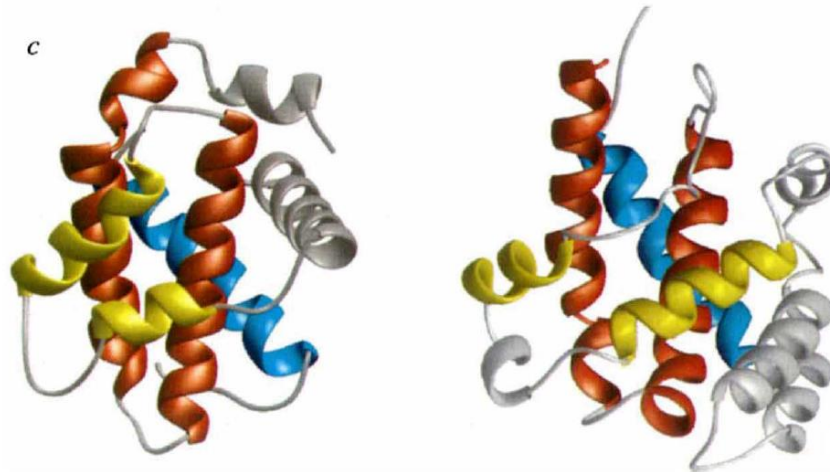


**FIGURE 1.11 Structural comparison between Bcl-xL and diphtheria toxin translocation domain.** The two central hydrophobic helices of Bcl-xL (**left**) and the T domain (**right**) are shown in red, while 2 amphipathic helices are colored in yellow. Figure taken from reference [66].

Other similarities between Bcl-xL and the T domain arise from their membrane interactions. First, both the soluble domain of Bcl-xL and the T domain are attached to independent domains that serve as anchors to the membrane: TM helix and R domain for Bcl-xL and T domain, respectively (See Fig. 2.2 and associated text for more details). Hence, the membrane interactions of the N-terminal region of Bcl-xL are analogous to that of the T domain. Second, it is suggested that the central hydrophobic helices of each protein ( $\alpha 5$ - $\alpha 6$  and TH8-TH9 in Bcl-xL and T domain, respectively) insert as transmembrane hairpins [51, 53, 57-60, 85, 96, 97]. Finally, Bcl-xL inserts into the bilayer as a monomer [83], which is similar to the case of the active form of the T domain [98, 99].

All these similarities led to suggest that the T domain would serve as a model for the understanding of Bcl-xL and other Bcl-2 proteins (Fig. 1.12) [64]. However, the molecular

details of the membrane interactions of Bcl-xL and other Bcl-2 proteins have not been studied, and it is unknown if they reflect what has been described for the T domain. For example, the T domain inserts into the membrane following a complex pathway with multiple intermediate states [43]. The membrane insertion pathway of Bcl-xL has not been described, and it is unknown if there are any intermediate states. In chapter 2, we show the membrane insertion pathway of Bcl-xL and systematically compare the features of that pathway described for the T domain to that determined for Bcl-xL.

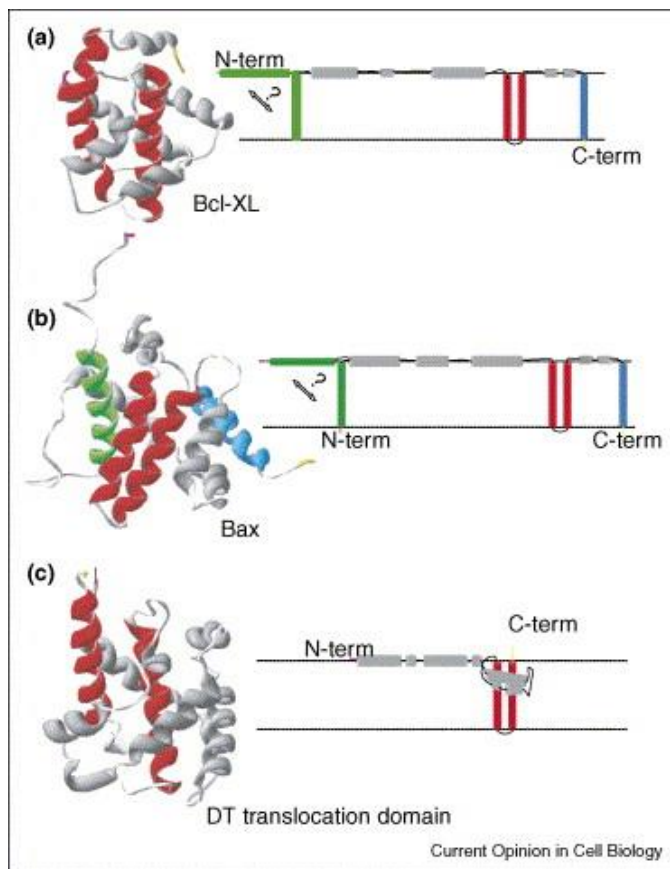


**FIGURE 2.12** Similarities between the membrane insertion models of Bcl-xL, Bax and the T domain as suggested in the literature [64]. The molecular details and the validity of these models have not been experimentally tested.

## *MEMBRANE LIPIDS AND APOPTOSIS*

There is growing evidence suggesting that different membrane lipids play a role in the regulation of Bcl-2 proteins, MOMP and apoptosis [100-111]. The most common example is that of cardiolipin, a phospholipid that in eukaryotes is found only in mitochondrial membranes [8]. Cardiolipin is a phospholipid with four acyl chains, and it has two negative charges in the headgroup under physiological conditions [112, 113]. Cardiolipin was first linked to apoptosis because cells with disrupted gene *CRD1*, which encodes cardiolipin synthase, showed altered mitochondrial functions, including increased cell death [114]. Subsequent studies suggested that cardiolipin is depleted during cell death [104] and is required for membrane interactions of Bid, Bax and Bcl-xL [83, 84, 103, 115, 116]. It is unclear what unique features of cardiolipin are important for regulation of apoptosis. Since some studies also have shown that the membrane interactions of Bcl-xL are regulated by phosphatidylglycerol [88, 90, 109], another anionic lipid, one possibility is that negative charges at the membrane interface are important for the action of the Bcl-2 proteins. A second possibility, however, is that cardiolipin and phosphatidylglycerol share some other common property because phosphatidylglycerol is precursor during biosynthesis of cardiolipin [8]. In chapter 4, we carry a detailed physicochemical characterization on the role of membrane lipids in the membrane interactions of Bcl-xL.

## SUMMARY, HYPOTHESES AND SPECIFIC AIMS

### Summary

- 1) The structure of the lipid bilayer consists of a double layer of lipids, where the acyl chains form the hydrocarbon core and the headgroups form relatively large and chemically complex membrane interfacial regions at each side of the hydrocarbon core.
- 2) Biological membranes are composed of an enormous variety of lipids that modulate the physicochemical properties of the lipid bilayer, at the hydrocarbon core and at the membrane interface.
- 3) The only two thermodynamically permitted folds of membrane proteins are transmembrane  $\alpha$ -helical bundles and  $\beta$ -barrels. Penetration of non-hydrogen bonded protein backbone into the hydrocarbon core is associated with prohibitive free energy penalty.
- 4) Membrane proteins insert into membrane by using either a translocon-assisted mechanism or upon receiving a cellular signal (e.g. protonation, proteolytic cleavage).
- 5) The diphtheria toxin T domain inserts into the membrane under acidic conditions *via* a multi-step pathway modulated by the protonation of various titratable residues. Initial stages of the refolding/insertion reaction are associated with the protonation of N-terminal histidines.
- 6) The Bcl-2 family proteins modulate apoptosis upon interaction with the mitochondrial outer membrane and pore formation. Bcl-2 proteins are structurally similar to the diphtheria toxin T domain and respond to acidification *in vitro*.

## *Hypotheses*

- 1) Given their functional differences, Bcl-xL and the T domain follow distinct pH-triggered membrane insertion pathways despite the structural similarities of their water-soluble states.
- 2) Membrane interactions of pH-induced membrane inserting proteins can be manipulated by protonation of key residues in the protein.
- 3) Properties of lipid bilayer modulate transmembrane insertion of proteins.

## *Specific aims*

In chapter 2, we determine the membrane insertion pathway of Bcl-xL and compare it to that of the diphtheria toxin T domain.

In chapter 3, we establish the effect of mutating individual C-terminal histidines on the folding and function of the diphtheria toxin T domain.

In chapter 4, we establish the regulatory role of cardiolipin and a variety of lipids on the membrane interactions of Bcl-xL.

## CHAPTER 2. COMPARING pH-DEPENDENT MEMBRANE INSERTION PATHWAYS OF BCL-XL AND DIPHTHERIA TOXIN T DOMAIN

### *INTRODUCTION*

Bcl-xL is an antiapoptotic member of the Bcl-2 family of proteins whose function is inhibiting the mitochondrial outer membrane permeabilization (MOMP) to prevent the cell from going into apoptosis [47, 73]. The mechanism by which Bcl-xL accomplishes its action is still under debate [75, 76, 81], although it is suggested that involves the redistribution of Bcl-xL between a cytosolic and a membrane-associated form [77, 80]. Given the similarities of the folded states between the diphtheria toxin translocation domain (T domain) and Bcl-xL (see introduction and below), it has been proposed that the T domain serves as model for the understanding of the action of Bcl-xL [64, 66] and other structurally similar Bcl-2 proteins [47] at the membrane. Here, we test this hypothesis by applying an array of spectroscopic methods to characterize the membrane insertion pathway of Bcl-xL, and compare it to that recently described for the T domain (Fig. 1.6) [53].

The diphtheria toxin is composed of three domains: the C domain (residues 1-199), the T domain (residues 200-378) and the R domain (residues 379-535) (Fig. 1.4A). The C domain inhibits protein synthesis in the target cell; the T domain is responsible for the translocation of the C domain inside the cell; and the R domain is responsible for the initial attachment of the toxin to the target cell through a direct interaction with a membrane receptor (Fig. 1.4B) [42]. The T domain is soluble in the aqueous extracellular fluid, but it undergoes a pH-triggered refolding and insertion into the endosomal membrane during endosomal acidification. The membrane insertion of the T domain results in the translocation of its own N-terminus across the

membrane, allowing the C domain or any other protein attached to the N-terminus to cross the membrane [117-119]. The isolated T domain has been a choice model for numerous biophysical studies on membrane binding and insertion [50-53, 57-60, 63, 68, 99, 119-124].

Bcl-xL shares significant structural and functional similarity with the diphtheria toxin T domain [64, 66, 85] (Fig. 2.1, detailed description in the introductory chapter). First, the high-resolution structure of Bcl-xL in the water-soluble state [66] shows a highly helical structure, with two central hydrophobic helices,  $\alpha 5$  and  $\alpha 6$  (red helices). The remaining helices (grey helices), as in the case of the T domain, surround the hydrophobic core. Bcl-xL, however, has an additional hydrophobic helix located at the C-terminus, TM helix, which is suggested to anchor the protein to the membrane prior to insertion [85]. Second, Bcl-xL also inserts into the bilayer in response to low pH [65, 84, 88, 90], although it is not clear if this is a prevailing signal that triggers insertion in the cell. Third, Bcl-xL inserts into the bilayer as a monomer [83], which is similar to what is described for the active form of the T domain [98, 99]. Finally, although the high-resolution structure of the membrane-inserted state of Bcl-xL is not available, the evidence suggests that helices  $\alpha 5$  and  $\alpha 6$  insert as transmembrane regions [85, 96], like TH8-TH9 of the T domain, while other regions might reside in the membrane interface.

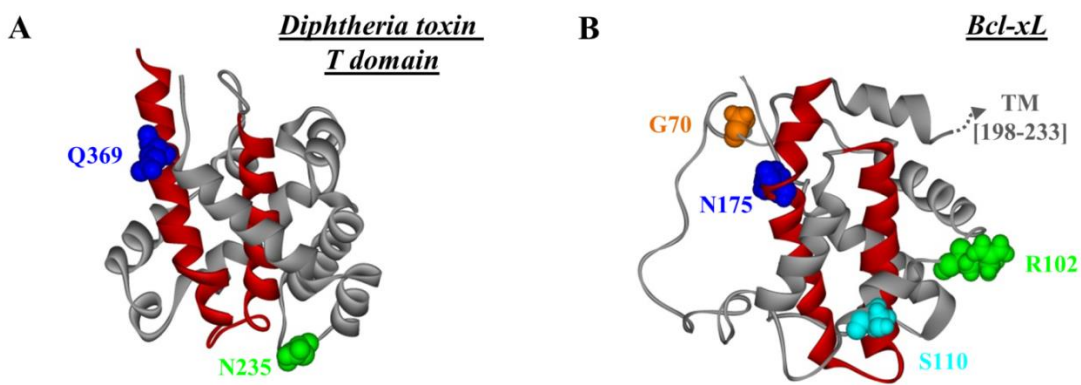


**FIGURE 2.1 High resolution structures of the T domain and Bcl-xL.** **A)** Crystal structure of the diphtheria toxin T domain (PDB 1MDT) in solution at neutral pH [49]. The central helices TH8-TH9 are shown as red ribbons. **B)** NMR structure of Bcl-xL (PDB 1LXL) in solution [66], with helices  $\alpha 5$  and  $\alpha 6$  shown as red ribbons. Residues used for cysteine replacement and site-selective labeling in reference [53] (for T domain) and in this chapter for Bcl-xL are shown as CPK. The putative location of the truncated C-terminal TM helix of Bcl-xL is schematized with a dotted arrow.

What would be an appropriate version of Bcl-xL to be compared to the T domain with regard to membrane insertion? The initial attachment of Bcl-xL to the mitochondrial membrane is ensured by a single TM helical fragment (residues 208-233). The folded N-terminal region (oval in Fig. 2.2) remains in a water-soluble state [85] and does not enter the membrane prior to the acidification. This arrangement is similar to that of the diphtheria toxin, with the TM fragment and the N-terminal domain of Bcl-xL being equivalent to the R domain and the T domain of the toxin, respectively. Therefore, most of the results presented here were generated with a Bcl-xL version in which the C-terminal helix has been truncated. The comparison made in this chapter corresponds to the membrane insertion processes of the N-terminal domain of Bcl-xL (residues 1-207) and the isolated T domain (residues 200-378), depicted as curved arrows in Fig. 2.2.

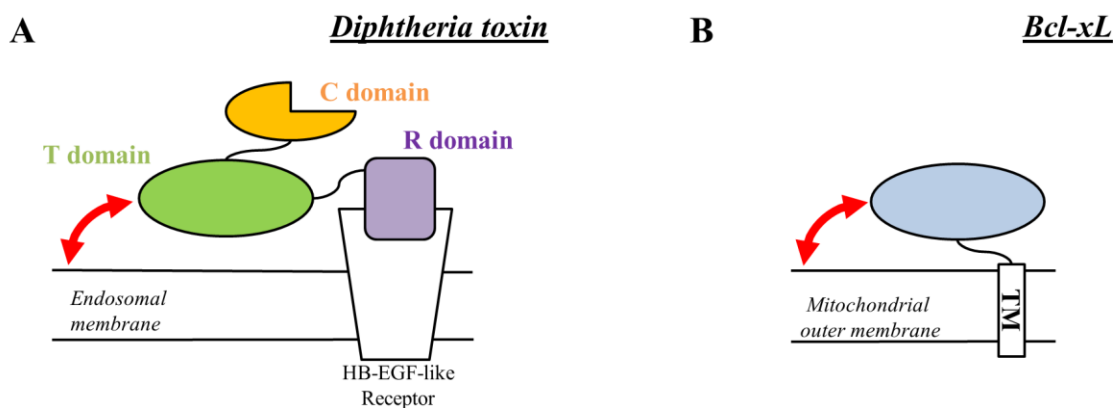


**FIGURE 2.2 Schematic representation of the mode of attachment of the diphtheria toxin and Bcl-xL to their target membranes.** The scheme illustrates the equivalent attachment/anchor function of the TM helix and the R-domain for Bcl-xL (**A**) and the diphtheria toxin (**B**), respectively. The membrane insertion of the T domain and the N-terminal region of Bcl-xL occur regardless of the attachment to the membrane. The processes addressed in this chapter are shown as curved red arrows (see text for more).

The truncation of the TM helix of Bcl-xL offers important additional advantages since it allows the study of the initial association of the protein with the membrane interface. The FRET assay used in this study for measuring this association was developed, and validated using independent FCS measurements, for the case of the T domain [53]. The assay uses the donor in the protein and the acceptor attached to a lipid head group, and requires that the protein and the membrane interface are not within the Förster distance of the donor/acceptor pair prior to the interaction. If the protein is already anchored to bilayer due to the TM helix, then the donor and acceptor would be within the Förster distance, and no spectral changes may be observed when triggering the binding of the N-terminal region of Bcl-xL to the membrane interface. Thus, by

truncating TM helix, we aim to prevent the N-terminal domain of Bcl-xL to be anchored to the bilayer, and ensure a detectable change in fluorescent signal upon donor/acceptor interaction.

## RESULTS

### *Folding and stability of Bcl-xL in solution: truncation of TM helix*

For the reasons discussed above, we truncated the TM helix of Bcl-xL using a standard site-directed mutagenesis that introduces a stop codon at the position 208 of the protein coding region. We then determined the effect of this truncation in the folding and stability of the protein in solution using circular dichroism (Fig. 2.3). Both the full-length and the truncated version of Bcl-xL show CD spectra that are typical of a protein with  $\alpha$ -helical secondary structure (minima at 220 and 208nm and maximum towards 190nm), consistent with the high resolution structure of Bcl-xL [66]. Both proteins also show similar ellipticity (compare black spectra of panels A and B), which indicates that the truncation did not cause substantial changes in the secondary structure of the protein. However, the refolding of Bcl-xL (blue spectra) after thermal unfolding (red spectra) was more complete in the truncated form, as judged by the recovery of CD signal after heating and cooling. The thermal unfolding experiments (Panels C and D) indicate that 1) the truncated form is more stable than the full-length Bcl-xL, 2) reversibility is only achieved for the truncated form, and 3) the process is rate-independent for both proteins. Together, these results indicate that Bcl-xL is less stable in solution, and possibly more prone to aggregation, when the TM helix is present. Hereafter, the truncated form of Bcl-xL is referred to as Bcl-xL.

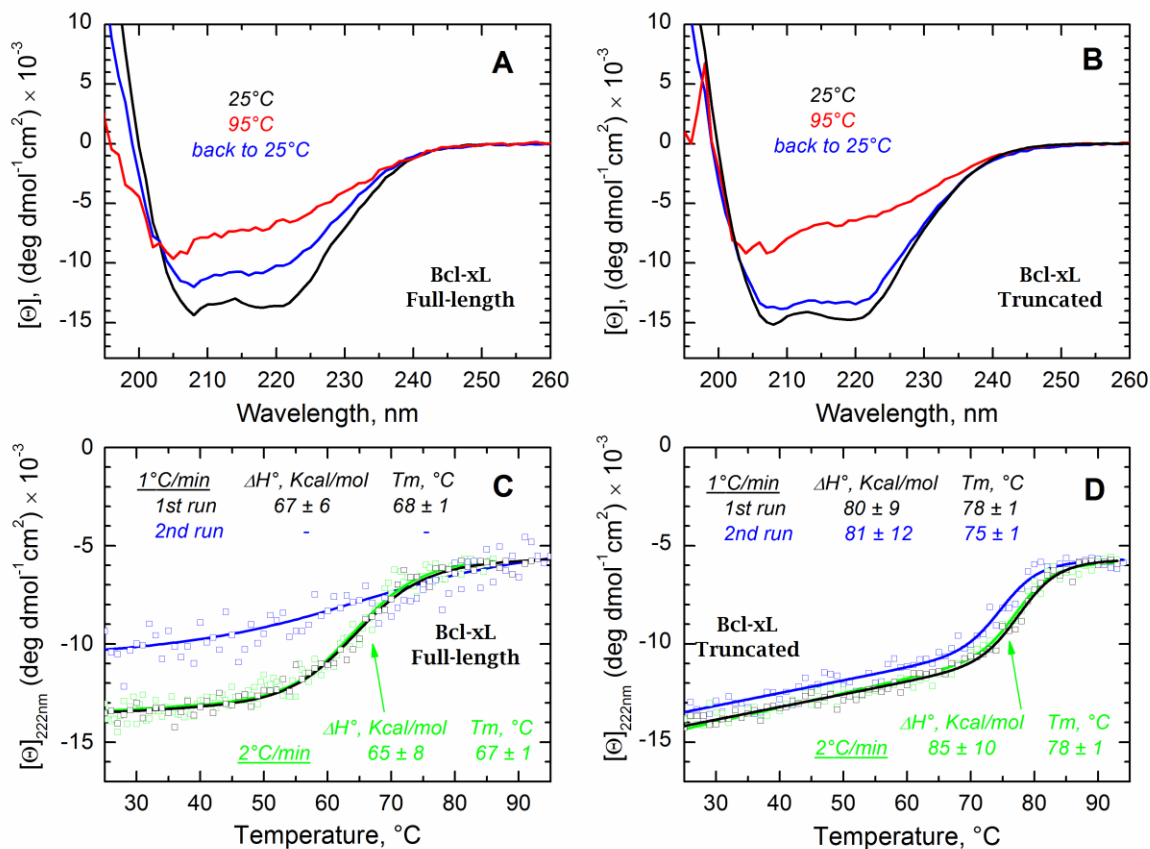


**FIGURE 2.3 Thermal unfolding of the full-length and truncated Bcl-xL in solution at pH 8.**

Panels **A** (truncated) and **B** (full-length) show the CD spectra before (black spectra) and after thermal unfolding (red spectra), and after the rapid cooling to 25°C (blue spectra). Panels **C** (truncated) and **D** (full-length) show the thermal unfolding of the folded (1st run, black data) and refolded (2nd run, blue data) Bcl-xL. The latter panels also show the thermal unfolding at double rate of heating (green data). The data suggest that reversible and rate-independent transitions in Bcl-xL, which are the prerequisite to quantitative analysis of thermal unfolding, can be achieved by deletion of the C-terminal TM helix.

### *Folding and pH-dependent stability in solution: comparison to T domain*

To determine whether or not Bcl-xL and the T domain share similar membrane insertion pathways, we first studied the stability of Bcl-xL at different pH. The first transition along the membrane insertion pathway of the T domain occurs in solution and is pH-dependent, and corresponds to the conversion of the water-soluble state (W-state) into the membrane-competent state (W<sup>+</sup>-state) (Fig. 1.6) [43]. This transition is characterized by partial refolding, reduction in the amount of secondary structure and loss of thermostability in a pH-dependent fashion [50, 52, 63, 124]. To determine whether the pH-triggered membrane insertion of Bcl-xL goes through the formation of a similar intermediate, we tested the pH-induced loss of secondary structure by CD spectroscopy (Fig. 2.4). Upon acidification, the CD spectrum of Bcl-xL maintains its characteristic shape and exhibits marginal reduction in molar ellipticity (Panel A), indicating that Bcl-xL does not experience a pH-induced loss of secondary structure. This behavior is different from that of the T domain (panel B), which loses substantial part of its ellipticity signal in the same pH range [121, 122].

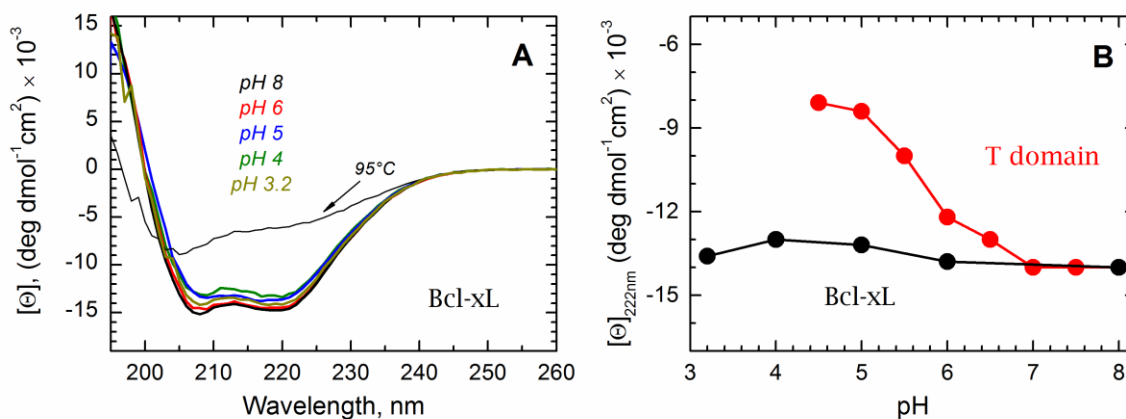


**FIGURE 2.4 pH-dependent variation in secondary structure of Bcl-xL and the T domain in solution.** **A)** CD spectra of Bcl-xL in solution at pH 8 (black spectrum), 6 (red spectrum), 5 (blue spectrum), 4 (olive spectrum) and 3.2 (dark yellow spectrum) at 25°C. The CD spectrum at pH 8 and 95°C is shown for reference (dotted line). **B)** pH-dependent changes in molar ellipticity measured at 222 nm for T domain (red symbols, data reproduced from [122] for visual comparison) and Bcl-xL (black symbols).

Next, we tested the pH-induced loss of thermodynamic stability by measuring changes in ellipticity at 222 nm as a function of temperature. In Fig. 2.3 we established that thermal unfolding of Bcl-xL is reversible and rate-independent, which are prerequisites for quantitative analysis. To provide a visual reference, we display the fits for the previously published thermal unfolding data for the T domain [124] in Fig. 2.5. These results indicate a substantial loss of stability when pH is reduced from 8 to 6, which follows from an over 15°C reduction in the melting temperature and a loss in transition enthalpy  $\Delta H^\circ$  (Thermodynamic parameters for the thermal denaturation of both proteins are summarized in Table 1). Cooperative melting transition is no longer observed at pH 5, when the T domain is converted to the  $W^+$ -state (Fig. 2.5A, blue line). In contrast, we observe identical thermal transitions of Bcl-xL at pH 8 and 6 (Fig. 2.5B). Moreover, further acidification up to pH 4 causes only a small decrease in melting temperature and transition enthalpy (Fig. 2.5B and Table 2.1). These results clearly indicate that the solution fold Bcl-xL is not destabilized by acid, complementing a previous report that showed Bcl-xL being equally resistant to chemical denaturation at neutral or acidic pH [89]. Together, our measurements suggest that Bcl-xL does not go through a CD-detectable pH-induced conformational change in the aqueous phase as does the T domain, demonstrating differences at the very early stages of the membrane insertion pathways.

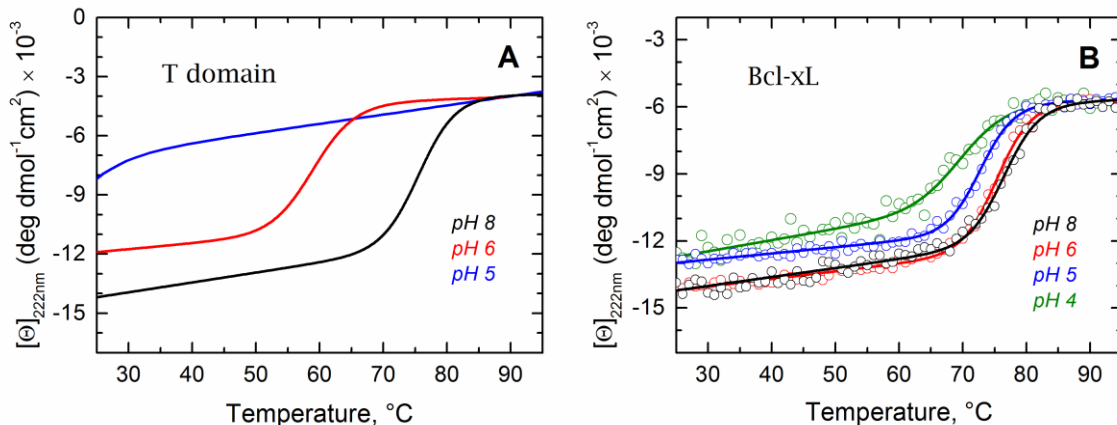


**FIGURE 2.5 pH-dependent variation in thermostability of Bcl-xL and the T domain in solution.** **A)** Fitting curves of the previously published data [124] on thermal unfolding of the T domain in solution at pH 8 and 6 are shown for reference. At pH 5 no cooperative melting transition can be detected. **B)** Thermal unfolding of Bcl-xL at pH 8 (black), pH 6 (red), pH 5 (blue) and pH 4 (olive). The figure illustrates the small effect of acidification on the thermal stability of Bcl-xL, contrasting with the dramatic loss of stability of the T domain. Corresponding thermodynamic parameters are summarized in Table 1.

**TABLE 2.1 Thermodynamic parameters for the thermal unfolding of the T domain and Bcl-xL in solution at the indicated pH.** \*Parameters for the T domain were published in reference [124].

pH	T domain*		Bcl-xL	
	T <sub>m</sub> , °C	ΔH°, kcal/mol	T <sub>m</sub> , °C	ΔH°, kcal/mol
8	75 ± 1	95 ± 7	77 ± 1	87 ± 6
6	59 ± 1	78 ± 6	76 ± 1	88 ± 4
5	No cooperative transition		73 ± 1	89 ± 4
4	No cooperative transition		70 ± 1	62 ± 8

## Membrane association

Previous studies have reported the pH dependence of membrane binding of the T domain to vesicles of various lipid compositions using several independent spectroscopic methods, which produced results with excellent agreement [50, 53]. One of them, based on FRET methodology, is used here for Bcl-xL. Briefly, the donor dye (Alexa488) is attached to the protein and the acceptor (Rhodamine) is incorporated in large unilamellar vesicles (LUV) as Rhodamine-PE. When protein and vesicles are mixed together at various pH, the binding can be measured by the decrease in the emission intensity of the donor or by the shortening of its fluorescence life-time. We show representative results of the steady-state (Fig. 2.6A) and life-time (Fig. 2.6B) fluorescence measurements for membrane interaction of the Bcl-xL R102C mutant with selectively attached dye to the cysteine residue. As expected, the data indicate a decrease in the fluorescence intensity and faster fluorescence decay when the interaction between the donor and acceptor is triggered by acidification (steps 1 and 2, black and blue). Importantly, the process is reversible, since the spectral features are recovered upon return to pH 8 (step 3, red), allowing the thermodynamic treatment to the data.

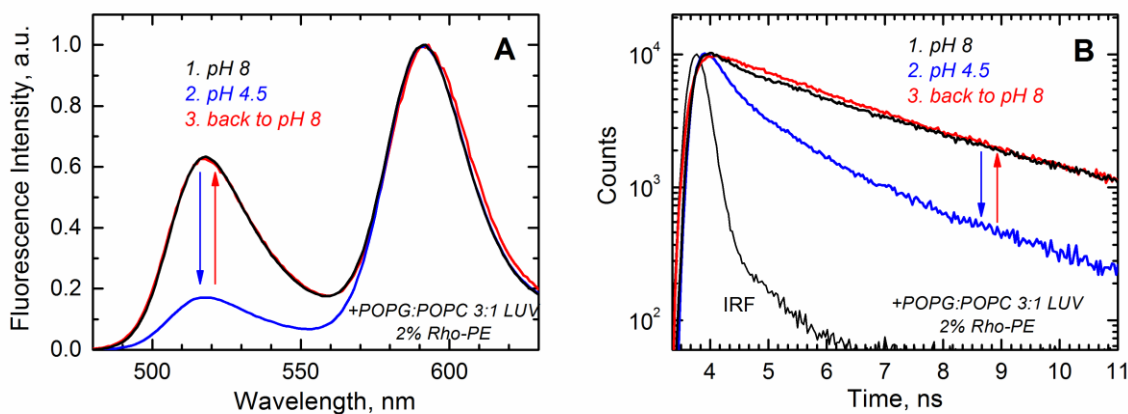


**FIGURE 2.6 Reversibility of pH-dependent membrane association of Bcl-xL examined by the FRET measurements between donor-labeled protein and acceptor-labeled LUV. A)** Emission spectra of the donor at pH 8 (step 1, black spectrum) and 4.5 (step 2, blue spectrum) in the presence of the acceptor. The loss of intensity is recovered upon addition of NaOH to return to pH 8 (step 3, red spectrum). **B)** Fluorescence decay of the donor at pH 8 (step 1, black trace) and 4.5 (step 2, blue trace) in the presence of the acceptor. The shortening of the decay is reversed upon return to pH 8 (step 3, red trace). The data indicate that the pH-triggered binding of Bcl-xL to the membrane is a reversible process.

Before proceeding into a full characterization of the membrane association of Bcl-xL, we performed two control experiments. In the first one, we measured the changes in fluorescence signal in the absence of acceptor-labeled membranes (Fig. 2.7A), and we did not observe any changes upon decrease in the pH. Therefore, the changes observed in Fig. 2.6 are consistent with association of labeled Bcl-xL with the membrane rather than an effect of pH on the probe. In the second control experiment, we changed the position of labeling from residue R102C to G70C or S110C and gradually decreased the pH (Fig. 2.7B). The resulting pH-dependent binding profiles are superimposable, indicating that we can label any of the three residues with the donor dye without affecting membrane binding).

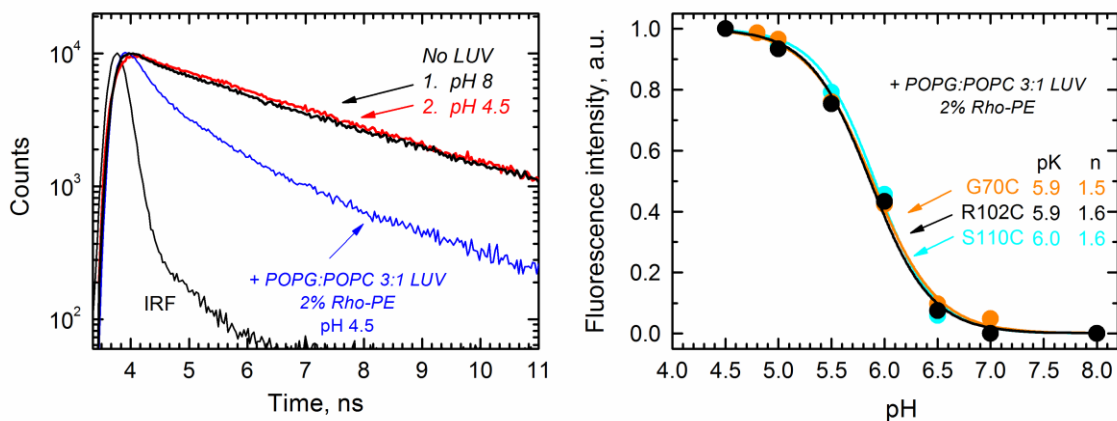


**FIGURE 2.7 Effect of acidification and labeling position on spectral features of the probe**

**Alexa488 attached to Bcl-xL.** **A)** Effect of acidification on the fluorescent signal of the Alexa488 attached to Bcl-xL in the absence of acceptor-labeled LUV. Fluorescence decay was measured in solution at pH 8 (step 1, black trace) and pH 4.5 (step 2, red trace). Measurement in the presence of acceptor-labeled LUV is shown for reference (blue trace). **B)** pH-dependence of binding of Bcl-xL labeled at three different positions to LUV composed of POPG:POPC 3:1. Measurements performed result in overlapping pH-dependent binding curves.

For the T domain, the initial binding proceeds through an interfacial intermediate I-state and is largely independent of the physical-chemical properties of the membrane interface [53]. We tested whether this would also hold true for Bcl-xL by measuring the association of the protein to LUV of different lipid compositions as a function of the pH. To do so, we used the FRET assay described above, and we calculated the FRET efficiency of binding at different pH values. In Fig. 2.8A, we show the titration curves previously reported for the case of the T domain [53], where it is clear that regardless of the proportion of the anionic lipid POPG in the LUV, the pK of the transition remains mostly unaltered. The case of Bcl-xL (Fig. 2.8B), however, appears to be different. In this case, the decrease of the POPG content causes a shift in the pK of the

transition, indicating that the binding of the protein to the bilayer depends on the physical-chemical properties of the membrane interface. Furthermore, Bcl-xL was unable to bind to LUV composed of only 10% anionic lipid (cyan) in the pH range studied, indicating that POPG is critical for binding of the protein to the membrane. Thus, in contrast to the case of the T domain, our results indicate that the formation of the membrane-competent state of Bcl-xL responds to changes in the physical-chemical environment of the membrane interface.

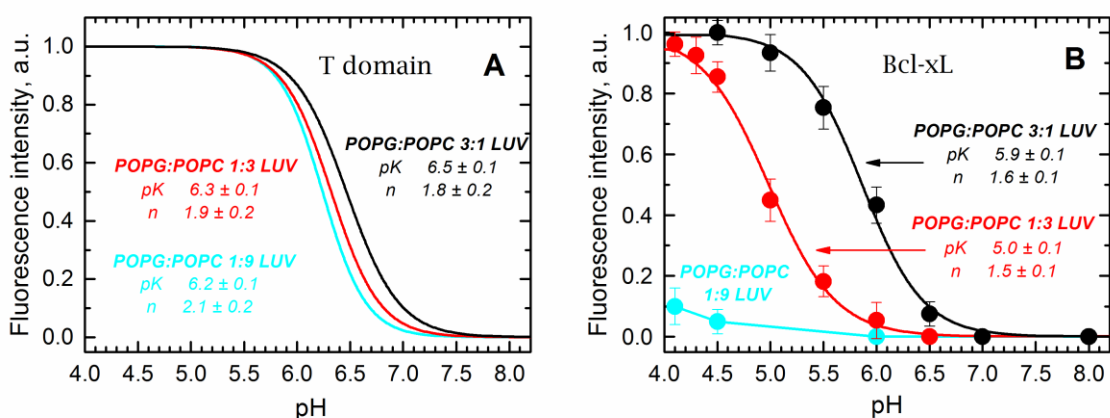


**FIGURE 2.8 Comparison of pH-dependent binding of Bcl-xL and the T domain to LUV composed of different mixtures of POPC and POPG. A)** The binding of the T domain to the membrane interface does not depend on the mole fraction of POPG, as the three lipid compositions result in almost overlapping titration curves (only fitting curves taken from reference [53] are shown). **B)** The titration curves of Bcl-xL shift to a lower pH when the mole fraction of POPG decreases. The pKs and n (Hill coefficient) were obtained by fitting the data to a two-state model as described in methods.

This difference in the binding to the membrane interface implies that both proteins respond to the pH changes at different stages of the process. In the case of the T domain, the protein would

respond to acidification when still in the bulk solution, because 1) the low pH causes conformational changes in the absence of membranes (Fig. 2.4 and 2.5, Table 2.1, and references [50, 52, 63, 121, 124]) and 2) binding to the bilayer does not depend on the physical-chemical properties of the membrane interface (Fig. 2.8 and reference [53]). In the case of Bcl-xL, however, the opposite is true: 1) no changes are observed during the acidification in the absence of membranes (Fig. 2.4 and 2.5 and Table 2.1), and 2) there is a strong dependence on the content of POPG (Fig. 2.8). The charges on the POPG head group will create a negative surface potential that can either affect the pK's of key titratable groups of Bcl-xL directly or possibly modulate the local pH near the interface, or both [125, 126].

#### *Membrane insertion of the hydrophobic helical hairpin*

The next step in the insertion pathway of the T domain is an interfacial refolding and membrane insertion of the hydrophobic helical hairpin TH8-TH9 (Fig. 2.1A) to form a transmembrane T-state [53]. The formation of this state can be followed experimentally by attaching the environment-sensitive fluorescent probe NBD to a single-cysteine mutant in the middle of helix TH9 [53, 68]. A similar transition is predicted to occur for Bcl-xL, as the helices  $\alpha 5$ - $\alpha 6$  (Fig. 2.1B) have been observed to adopt a transmembrane topology in the context of the isolated fragments [85]. To confirm that these helices can be inserted in the context of protein, we labeled helix  $\alpha 6$  at position N175C with NBD. We show a typical measurement in Fig. 2.9, where the acidification of the medium in the presence of LUV (steps 1 and 2, black and blue) results in a 12 nm blue-shift and 7-fold increase of the intensity in the emission spectra (Panel A), and longer fluorescence decay (Panel B) of the NBD-labeled Bcl-xL. The return to pH 8.0

causes the recovery of the spectral features and life-time decay, which indicates that this insertion process is reversible (step 3, red).

In a control experiment, we measured the emission spectra of Bcl-xL labeled with NBD in the absence of LUV (Fig. 2.10). The results showed that acidification caused little changes in the steady-state and life-time profiles, indicating that pH does not cause spectral changes of the NBD probe. Therefore, data of Fig. 2.9 are consistent with the repositioning of the probe to a non-polar environment. The addition of membranes to the previously acidified sample resulted in the characteristic spectral signature of the NBD probe locating in the hydrophobic environment of the membrane (Fig. 10, blue data), suggesting that the membrane insertion of Bcl-xL is path-independent.

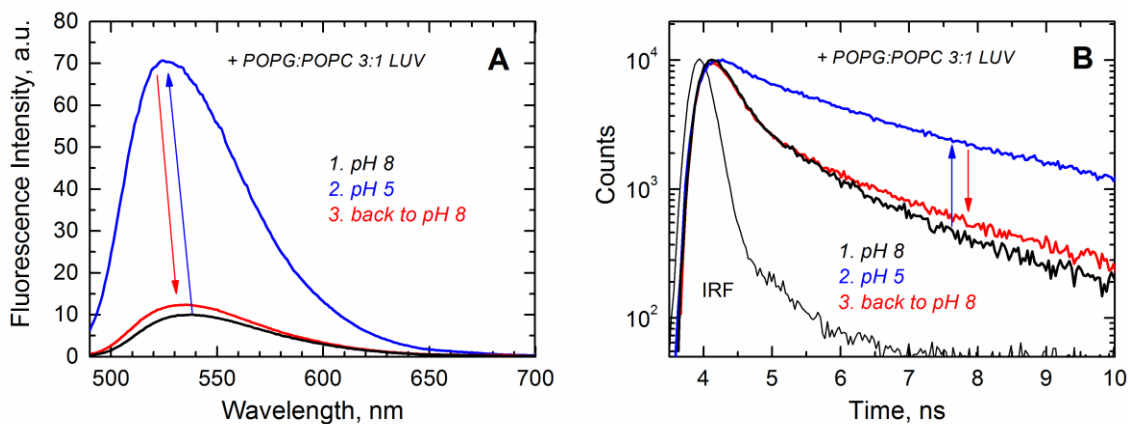


**FIGURE 2.9 Membrane insertion of Bcl-xL monitored by fluorescence of the environment-sensitive probe NBD attached to the residue N175C (the middle of helix  $\alpha_6$ ).** A) Steady-state spectra in the presence of LUV at pH 8 (black spectrum) and 5 (blue spectrum) shows gain in intensity and blue shift at acidic pH, and recovery of spectral features upon return to pH 8 (red

spectrum). **B)** Fluorescence decay of the same samples showing the lengthening of the decay at acidic pH.

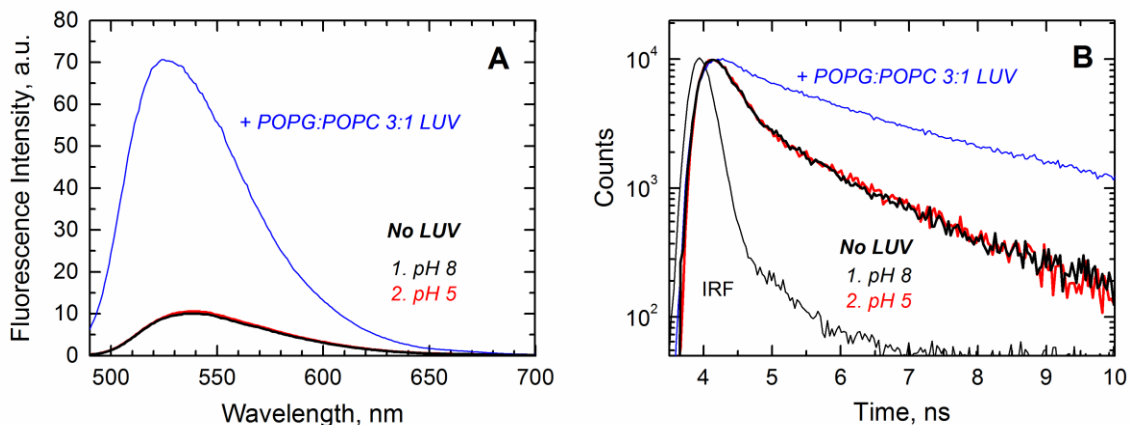


**FIGURE 2.10** Effect of pH on spectral features of probe NBD selectively attached to Bcl-xL. Steady-state (**A**) and life-time (**B**) emission of Bcl-xL labeled at position N175C with NBD were measured in solution at pH 8 (step 1, black). Acidification of the solution causes no changes in the fluorescence intensity, position of maximum emission, and fluorescence decay (step 2, red). Addition of LUV to the previously acidified sample results in increase of emission intensity, blue-shift of the spectrum and longer fluorescence decay (blue).

The pH dependence of this insertion is affected by the mole fraction of POPG in the T domain, where a high proportion of anionic lipid is required for the protein to adopt the T-state [53]. We show the fitting curves for the pH-dependence of the insertion of the T domain in Fig. 2.11A as reference. We made the parallel analysis for the hairpin of Bcl-xL by using the NBD-labeled protein and measuring the changes in intensity as a function of the pH. The data for Bcl-xL (Fig. 2.11B) shows that the pH dependence varied just slightly with a decreasing mole fraction of POPG. Measurements for LUV composed of 10% POPG were excluded from the analysis because of the lack of membrane association of Bcl-xL in the first place (see Fig. 2.8B). The T

domain is fully bound to the membrane under those conditions, and lack of membrane insertion is due to the protein being trapped in a kinetic intermediate in the membrane interface [53, 63]. In contrast, pH-dependencies of insertion of Bcl-xL only marginally differ from those of initial association, suggesting that the non-inserted state on membrane interface exists only transiently. Thus, the insertion of the helical hairpins also takes place by a different mechanism, where the T domain responds to the presence of anionic lipid for this step, but not Bcl-xL.

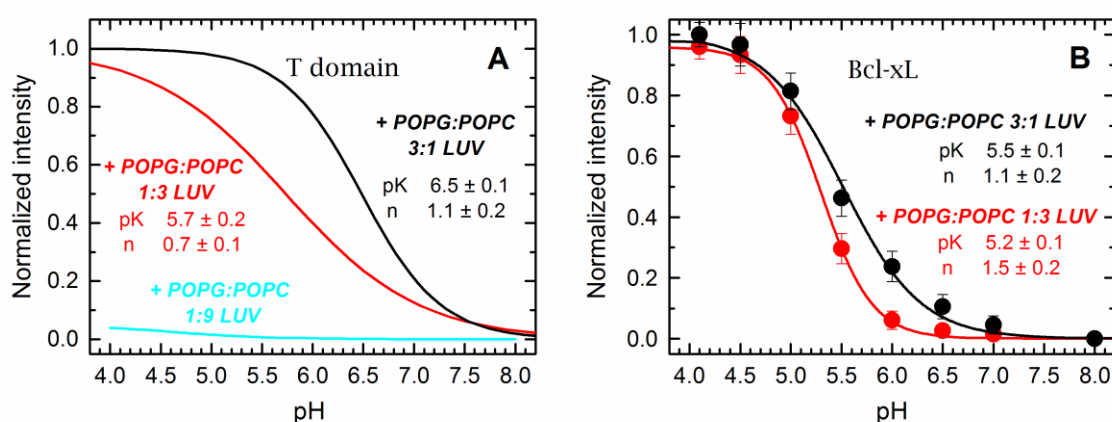


**FIGURE 2.11 Comparison of pH-dependent membrane insertion of the hydrophobic helical hairpins of the T domain and Bcl-xL.** **A)** The membrane insertion of the T domain into LUV, determined as a function of the pH, strongly depends on the mole fraction of POPG in the LUV (only fitting curves from reference [53] are shown). **B)** The membrane insertion of Bcl-xL, studied as a function of the pH by following the changes in emission intensity at 525 nm, does not strongly depend on the POPG content of LUV. Data for LUV composed of POPG:POPC 9:1 was omitted due to lack of membrane association.

## DISCUSSION

We summarize our findings in Fig. 2.12, where we illustrate the comparison of the insertion pathways for the T domain and Bcl-xL. The structures of the soluble W-states are similar for the two proteins [49, 66], featuring a pair of long hydrophobic helices in the middle of the structure (highlighted red in Fig. 2.1): TH8-TH9 and  $\alpha 5$ - $\alpha 6$  for the T domain and Bcl-xL, respectively. While these helices will adopt a transmembrane conformation in the final inserted T-state in both cases, the similarities between the two proteins end there. For the case of the T domain (Fig. 2.12A), the folded soluble W-state is initially converted to the low-stability membrane-competent  $W^+$ -state as a result of acidification in solution. This  $W^+$ -state then interacts with the membrane in a manner that is independent of the properties of the membrane interface. The latter indicates that the protein is ready to associate with the membrane when still in solution, and therefore senses the pH change within the bulk solution [50, 53]. The physiological reason for this feature is likely to be related to the fact that the toxin may dissociate from its receptor inside the endosome [127] and the T domain is no longer localized close to membrane interface. The pathway proceeds through a series of intermediate states, such as interfacial I-state and activated insertion-competent  $I^+$ -state [53]. The final insertion to T-state is regulated by additional protonation on the membrane interface and by the presence of anionic lipids, presumably promoting formation of productive intermediates via electrostatic interactions with cationic groups on the T domain.

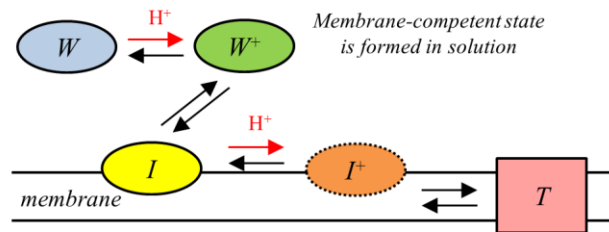
Remarkably, the soluble W-state of Bcl-xL is not destabilized by acidification and the formation of the membrane-competent state does not appear to require a conformational change to occur in solution (Fig. 2.4 and 2.5, and Table 2.1). Unlike in the case of the T domain, the

conformational switching initiating the insertion cascade requires the membrane interface and is modulated by the presence of anionic lipids (Fig. 2.8). Once the protein is on the interface, the insertion proceeds without the requirement of additional protonation in a lipid-independent manner, which is again different from the behavior of the T domain (Fig. 2.11). Thus, our study clearly indicates that Bcl-xL and the diphtheria toxin T domain insert into the lipid bilayer following different membrane insertion and protonation pathways.

We suggest that the difference in the nature of the conformational switching in both proteins evolved to best serve their physiological function. For the T domain, the robustness of delivery of its cargo (the catalytic domain, ultimately responsible for toxicity) requires no regulation step and is achieved by a single copy of the protein. In contrast, Bcl-xL and other proteins of the Bcl-2 family act collectively, and their function is very tightly regulated [47, 75, 76]. Subsequently, lipid-dependent triggering of the insertion (Fig. 2.8) can be a part of such regulatory machinery. Another important aspect of membrane interactions of Bcl-xL is the complete reversibility of binding (Fig. 2.6) and insertion (Fig. 2.9), also suggested previously [90], which may be required for proper functioning of this protein.

*pH-TRIGGERED MEMBRANE INSERTION*

**A** *Diphtheria toxin T-domain*



**B** *Bcl-xL*

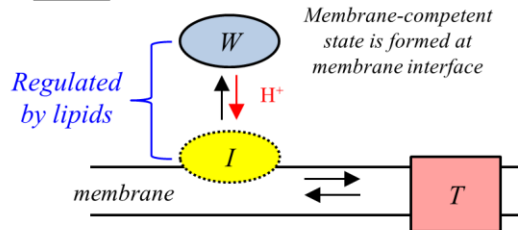


**FIGURE 2.12 Schematic representations of the pH-triggered membrane insertion pathways of the diphtheria toxin T domain and apoptotic regulator Bcl-xL.** Each starts with a similarly folded soluble W-state (Fig. 2.1) and ends with membrane-inserted T-state, in which two central hydrophobic helices, TH8-TH9 of the T domain and  $\alpha 5$ - $\alpha 6$  of the Bcl-xL, adopt a transmembrane conformation. The pathway connecting the two states, however, is very different in the two proteins. T domain goes through a set of intermediate states and undergoes several protonation transitions, both in solution and on membrane interface, characterized by staggered pH-dependencies [53]. Unlike the T domain, Bcl-xL is not destabilized by acidic pH in solution, and protonation resulting in the formation of its membrane-competent form occurs on membrane interface where it can be regulated by lipid composition. The interfacial intermediate state for Bcl-xL appears to be transient (as indicated by dotted border line of I-state on the scheme) with insertion closely following initial association with membrane interface (see Figs. 2.8 and 2.11, and text for details).

## *MATERIALS AND METHODS*

*Materials:* Palmitoyl-oleoyl-phosphatidylcholine (POPC), palmitoyl-oleoyl-phosphatidylglycerol (POPG) and Rhodamine-PE were purchased from Avanti Polar Lipids (Alabaster, AL). IANBD-ester and AlexaFluor488-maleimide were obtained from Invitrogen (Carlsbad, CA).

*Cloning and mutagenesis:* Full-length Bcl-xL (residues 1-233) was PCR-amplified from cDNA obtained from K562 human lymphoma cells and ligated into the pET28b vector using the NdeI and EcoRI cloning sites. The truncated version of Bcl-xL (residues 1-207) was generated by introducing a stop codon in the position corresponding to residue 208. For the purposes of Cys-labeling with fluorescent dyes, Cys-less mutant (C151S) was created and used as template for site-directed mutagenesis. All the constructs contained an N-terminal 6xHis-tag for purification.

*Expression, purification and labeling:* The expression and purification of Bcl-xL was based on the previously described procedure for the pET system [128]. Briefly, BL-DE23pLysE E.coli cells were transformed with the corresponding pET plasmid and grown to OD<sub>600nm</sub> ~ 0.6, after which expression was induced by addition of 0.8M IPTG and the cells grown for an additional 16 hours at 24°C. The cells were pelleted by centrifugation, lysed by sonication and clarified by centrifugation for 30 min at 4000 rpm and 4°C. The proteins were then incubated with Ni-NTA beads, washed with washing buffer (50mM Tris-HCl, 300mM NaCl, 5mM imidazole, pH 8) and eluted with 0.5M imidazole in the same buffer. The eluted proteins were subjected to size-exclusion chromatography on a Sepharose12 1x30cm column in 50mM phosphate buffer at pH 8, and quantified by measuring their absorbance spectra in the range 200-350 nm (we used molar

extinction coefficient of 41,200 M<sup>-1</sup>cm<sup>-1</sup> at 280 nm). Labeling with fluorescent dyes was performed using a standard procedure for thiol-reactive derivatives [53, 129] and the unreacted dye was removed by gel filtration chromatography in the same column and buffer.

*LUV preparation:* Large unilamellar vesicles (LUV) containing molar mixtures POPG:POPC (3:1, 1:3 and 1:9) of 0.1 μm diameter were prepared by extrusion as previously described [130, 131]. Rhodamine-labeled LUV were prepared by the addition of 2% of Rhodamine-PE to the lipid mixture.

*Circular dichroism and thermal unfolding:* CD measurements were performed using an upgraded Jasco-720 spectropolarimeter (Japan Spectroscopic Company, Tokyo). Normally, 100 scans were recorded between 190 and 260 nm with a 1 nm step at 25°C and 95°C using a 1 mm optical path cuvette. The sample contained 4μM of Bcl-xL in 50mM phosphate buffer at pH 8.0 or a mixture of phosphate and acetic/acetate buffer at pH 6.0, 5.0 or 4.0. Further acidification was reached by equilibrating the sample in 50mM glycine-HCl buffer. All spectra were corrected for background. The thermal unfolding was followed at 222 nm with a 1 degree/minute scan rate, unless indicated. The data was fitted to a two-state transition as described before [68, 124], obtaining the transition temperature  $T_m$  and transition enthalpy  $\Delta H^\circ$  with the following equations:

$$Y = (Y_N + m_N T) X_N + (Y_U + m_U T) (1 - X_N) \quad (\text{Eq. 2.1})$$

$$X_N = 1 / [1 + \exp(-\Delta H^\circ (1 - T / T_m) / RT)] \quad (\text{Eq. 2.2})$$

where  $Y$  is the experimentally observed CD signal at a given temperature,  $Y_N$  and  $Y_U$  represent the signals of the pure native and unfolded state at 0K, and  $m_N$  and  $m_U$  are the temperature-

dependencies of these CD signals for the native and unfolded states, respectively, and  $X_N$  is the fraction of the native state at temperature  $T$ .

*Fluorescence measurements and analysis:* Steady-state fluorescence emission was measured using a SPEX Fluorolog FL3-22 steady-state fluorescence spectrometer (Jobin Yvon, Edison, NJ) equipped with double-grating excitation and emission monochromators. The measurements were made in a 2x10 mm cuvette oriented perpendicular to the excitation beam and maintained at 25°C using a Peltier device from Quantum Northwest (Spokane, WA) in 1 nm steps. For Alexa488 measurements, we recorded the emission spectra from 470 to 700 nm with excitation wavelength of 455 nm and slits of 2 nm for both excitation and emission. For NBD measurements, we collected the emission spectra from 490 to 700 nm, and the excitation wavelength was 470 nm, using slits of 5 nm on both monochromators. For each spectrum, we averaged 5 scans after incubating the samples during 30 min for equilibration.

Fluorescence decays were measured with a time-resolved fluorescence spectrometer, FluoTime 200 (PicoQuant, Berlin, Germany), using a standard time-correlated single-photon counting scheme as previously described [132]. Samples were excited at 440 nm by a subnanosecond pulsed diode laser, LDH 440 (PicoQuant, Berlin, Germany), with a repetition rate of 10 MHz. Fluorescence emission was detected at 535 nm, selected by a Scientech Model 9030 monochromator, using a PMA-182 photomultiplier (PicoQuant, Berlin, Germany). The samples normally contained 0.3 $\mu$ M protein and 0.5mM lipid. The fluorescence intensity decay was analyzed using FluoFit iterative-fitting software based on the Marquardt algorithm (PicoQuant, Berlin, Germany).

The pH-dependencies of the fraction of membrane-bound or membrane-inserted states generated by corresponding spectroscopic experiments ( $F$ ) were fitted to the following equation [133]:

$$F = \frac{1}{1 + 10^{n(pH - pK)}} \quad (\text{Eq. 2.3})$$

where  $pK$  is a negative logarithm of the dissociation constant, and  $n$  is the Hill coefficient.

*Data analysis and illustrations:* Data analysis, fittings and preparation of graphs were performed with the commercial software packages OriginPro versions 8.5, 9.0, 9.1 and 2015 (OriginLab Corporation, Northampton, MA). Structural visualization and preparation of illustrations were performed with DS Viewer 6.0 and Discovery Studio 4.1 (Accelrys Software Inc., San Diego, CA)

## CHAPTER 3 ROLE OF C-TERMINAL HISTIDINES IN THE MEMBRANE INSERTION OF THE DIPHTHERIA TOXIN T DOMAIN

### *INTRODUCTION*

Diphtheria toxin, like many other bacterial toxins [42, 134-136], enters the cell via the endosomal pathway of internalization, where a set of environment-induced conformational changes result in the delivery of its active moiety into the cytosol. The toxin is composed of three domains (Fig. 1.4A): the receptor-binding domain (R domain), the translocation domain (T domain) and the catalytic domain (C domain). The general mechanism of toxin's entry is shown in the introductory chapter of this manuscript (Fig. 1.4B), where the attachment of the R domain to its receptor in the plasma membrane induces the endocytosis of the toxin. The acidification of the endosomal lumen in the subsequent step triggers a series of conformational changes in the T domain, which refolds and inserts into the membrane, and translocates the catalytic domain attached to its N-terminus [42, 43]. This chapter focuses on the pH-triggered membrane insertion and refolding of the translocation domain, particularly at the role of three histidine residues of C-terminal location.

The pH-triggered membrane insertion of the T domain occurs through a multistep mechanism [53], with intermediate states populated in solution and in the membrane (Fig. 1.6). The first step is a pH-induced refolding in solution, where a membrane-incompetent state (W-state) is converted into a membrane-competent state ( $W^+$ -state). The second step is the partitioning of the  $W^+$ -state into the membrane interface to form the interfacial state (I-state). The fate of the T domain in the membrane is determined by the lipid composition: a low mole fraction of anionic lipids results in the T domain being kinetically trapped in the I-state, while a high mole fraction

of negatively charged lipids promotes the formation of the final functional transmembrane state (T state, also known as open-channel state or OCS).

The high resolution structure of the W-state (determined in solution at neutral pH [49]) consists of nine alpha helices arranged in a globular fold (Fig. 3.1). Helices TH8 and TH9 (red ribbons) form the central hydrophobic core of the domain, while the remaining helices surround them. High resolution structures for the other states are not yet available through experimental techniques. However, that of the  $W^+$ -state was recently modeled through molecular dynamic simulations and validated with spectroscopic techniques, consisting in a rearrangement of the structure that retains the overall globular fold of the protein (details can be found in reference [50]). For the topography of the T domain in the membrane, multiple studies suggest that helices TH8-TH9 and possibly TH5 become transmembrane [51, 57-59, 97], while the remaining helices take a variety of topologies depending on the intermediate [59, 60, 97, 137]. Therefore, identifying mutations capable of altering the insertion pathway provides not only insights into the nature of acid-induced conformational switching, but also potential for future high-resolution studies of key intermediates.

It has been suggested that the pH-triggered membrane insertion of the T domain is modulated by protonation of the six histidines residues in various stages of the process [43, 67]. Based on their location in the protein, these histidine residues are classified as the N-terminal (H223, H251 and H257) and C-terminal (H322, H323 and H372) cluster of histidines. Protonation of H223 and H257 has been linked to the early stages of the conformational switching, involving the destabilization of the folded structure of the T domain in solution and the formation of the membrane-competent state [50, 52]. The role of the C-terminal cluster of histidines, flanking the

consensus insertion unit TH8-TH9 (Fig. 3.1), is less clear. Based on an approach that combined site-directed mutagenesis and spectroscopic and functional assays, it was demonstrated that the triple replacement of all C-terminal histidines to either arginine or glutamine greatly decreases the translocation and impaired the formation of the OCS [68]. However, the transmembrane insertion of the TH8-TH9 helical hairpin was not affected. This suggests that the transmembrane insertion of the T domain can be uncoupled from the translocation of its N-terminus and formation of an open-channel state.

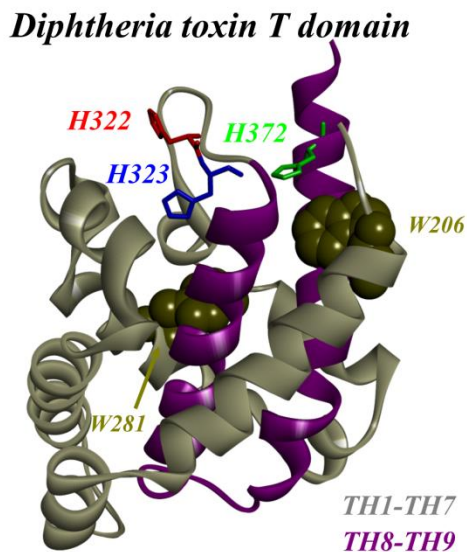


**FIGURE 3.1** Crystal structure of the T domain showing the consensus insertion unit TH8-TH9 and the C-terminal histidines. Histidine residues H322, H323 and H372 are presented red, blue and green sticks, respectively. Tryptophan residues W206 and W281 are shown as dark yellow CPK.

This chapter focuses in the further investigation of the role of the C-terminal histidines in the membrane interactions of the T domain. It specifically addresses two open questions left by the study of Rodnin et al. [68]: 1) why does the replacement of C-terminal histidines result in a loss

of activity despite the apparently normal interactions with the lipid bilayer, and 2) are any of the three histidines more important than the other, or will single and double replacements show a cumulative effect? To answer these questions, we generated a series of mutants that mimic the either protonated or deprotonated state of the residues. We use spectroscopic assays to determine mutation-induced changes along the membrane insertion pathway of the T domain, and functional assays to establish the ability of the mutants to fold into a functional open-channel state.

## *RESULTS*

First, we generated single mutations in the T domain to determine if the protonation of any of these histidines alone is responsible for the loss of function reported in the literature [68]. The residues were replaced by either glutamine or lysine because these residues are neutral or positively charged, respectively, at the pH range tested in this study. Hence, these mutations are expected to mimic the non-protonated and protonated states of histidines. Then, we tested the activity of single mutants by measuring the conductance in planar lipid bilayers<sup>1</sup> as described previously [68, 118, 138]. As shown in Table 3.1 (full set of conductance measurements can be found in reference [124]), the relative activity of the T domain is decreased in all the mutants. However, the mutations of H322 resulted in the most dramatic effect, as the activities of both mutants H322Q and H322K were almost two orders of magnitude lower than that of the WT protein. The effect of substituting H323 and H372 was less pronounced, resulting in relative activities within a factor of four of that of the WT protein. These results suggest that each of the three C-terminal histidines affects the formation of the OCS, but the role of H322 appears to be critical. We then moved on the characterization of membrane interactions of the mutants.

---

<sup>1</sup> Conductance measurements were performed by our collaborators at the Department of Physiology and Biophysics, Albert Einstein College of Medicine, Bronx, New York. We are thankful to Dr. Paul Kienker and Dr. Alan Finkelstein for complementing this study.

T domain mutant	Relative Activity
WT	1
H322K	$0.028 \pm 0.004$
H322Q	$0.011 \pm 0.005$
H323K	$0.38 \pm 0.06$
H323Q	$0.26 \pm 0.04$
H372K	$0.83 \pm 0.09$
H372Q	$0.41 \pm 0.04$
H322,323Q	0.007
H322,323,372Q	0.002

**TABLE 3.1 Relative activities of the C-terminal histidine mutants of the diphtheria toxin T domain.** The values are calculated relative to the total increase of conductance of the WT. For the single replacements, the values correspond to the average and standard deviation of 3 independent assays.

The first step in the membrane insertion pathway of the T domain corresponds to the conformational switching between the W-state and the W<sup>+</sup>-state (Fig. 1.6) [43]. The structural changes have been shown by MD simulations [50], and experimentally through differences in thermodynamic stability [63]. We examined the stability of the WT and mutant proteins by measuring temperature-dependent changes in ellipticity using CD spectroscopy. Data collected at pH 8 and 6 (Fig. 3.2), corresponding to the W and W<sup>+</sup> states, respectively, indicate a very similar behavior for all proteins. Mild acidification results in similar reduction in transition temperature and enthalpy (Table 3.2). No reproducible data, however, could be collected at lower pH as protein aggregation in the denatured state renders thermodynamic analysis impossible [63, 99, 121]. Nevertheless, it is clear that the reason for the loss of functional activity due to histidine replacements is not associated with changes in stability in solution, but is

rather related to altered interactions with the membranes at some point along the insertion pathway.

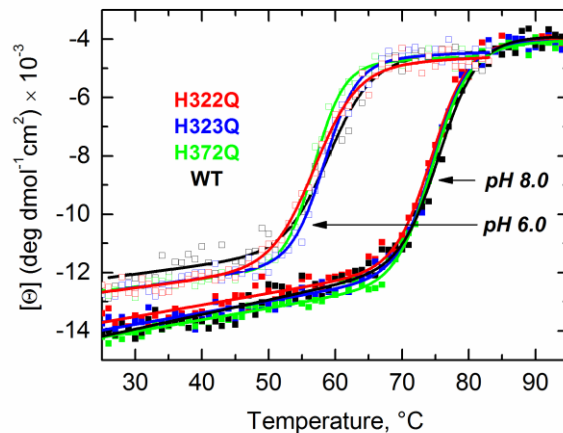


**FIGURE 3.2 Thermal stability of mutants H322Q, H323Q and H372Q at pH 8 and pH 6.**

Data at pH 8 (solid symbols) and pH 6 (open symbols) indicate that replacement of C-terminal histidines does not alter the acid destabilization process in solution. The thermal unfolding was monitored by circular dichroism. The temperature-dependent loss of ellipticity at 222 nm was fitted to a two-state unfolding transition as described in the methods section (thermodynamic parameters are summarized in Table 2.2).

T domain mutant	pH 8		pH 6	
	$\Delta H^\circ$ , kcal/mol	$T_m$ , °C	$\Delta H^\circ$ , kcal/mol	$T_m$ , °C
WT	$95 \pm 7$	$74.6 \pm 0.4$	$78 \pm 6$	$58.4 \pm 0.4$
H322K	$82 \pm 6$	$74.2 \pm 0.3$	$85 \pm 6$	$57.7 \pm 0.2$
H322Q	$84 \pm 5$	$75.4 \pm 0.3$	$74 \pm 7$	$57.4 \pm 0.4$
H323K	$93 \pm 8$	$74.1 \pm 0.1$	$88 \pm 4$	$56.8 \pm 0.6$
H323Q	$82 \pm 5$	$75.2 \pm 0.4$	$85 \pm 5$	$59.2 \pm 0.5$
H372K	$94 \pm 8$	$74.3 \pm 0.3$	$87 \pm 7$	$59.0 \pm 0.3$
H372Q	$87 \pm 4$	$75.1 \pm 0.2$	$90 \pm 8$	$56.9 \pm 0.2$

**TABLE 3.2 Thermodynamic parameters derived from the fitting of thermal unfolding data of mutants of T domain.** Data presented correspond to single C-terminal histidine mutants and WT T domain for soluble state (pH 8) and membrane-competent state (pH 6).

Previously, it was demonstrated that triple substitutions of C-terminal histidines do not prevent efficient insertion of the TH8-TH9 helical hairpin [68] (purple helices in Fig. 3.1), suggesting that they affect proper insertion of the rest of the structure. Here we follow up on this result using intrinsic fluorescence from W206 and W281, located in the N-terminal helices TH1 and TH5, respectively (shown in dark yellow in Fig. 3.1). Representative examples of fluorescence spectra of the WT and mutant H322Q in the presence of large unilamellar vesicles are shown as open symbols in Fig. 3.3. Although the spectra in the membrane-incompetent W-state are superimposable (panel A), there is a pronounced difference when the WT and the mutant interact with the membrane (panel B). Fluorescence spectra were fitted to a log-normal distribution (fits are shown as solid lines) as described in methods. This procedure allows for accurate and reliable measurements of subtle changes in tryptophan spectral position [139].

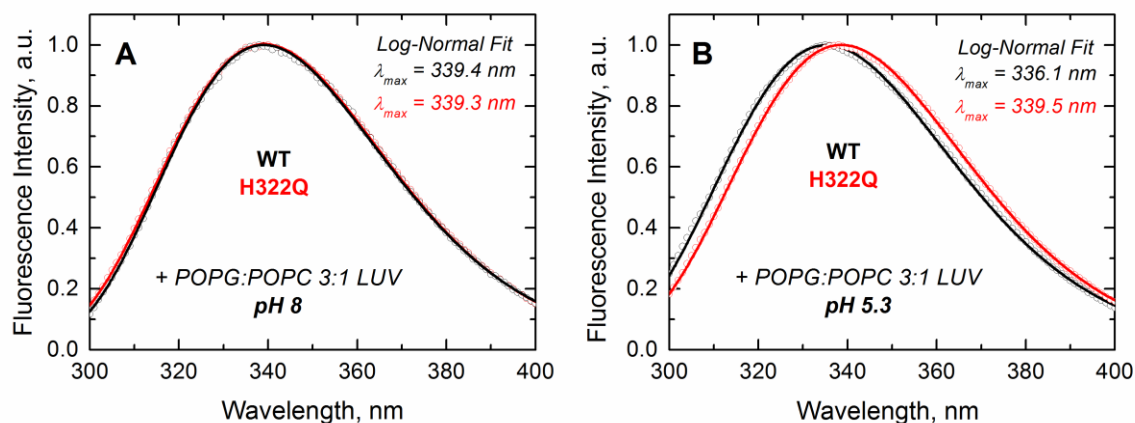


**FIGURE 3.3 Tryptophan spectra of WT and H322Q mutant in the presence of LUV at pH 8 and pH 5.3.** Panels A and B correspond to recordings at pH 8 and 5.3, respectively. All spectra (open symbols) were corrected for background, normalized to maximal intensity for visual comparison of spectral changes and fitted to a log-normal function (lines) [139] to estimate the position of maximum.

The analysis of the position of maximum emission as a function of the pH indicates that mutants of H322, the least active mutants (Table 3.1), experience a pH-dependent red spectral shift in solution (Fig. 3.4A). A red-shift is normally associated with increased exposure of tryptophans to the aqueous phase [52, 139]. The magnitude of the red-shift is similar for the mutants and the WT, complementing our thermal stability CD results and confirming that the mutations do not alter either of the conformations of the T domain in solution. On the other hand, both mutants show a distinct red-shift of emission in the presence of large unilamellar vesicles (LUV) that is not observed for the WT T domain (Fig. 3.4B), suggesting a membrane-induced misfolding of intermediate states on the path toward the OCS. These changes are detected at all lipid compositions that we tested, and appear to be exactly the same for 3:1 mixtures of anionic:neutral lipids, regardless of the substitution of phosphatidylcholine (POPC) with phosphatidylethanolamine (POPE), or phosphatidylglycerol (POPG) with phosphatidylserine (POPS) (Fig. 3.4C). At lower anionic content, the same effect is observed, but the curves are shifted to more acidic pH (Fig. 3.4D). Thus, our results suggest that mutants H322K and H322Q misfold within the membrane regardless of the membrane composition.

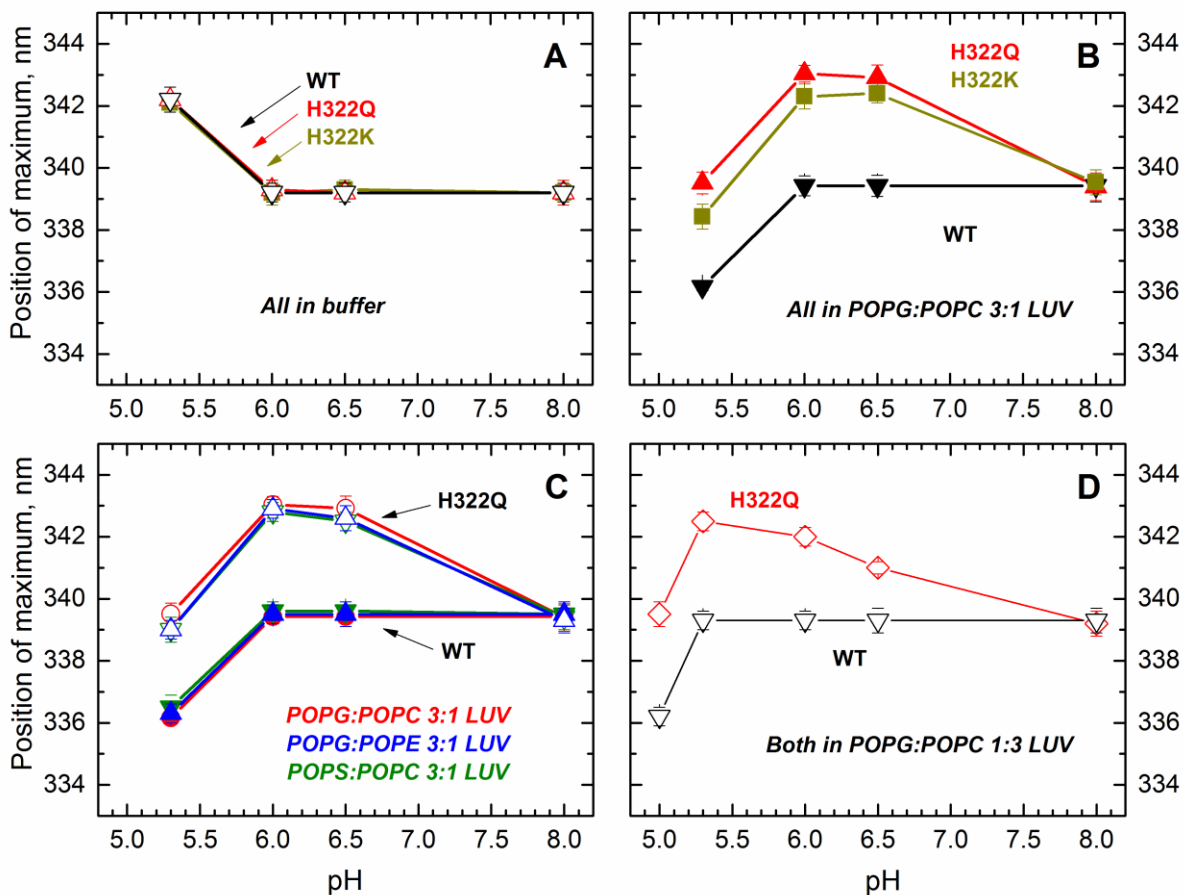


**FIGURE 3.4 Membrane-induced misfolding of T domain's mutants of H322 followed by tryptophan fluorescence.** **A** and **B**) Position of maximum emission as a function of pH for WT and mutants H322Q and H322K in the absence of LUV (**A**), or in the presence of POPG:POPC 3:1 LUV (**B**). Membranes induce a distinct red-shift of tryptophan emission spectra for the mutants at pH 6-6.5. Further acidification induces blue-shift of the spectra for the WT and mutant. **C** and **D**) Position of maximum emission as function of pH for WT and the mutant H322Q in the presence of LUV composed of POPG:POPC 3:1, POPG:POPE 3:1 and POPS:POPC 3:1 (**C**), and POPG:POPC 1:3 (**D**). Membrane-induced misfolding of mutant H322Q is observed regardless of the membrane composition. Error bars represent the standard deviation of at least three independent measurements.

Next, we recorded the tryptophan emission spectra in the presence of LUV for the rest of the mutants, including a double and triple glutamine replacement (Fig. 3.5A). As in the case of the inactive mutant H322Q, most mutants undergo a membrane-induced red shift at pH 6.0-6.5. However, some mutants also undergo a blue-shift under more acidic conditions, which is the characteristic spectral signature of the WT protein. These results suggest that mutants of H323 and H372 (blue and green symbols), but none of the mutants of H322 (red, orange and magenta symbols), partially regain the WT-like spectroscopic signature at pH 5.3. Notably, these results correlate with the electrophysiological measurements of conductance (Table 3.1). Those mutants experiencing a WT-like refolding in the membrane are relatively active in electrophysiological measurements (black box), while those that do not are the least active (red box). We do not discard a blue-shift in the fluorescence spectra of the inactive mutants under even more acidic conditions; however, this will not be physiologically relevant. These results suggest that the membrane-induced misfolding is connected to the open-channel function of the T domain.

To confirm that the inactive mutants indeed adopt a misfolded conformation within the bilayer, we recorded the CD spectra of the T domain WT and the active and inactive mutants in the presence of LUV (POPG:POPC 3:1) at pH 5.3 (Fig. 3.5B). The CD spectra of the membrane-inserted state of the WT protein (black spectrum) and the active mutant H372Q (green spectrum) are identical and exhibit the characteristics of an  $\alpha$ -helical structure, with minima at 222 and 208 nm. In contrast, inactive mutants H322Q (red spectrum), H322,323Q (orange spectrum) and H322,323,372Q (magenta spectrum) showed CD spectra with loss of ellipticity and atypical changes in shape. These changes have been previously associated with misfolding and aggregation of membrane proteins [140, 141], suggesting that mutants of H322 do not fold into a WT-like structure in the membrane. The relatively active mutant, H323Q (blue spectrum), does

not follow this pattern; it has a similar CD spectrum to that of the inactive mutant H322Q. Fluorescence data indicate that H323Q is strongly misfolded at the intermediate pH of 6.0, yet inserts like the WT at pH 5.3. The likely reason why it cannot regain a proper fold under the conditions of the CD experiment is that the latter requires much higher concentrations than those used in fluorescence or conductance measurements. Indeed, when the concentration of this mutant in the tryptophan fluorescence assay was increased, the spectrum no longer returned to the WT position (data not shown).

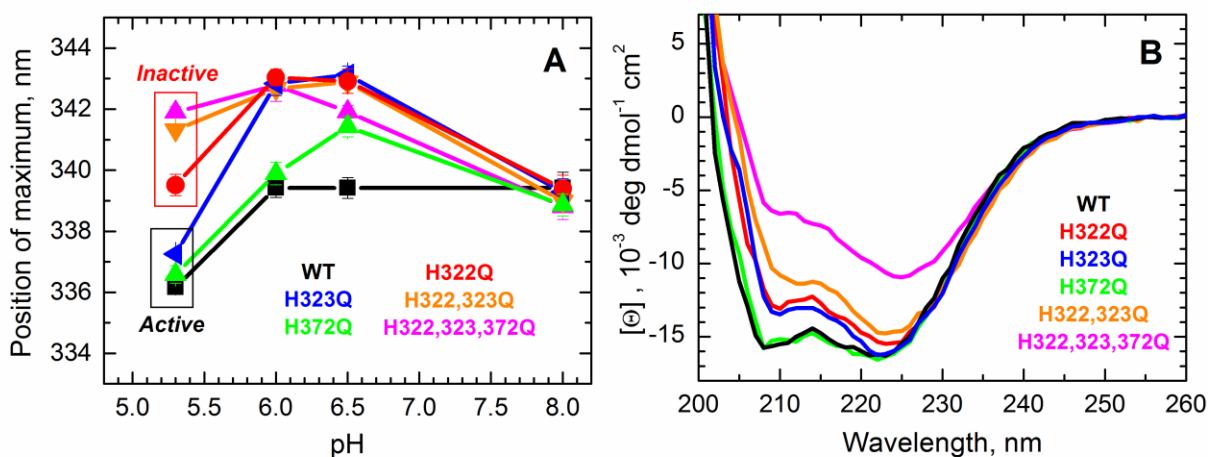


**FIGURE 3.5 Membrane-induced misfolding of C-terminal histidine mutants correlates with loss of function.** **A)** Position of maximum emission as function of the pH for mutants carrying histidine-to-glutamine mutations. Mutants experiencing a WT-like spectral blue-shift at pH 5.3 (reference is spectrum at pH 8) are active in electrophysiology measurements (Table 3.1). Data for active and inactive mutants are shown in a black or red box, respectively. The error bars represent the standard deviation of three independent measurements. **B)** CD spectra of T domain WT and active and inactive mutants at pH 5.3 in the presence of LUV. The inactive mutants show atypical CD spectral shape and decreased ellipticity.

## *DISCUSSION*

Previous studies have demonstrated that histidine protonation plays a role in the pH-triggered membrane insertion of the diphtheria toxin T domain [50, 52, 67, 68]. In the case of the C-terminal cluster of histidines (H322, H323 and H372), the triple replacement to arginine or glutamine was shown to cause loss of translocation activity and channel formation [68]. However, there were no apparent changes in the membrane interactions of those triple mutants, as judged by the unaffected transmembrane insertion of TH8-TH9, suggesting that the membrane action of the T domain is uncoupled from the transmembrane insertion of the helical hairpin. Here, we have answered two immediate questions regarding the role of this cluster of histidines on the membrane action of the T domain. First, we determined that protonation of the three histidines modulate the activity of the T domain, but H322 appears to be the most crucial. Second, we found that the loss of activity of T domain correlates with misfolding within the membrane of the N-terminal helices, rather than TH8-TH9. This type of conformational switching is clearly different from that occurring in solution and involving the protonation of N-terminal histidines [50, 52], which is required for the formation of a membrane competent state.

We illustrate our findings in the scheme of Fig. 3.6, which summarizes the membrane insertion pathway of the T domain WT (upper panel) and the mutants carrying substitutions of the C-terminal histidines (lower panel). Upon initial formation of the membrane-competent state and binding to the membrane (omitted in the scheme for simplicity), the process continues through the insertion of TH8-TH9 into the bilayer and the subsequent refolding of the rest of the protein until reaching the open-channel state [53]. In the case of the WT protein, we propose that the C-terminal histidines are involved in guiding the conformation of the N-terminal helices through

productive folding intermediate states towards the OCS. The WT protein also shows a characteristic closing of the channels by the N-terminal His-tag when a negative potential is applied [51]. Since the mutants show the same behavior [124], including the least active mutants, it is likely that the loss of function is associated with reduction in the number of channels rather than in the properties of the channels. Thus, when C-terminal histidines are replaced, the protein still undergoes a proper pH-dependent destabilization in solution (Fig. 3.2), binds to membranes and inserts a TH8-TH9 helical hairpin [68]. Histidine replacement, however, leads to the formation of an intermediate that is not productive for formation of open-channels. This non-productive intermediate is characterized by greater exposure of W206 (TH1) or W281 (TH5) to the aqueous phase at pH values of ~6-6.5, manifesting itself in red-shifted fluorescence spectra (Figs. 3.4 and 3.5), which then aggregates in the interface. Previously we demonstrated that non-inserted intermediates of another protein that undergoes pH-dependent membrane insertion, annexin B12, are prone to aggregation on the interfaces [126, 142].

There is no high resolution structure of the OCS available (or that of any membrane-associated intermediate). Electrophysiological data, however, are consistent with helices TH8, TH9 and TH5 adopting a transmembrane conformation [51], where proper folding of TH5 is required for channel formation. We hypothesize that protonation of C-terminal histidines regulate the membrane interactions leading to proper folding of helix TH5. Since W281 is located in the middle TH5, its abnormal membrane penetration would explain the red-shift observed in Figs. 3.4 and 3.5 for the inactive mutants. This abnormal folding of TH5 has indeed been observed using quenchers attached to the acyl chains of membrane lipids: W281 penetration was shallow upon triple replacement of the C-terminal histidines (C.Ghatak, M.V.Rodnin and A.S.Ladokhin, unpublished data).

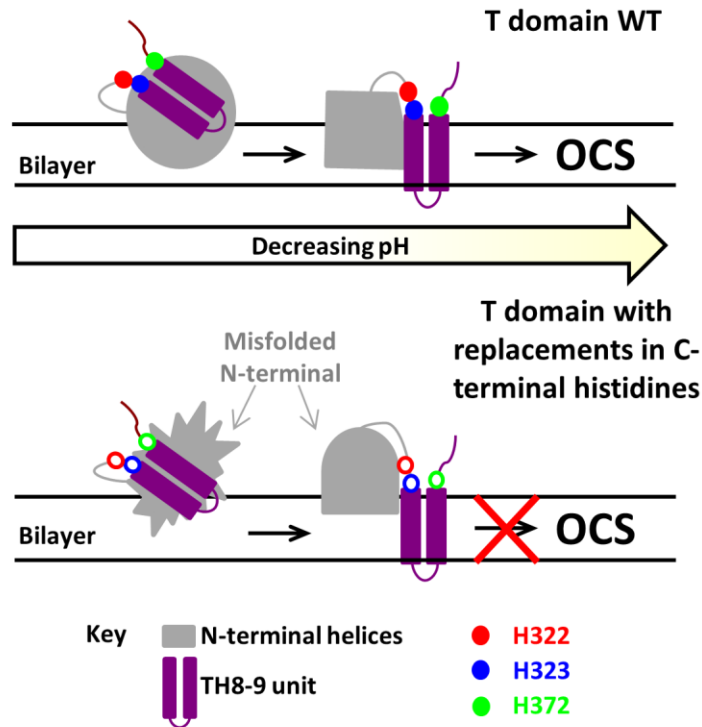


**FIGURE 3.6 Model of the role of the C-terminal histidines in the refolding process of the T domain within the bilayer.** **Top (WT):** Upon initial destabilization of the protein and association with the lipid bilayer, the N-terminal region of the protein adopts a conformation that leads to the insertion of the TH8-TH9 unit into the bilayer. The N-terminal region refolds to form the OCS. **Bottom (mutants with C-terminal histidine replacements):** Membrane interaction of these mutants results in a different membrane conformation from that of the WT, specifically in the more exposed N-terminal helices. While the insertion of TH8-TH9 is not compromised [68], replacement of C-terminal histidines, especially that of H322, affects the efficient folding of the T domain into the OCS.

The replacement of H322 appears to be particularly damaging, with mutants H322Q and H322K showing the least channel activity (Table 3.1) and also misfolding on the membrane

(Figs. 3.4 and 3.5). Interestingly, the replacement of H322 with the charged lysine or neutral glutamine has a similar effect on the folding pathway (Fig. 3.4). This is different from replacements of another critical residue, H257, involved in destabilization of the folded structure in solution [52]: while replacement with a charged residue promoted unfolding, replacement with a neutral residue slowed it down. Thus, we propose that the C-terminal histidines play a crucial role in guiding the folding of the N-terminal region into the OCS, where the residue H322 would have particular importance that likely goes beyond its mere protonation. It is possible that the changes in protonation of the C-terminal histidines are required to occur on a very specific step or multiple protonation/deprotonation cycles may take place.

## MATERIALS AND METHODS

*Materials:* POPC, POPG, POPS and POPE were purchased from Avanti Polar Lipids (Alabaster, AL). Diphtheria toxin T domain (amino acids 202-378) was cloned into NdeI-EcoRI-treated pET15b vector containing an N-terminal 6xHis-tag and a thrombin cleavage site. Both the mutants and the WT protein were expressed and purified as described in [121]. Briefly, BL-DE23pLysE E.coli cells were transformed with the plasmid and grown to OD<sub>600nm</sub> ~ 0.6, after which expression was induced by addition of 0.8M IPTG and the cells grown for an additional 16 hours at 24°C. Cells were pelleted by centrifugation, lysed by sonication and clarified by centrifugation for 30 min at 4000 rpm and 4°C. The proteins were then incubated with Ni-NTA beads, washed with washing buffer (50mM Tris-HCl, 300mM NaCl, 5mM imidazole, pH 8) and eluted with 0.5M imidazole in the same buffer. The eluted proteins were subjected to size-exclusion chromatography on a Sepharose12 1x30cm column in 50mM phosphate buffer at pH 8, and quantified by measuring their absorbance spectra in the range 200-350 nm (we used molar extinction coefficient of 17000 M<sup>-1</sup>cm<sup>-1</sup> at 280 nm).

*Conductance assays in planar bilayers:* The current response was measured under voltage-clamp conditions in planar phospholipid bilayers separating two compartments: the *cis* compartment with acidic buffer into which the proteins were injected from a stock solution and the *trans* compartment with neutral buffer, as previously described [118]. Asolectin planar bilayers were formed and voltage-clamp recordings were performed as previously described [138]. The voltage is defined as the potential of the *cis* compartment, relative to that of the opposite *trans* compartment. Both aqueous solutions contained 1 M KCl, 2 mM CaCl<sub>2</sub>, and 1

mM EDTA; in addition, the *cis* compartment contained 20 mM malic acid, pH 5.3, and the *trans* compartment contained 20 mM HEPES, pH 7.2.

*LUV preparation:* Large unilamellar vesicles (LUV) of 0.1  $\mu\text{m}$  diameter were prepared by extrusion as previously described [130, 131]. The vesicles were composed of molar mixtures of POPG:POPC 3:1, POPG:POPC 1:3, POPG:POPE 3:1, and POPS:POPC 3:1.

*Tryptophan fluorescence measurements:* Fluorescence was measured using a SPEX Fluorolog FL3-22 steady-state fluorescence spectrometer (Jobin Yvon, Edison, NJ) equipped with double-grating. The measurements were made at 25°C in 2x10 mm cuvettes oriented perpendicular to the excitation beam. Tryptophan residues were excited at 280 nm and the emission spectra were recorded between 290-500 nm using excitation and emission spectral slits of 2 and 4 nm, respectively. Normally, we added purified T domain WT or mutant from a concentrated stock to 50 mM of sodium phosphate buffer at pH 8.0. We mixed the sample with LUV to reach final concentrations of 1  $\mu\text{M}$  and 1 mM of T domain and LUV, respectively, and rapid acidification was achieved by addition of small amounts of concentrated acetic buffer. We recorded at least 5 scans after an incubation time of 30 min to assure the equilibration of the sample. All spectra were corrected for background and fitted to a log-normal distribution as described in [139] with the following equations to determine the position of maximum of emission:

$$\text{For } \lambda > \lambda_{\max} - \frac{\rho\Gamma}{\rho^2 - 1},$$

$$I(\lambda) = I_0 \exp\left[\frac{\ln 2}{\ln^2 \rho} \ln^2\left(1 + \frac{(\lambda - \lambda_{\max})(\rho^2 - 1)}{\rho\Gamma}\right)\right],$$

$$\text{while for } \lambda < \lambda_{max} - \frac{\rho\Gamma}{\rho^2 - 1}, \quad I(\lambda) = 0, \quad (\text{Eq. 3.1})$$

where  $I_0$  is the intensity observed at the wavelength of maximum intensity  $\lambda_{max}$ , and  $\Gamma$  is the full width of the spectrum at half-maximum intensity. The asymmetry of the distribution is described by the parameter  $\rho$ . Normally, positions of maximum for 3 to 6 samples were averaged.

*CD measurements and analysis of thermal unfolding:* CD measurements were performed using an upgraded Jasco-720 spectropolarimeter (Japan Spectroscopic Company, Tokyo). Normally, 100 scans were recorded between 190 and 260 nm with a 1 nm step at 25°C, using a 1 mm optical path cuvette. The sample contained 4  $\mu\text{M}$  of T domain, either WT or mutant, and 1 mM of LUV in 50 mM phosphate buffer at pH 8.0. The rapid acidification was reached as described in the fluorescence experiments. All spectra were corrected for background; however, only the data collected at wavelengths longer than 200 nm, where effects of scattering are negligible [143], were presented.

For the thermal unfolding measurements, the ellipticity was measured at 222 nm with a 1 degree/minute scan rate. The analysis of thermal stability, yielding transition temperature  $T_m$  and transition enthalpy  $\Delta H^\circ$ , was performed by fitting the data to a two-state transition as previously described [68, 121] with the following equations [144]:

$$Y = (Y_N + m_N T) X_N + (Y_U + m_U T) (1 - X_N) \quad (\text{Eq. 3.2})$$

$$X_N = 1 / [1 + \exp(-\Delta H^\circ (1 - T / T_m) / RT)] \quad (\text{Eq. 3.3})$$

where  $Y$  is the experimentally observed CD signal at a given temperature,  $Y_N$  and  $Y_U$  represent the signals of the pure native and unfolded state at 0K, and  $m_N$  and  $m_U$  are the temperature-dependencies of these CD signals for the native and unfolded states, respectively, and  $X_N$  is the fraction of the native state at temperature  $T$ .

*Software for data analysis:* Data analysis, fittings and figure preparation were performed with commercial software packages OriginPro versions 8.5 and higher (OriginLab Corporation, Northampton, MA). Structural visualization and preparation of figures were performed with DS Viewer 6.0 and Discovery Studio 4.1 (Accelrys Software Inc., San Diego, CA).

## CHAPTER 4 REGULATION OF THE MEMBRANE INTERACTIONS OF BCL-XL BY LIPIDS

### INTRODUCTION

The Bcl-2 family of proteins control the mitochondrial outer membrane permeabilization (MOMP) during apoptosis [47]. The process is considered as the point of no return in cell death because it irreversibly releases mitochondrial proteins (*e.g.* cytochrome C and SMACs) into the cytosol, activating a cascade of caspases that execute apoptosis [71, 73]. The Bcl-2 family of proteins are subdivided into three classes [74]: the pro-apoptotic (*e.g.* Bax, Bak), which promote MOMP; the anti-apoptotic (*e.g.* Bcl-xL, Bcl-2), which prevents MOMP; and the BH3-only (*e.g.* Bid, Bim), which either inhibit anti-apoptotic members or activate pro-apoptotic members. The mode of action of the Bcl-2 family of proteins is a matter of active debate, and the molecular mechanism is not clearly understood. The current models acknowledge that the mitochondrial outer membrane is a critical platform for Bcl-2 proteins' action [75, 76, 81, 145], however the role of specific lipids and properties of the membrane itself have not been characterized. Here, we test the effect of various lipids of biological relevance on the membrane interactions of the anti-apoptotic protein Bcl-xL.

*In vivo*, Bcl-xL exists in at least two forms: soluble in the aqueous environment of the cytosol, and bound to the mitochondrial outer membrane. It is suggested that the dynamic exchange between these two forms (*i.e.* membrane association and dissociation) is part of the mechanism of action of Bcl-xL [77, 78, 80, 83, 146]. The high resolution structure of the water-soluble conformation is known [66], and consists of globular arrangement of  $\alpha$ -helices, with helices  $\alpha$ 5- $\alpha$ 6 at the hydrophobic core (colored in red in Fig. 4.1). In contrast, the high resolution structure

of the membrane-bound state of Bcl-xL is unknown, but it is suggested that helices  $\alpha 5$ ,  $\alpha 6$  and the TM helix adopt a transmembrane topology [85]. *In vitro*, the membrane association of Bcl-xL can be triggered by low pH [65, 84, 88, 90, 109], although it is not clear how acidification contributes to the process *in vivo*. In chapter 2 and reference [109], we described the general features of the pH-triggered membrane insertion pathway of Bcl-xL, which consists of an initial membrane binding step followed by a refolding/insertion step (Fig. 4.1).

### *Membrane insertion pathway of Bcl-xL*

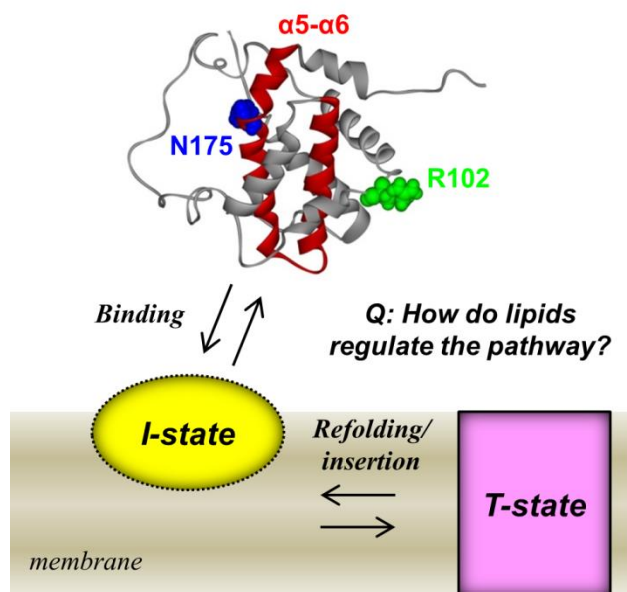
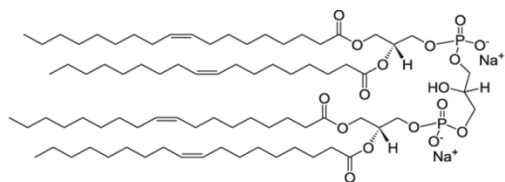


**FIGURE 4.1 pH-triggered membrane insertion pathway of Bcl-xL** [109]. Figure displays the NMR structure of Bcl-xL (PDB 1LXL) in solution at neutral pH [66] and its pH-triggered membrane insertion pathway. Helices  $\alpha 5$  and  $\alpha 6$ , suggested to span the lipid bilayer, are colored in red. Residues R102 and N175 were replaced to cysteine for specific labeling with Alexa488 and NBD, respectively. We suggest that both binding and insertion of the protein into the membrane are regulated by lipids.

There is emerging evidence emphasizing the role of the membrane itself in the action of the Bcl-2 family of proteins, MOMP and apoptosis [84, 88, 90, 100-111]. For example, cardiolipin, a phospholipid that is generally found in the mitochondrial membrane [8] and depleted during apoptosis [104], is required for the membrane interactions of Bid, Bax and Bcl-xL [83, 84, 103, 115]. Our research group and others have shown that the membrane interactions of Bcl-xL can also be regulated by the mole fraction of phosphatidylglycerol [88, 90, 109]. Interestingly, cardiolipin and phosphatidylglycerol have a common chemical and physical property: the headgroup is negatively charged at pH values higher than 3.5 [112, 113]. It can then be hypothesized that Bcl-xL is regulated by a negatively charged membrane interface rather than distinct properties of cardiolipin or phosphatidylglycerol. However, phosphatidylglycerol is also a precursor of cardiolipin during cardiolipin biosynthesis [8], and they might share some additional chemical or physical properties sensed by Bcl-2 proteins. To distinguish between these alternatives, and determine the role of other lipids of biological relevance, it is necessary to characterize the role of membrane lipids on the membrane interactions of Bcl-2 proteins at the biophysical level.

Here, we determine the effect of membrane lipids on the binding and insertion of Bcl-xL into the membrane using an array of fluorescence-based assays. We tested the anionic lipids cardiolipin, phosphatidylglycerol, phosphatidylserine and phosphatidic acid; and the non-bilayer forming lipids phosphatidylethanolamine and lysophosphatidylcholine (Fig. 4.2). These lipids are regularly found in different proportions in mitochondrial membranes [147], some of them varying their mole fractions during apoptosis [104], or inducing mechanical changes in bilayers that are important for biological processes [148-150].

### ***Negatively charged lipids***

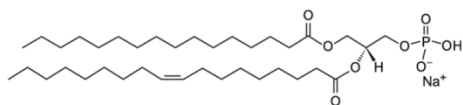


#### **Cardiolipin (TOCL)**

Net charge: -2

Abundance in mitochondria: 10-25%

*Decreases during apoptosis*

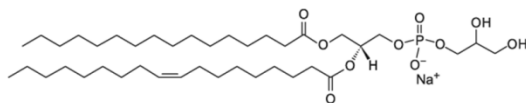


#### **Phosphatidic acid (POPA)**

Net charge: -1

Abundance in mitochondria: 0-5%

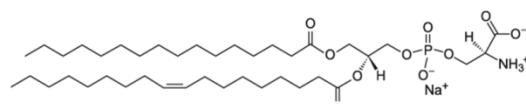
*Increases during apoptosis*



#### **Phosphatidylglycerol (POPG)**

Net charge: -1

Abundance in mitochondria: 0-10%

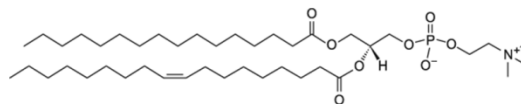


#### **Phosphatidylserine (POPS)**

Net charge: -1

Abundance in mitochondria: 0-15%

### ***Zwitterionic lipids***

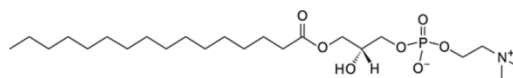


#### **Phosphatidylcholine (POPC)**

Net charge: 0

Abundance in mitochondria: 40-50%

*Used as matrix lipid*



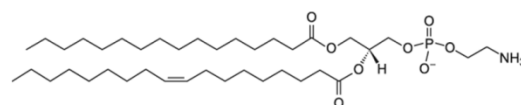
#### **Lysophosphatidylcholine (LysoPC)**

Net charge: 0

Abundance in mitochondria: 0-5%

*Induces positive curvature*

*Increases during apoptosis*



#### **Phosphatidylethanolamine (POPE)**

Net charge: 0

Abundance in mitochondria: 20-35%

*Induces negative curvature*

**FIGURE 4.2 Structure and properties of membrane lipids used in this study.** Negatively charged lipids and zwitterionic lipids are on the left and right columns, respectively, with abbreviations in parenthesis. The net charge and relative abundance of each lipid are indicated below each structure [147, 151]. Changes in relative abundance during apoptosis are indicated for TOCL, POPA, POPC and LysoPC [104]. The abundance of the remaining lipids is either unknown (POPG and POPE) or unchanged (POPS). LysoPC and POPE induce positive and negative curvature stress, respectively.

## RESULTS

### *Effect of anionic lipids on membrane binding*

The pH-triggered membrane insertion pathway of Bcl-xL consists of a membrane binding and a membrane insertion/refolding step [109]. We first tested the effect of lipids on the membrane binding step, starting with cardiolipin because of its suggested relevance in regulating MOMP and apoptosis [103, 115]. We monitored the membrane binding transition using the binding assay described in Chapter 2 and references [53, 109], where we follow the fluorescence changes associated with FRET between donor-labeled protein and acceptor-labeled LUV (we used Alexa488/Rhodamine as donor/acceptor pair). In Fig. 4.3, we show a set of pH titrations for the binding of Bcl-xL to LUV composed of various mole fractions of 1,1,2,2-tetraoleoyl-cardiolipin (hereafter referred as cardiolipin or TOCL) in a POPC matrix. For clarity, we normalized the FRET signal, where 100% represents the maximum change in intensity recorded in a set of experiments. The results show that the binding isotherms are dependent on the mole fraction of TOCL. We fitted the data to estimate the  $pK_a$  and the cooperativity  $n$  of the process with Eq. 4.1 [133]. This analysis indicates that the  $pK_a$  of membrane binding of Bcl-xL shifts toward lower values upon reduction of the mole fraction of cardiolipin.

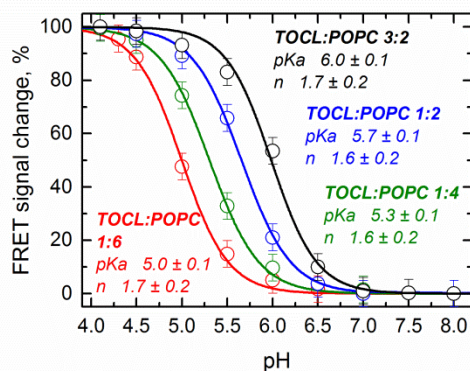


**FIGURE 4.3 pH-dependence of binding of Bcl-xL to LUV composed of various mole fractions of cardiolipin (TOCL) and phosphatidylcholine (POPC).** Process was monitored by FRET between Bcl-xL/Alexa488 and LUV/Rhodamine-PE, where 100% represents the maximum signal change in a set of experiments.  $pK_a$  and  $n$  were determined by fitting the data with Eq. 4.1. Results indicate that membrane binding of Bcl-xL depends on the mole fraction of cardiolipin.

Previously, we reported that the membrane binding of Bcl-xL also depends on the mole fraction of phosphatidylglycerol [109] (See Chapter 2). Both phosphatidylglycerol and cardiolipin have a negatively charged headgroup at pH values higher than 3.5 [112, 113], suggesting that Bcl-xL is responsive to a negatively charged membrane interface. Alternatively, both lipids may share a common property that is sensed by Bcl-xL because phosphatidylglycerol is precursor in the biosynthesis of cardiolipin [8]. To distinguish between both possibilities, we performed pH titrations for the binding of Bcl-xL to LUV composed of other anionic lipids. The results are summarized in Table 4.1, where we show the  $pK_a$  and  $n$  values for the binding of Bcl-xL to LUV whose lipid composition consists of various mole fractions of phosphatidylserine (POPS), phosphatidic acid (POPA), cardiolipin (TOCL) or phosphatidylglycerol (POPG) in a POPC matrix. These results indicate that the  $pK_a$  of membrane binding depends on the mole fraction of anionic lipids in all the cases. Thus, it is likely that Bcl-xL senses the charge density at the membrane surface rather than a property unique to cardiolipin and phosphatidylglycerol.

<b>Lipids mole fraction</b>	<b><math>pK_a</math> (<math>\pm 0.1</math>)</b>	<b><math>n</math> (<math>\pm 0.2</math>)</b>
TOCL:POPC 3:2	6.0	1.7
TOCL:POPC 1:2	5.7	1.6
TOCL:POPC 1:4	5.3	1.6
TOCL:POPC 1:6	5.0	1.7
POPG:POPC 3:1	6.0	1.6
POPG:POPC 1:3	5.0	1.5
POPS:POPC 3:1	5.9	1.4
POPS:POPC 1:1	5.7	1.5
POPS:POPC 1:3	5.1	1.5
POPA:POPC 3:1	5.9	1.3
POPA:POPC 1:1	5.6	1.4
POPA:POPC 1:3	5.0	1.4

**TABLE 4.1 pH-dependent binding parameters of Bcl-xL to LUV of various lipid compositions.**  $pK_a$  and cooperativity  $n$  was estimated fitting the FRET binding data with Eq. 4.1. Lipid compositions are expressed as the mole fractions.

To verify that the membrane binding of Bcl-xL depends on the charge density at the membrane interface, we tested the effect of ionic strength on the membrane binding of Bcl-xL. The theory of the electrical double layer predicts that counterions are attracted to a charged surface and modulate the effective electrostatic potential [152]. Fig. 4.4A shows that the  $pK_a$  of binding is indeed modulated by the ionic strength, as it shifts toward lower values upon addition of NaCl. Because membrane is promoted by increasing mole fractions of anionic lipids and hindered by increasing ionic strength, we conclude that electrostatic interactions modulate the membrane interactions of Bcl-xL.

In order to quantitatively characterize these interactions, we calculated the electrostatic surface potential ( $\psi_0$ ) using the Gouy-Chapman equation (Eqs. 4.3 and 4.4), which describes  $\psi_0$  as function of the charge per area of lipid and ionic strength [152]. Despite being a theoretical approximation, this equation predicts experimental measurements with remarkably agreement

[152-154]. We plotted the  $pK_a$  of membrane binding modulated by both methods as function of  $\psi_0$  (Fig. 4.4B), and found that both variables are linearly correlated. We applied linear fitting with Eq. 4.5 and free fitting parameters for the binding of Bcl-xL to the different membrane systems (only that of cardiolipin-containing LUV is shown in the figure). According this equation the slope ( $0.019 \text{ mV}^{-1}$ ) describes the dependence of the apparent  $pK$  value ( $pK_a$ ) on the membrane surface potential, while the intercept (3.8) corresponds to the intrinsic  $pK$  value ( $pK_i$ ). The fact that the rest of the data fall within the same linear fit, regardless of the mode of modulation of the membrane surface potential, demonstrates that the partitioning of Bcl-xL to the membrane depends on the electrostatic potential at the membrane interface.

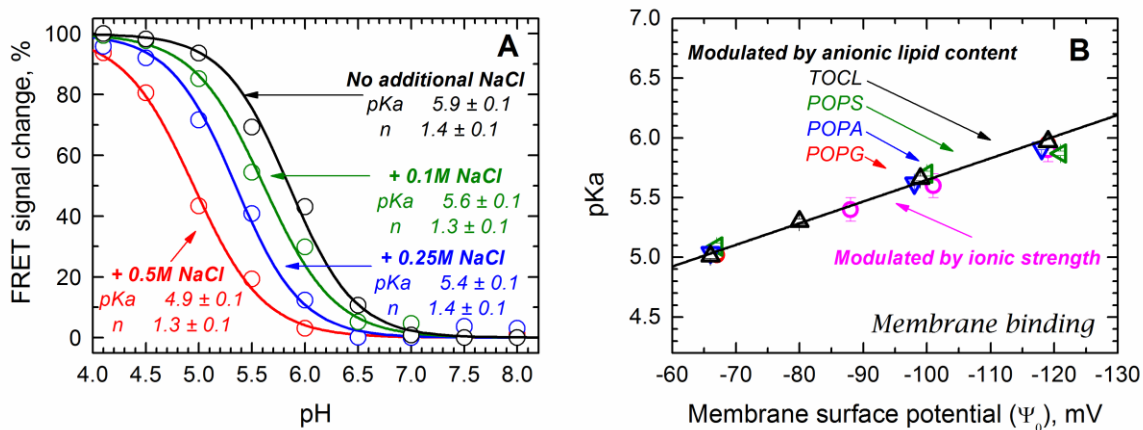


**FIGURE 4.4 Regulation of membrane binding of Bcl-xL by membrane surface potential.**

**A)** pH-titrations for membrane binding of Bcl-xL in the presence of additional NaCl.  $pK$  and cooperativity  $n$  were determined by fitting the data to Eq 4.1. **B)**  $pK_a$  of membrane binding of Bcl-xL as function of the membrane surface potential ( $\psi_0$ ) calculated with Eqs. 4.3 and 4.4. There is a linear correlation between the  $pK_a$  and  $\psi_0$ , regardless of its mode of manipulation.

To complete the thermodynamic characterization, we converted the  $pK_a$  values into apparent free energies of protonation ( $\Delta G_a$ ) using Eq. 4.2. The resulting  $\Delta G_a$  values were plotted against the corresponding membrane surface potential and fitted with Eq. 4.6 with free fitting parameters (Fig. 4.5, black linear fit). Remarkably, the free fitting of the experimental values overlaps with a theoretical fit (red fit) whose slope is fixed in  $0.023 \text{ kcal mol}^{-1}\text{mV}^{-1}$ . According Eq. 4.6, this slope (Faraday constant) corresponds to the ideal modulation of free energy of protonation by the membrane surface potential. Thus, this analysis not only confirms that membrane binding of Bcl-xL depends on the membrane surface potential, but also suggests that it is the main regulatory component for initial membrane association.

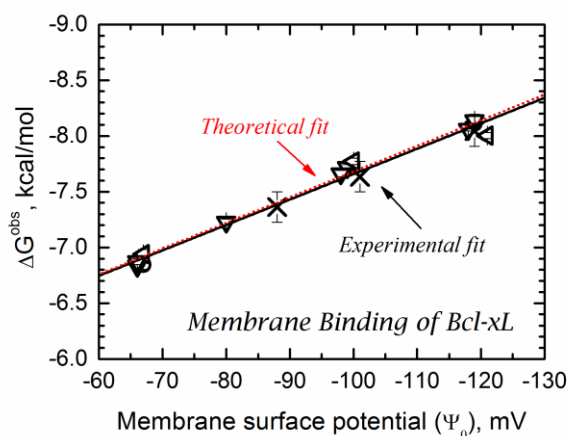


**FIGURE 4.5 Thermodynamics of membrane binding of Bcl-xL to LUV.**  $pK_a$  values were converted into free energies of protonation with Eq. 4.2 and plotted against the membrane surface potential. While the experimental fit has free fitting parameters, the theoretical fit has a fixed slope of  $0.023 \text{ kcal mol}^{-1}\text{mV}^{-1}$ . According to Eq. 4.6, this slope describes the ideal modulation of free energy by the membrane surface potential.

## Effect of anionic lipids on membrane insertion/refolding

Next, we tested the effect of lipids on the membrane insertion/refolding step, where helices  $\alpha 5$  and  $\alpha 6$  are suggested to insert as a hairpin into the lipid bilayer [85, 109]. To monitor the insertion of helix  $\alpha 6$ , we performed site-directed labeling at residue 175 with the environment sensitive probe NBD. In Chapter 2 and reference [109], we showed that membrane insertion of the labeled helix results in blue shift and increase of fluorescence intensity of NBD. In Fig. 4.6A, we show representative pH-titrations for the membrane insertion of Bcl-xL into LUV composed of various mole fractions of cardiolipin. The change in signal, normalized to the maximum change in NBD intensity in a set of experiments, demonstrates that Bcl-xL inserts into cardiolipin-containing LUV. However, as in the case of the membrane binding experiments (Fig.4.2), the membrane insertion depends on the mole fraction of cardiolipin. The fitting analysis with Eq. 4.1 (solid lines) indicates a shift of  $pK_a$  toward lower values as the mole fraction of cardiolipin is decreased. These fitting parameters are comparable to those obtained in the binding experiments under the same conditions (Fig 4.2), suggesting that initial binding and membrane insertion cannot be distinguished by modulating the mole fraction of cardiolipin.

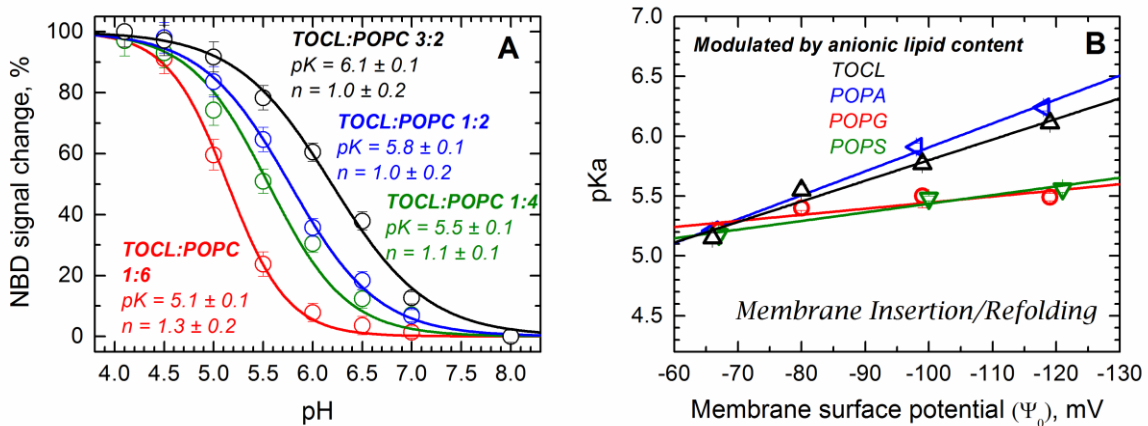


**FIGURE 4.6 Effect of anionic lipids on the insertion/refolding of helices  $\alpha 5$ - $\alpha 6$  into the bilayer monitored through changes in the fluorescence intensity of NBD-labeled Bcl-xL.** **A)** pH-titrations for the insertion/refolding of Bcl-xL into LUV of various mole fractions of cardiolipin (TOCL) and phosphatidylcholine (POPC).  $pK_a$  and cooperativity  $n$  were determined by fitting the data with Eq. 4.1. **B)**  $pK_a$  of membrane insertion/refolding of Bcl-xL plotted as a function of the membrane surface potential ( $\psi_0$ ). There are linear correlations between the  $pK_a$  values and the membrane surface potential, but the slopes are different for each lipid.

On the next step, we characterized the insertion/refolding of Bcl-xL into LUV composed of other anionic lipids (POPG, POPS and POPA). Table 4.2 summarizes the parameters obtained by fitting each of the pH titrations with Eq. 4.1, where it is clear that the  $pK_a$  of membrane insertion was affected by the lipid composition in different degrees. In order to better visualize these effects, we plotted the  $pK_a$  values as function of the membrane surface potential (Figure 4.5B). The data show that the correlation between  $pK_a$  and membrane surface potential is different in all the lipid systems (note the different slopes). This suggests that the membrane insertion/refolding of Bcl-xL is not regulated by the membrane surface potential alone, but there are additional properties playing a role. The further analysis of the data with Eq. 4.5 supports the possibility of differential regulation at the level of the membrane insertion/refolding. While the slopes for the TOCL and POPA lipid systems ( $0.020 \text{ mV}^{-1}$  and  $0.017 \text{ mV}^{-1}$ , respectively) are similar to the slope of the initial binding step ( $0.019 \text{ mV}^{-1}$ ), the slopes for the POPG and POPS systems are clearly different ( $0.005 \text{ mV}^{-1}$  and  $0.007 \text{ mV}^{-1}$ , respectively). This shows that the pH required for membrane insertion of Bcl-xL into membranes made of TOCL or POPA is the same pH required for initial binding. However, if the membrane contains POPG and POPS, Bcl-xL requires a specific pH regardless of that required for membrane binding.

<b>Lipids mole fraction</b>	<b><math>pK_a</math> (<math>\pm 0.1</math>)</b>	<b><math>n</math> (<math>\pm 0.2</math>)</b>
TOCL:POPC 3:2	6.1	1.0
TOCL:POPC 1:2	5.8	1.0
TOCL:POPC 1:4	5.6	1.1
TOCL:POPC 1:6	5.2	1.3
POPG:POPC 3:1	5.5	1.1
POPG:POPC 1:1	5.5	1.1
POPG:POPC 1:2	5.4	1.0
POPG:POPC 1:3	5.2	1.4
POPS:POPC 3:1	5.6	1.1
POPS:POPC 1:1	5.5	1.2
POPS:POPC 1:3	5.2	1.1
POPA:POPC 3:1	6.2	1.3
POPA:POPC 1:1	5.9	1.0
POPA:POPC 1:3	5.2	1.0

**TABLE 4.2 Parameters of pH titrations of insertion/refolding of Bcl-xL into LUV of various lipid compositions.**  $pK_a$  and cooperativity  $n$  was estimated fitting the data of Fig. 4.6 with Eq. 4.1. Lipid compositions are expressed as mole fractions.

#### *Kinetic regulation of the membrane insertion/refolding*

To test if anionic lipids also modulate the rate of membrane insertion/refolding in a lipid-specific manner, we measured the time course of helix  $\alpha_6$  insertion using NBD fluorescence. We used lipid compositions with low membrane surface potential (-67mV) because the insertion of Bcl-xL reached completion within the dead time (~5 seconds) in LUV of high anionic content. Also, we used pH 4.5 to ensure formation of the membrane-inserted state (Fig. 4.6 shows that at pH 4.5, the formation of the transmembrane state is almost complete). Fig. 4.7 displays the time course of membrane insertion/refolding of Bcl-xL into LUV of the various lipid compositions. The rate of insertion appears to be similar in all the cases but when POPS is used. This lipid is reported to have a  $pK_a$  of protonation of about 5, which complicates the analysis because the effective charge is <1. We fitted the data to an empirical exponential association (see methods)

of two components ( $k_1$  and  $k_2$ ) and one fast step ( $k_0 = 0$ ). Although the rate ( $k_i$ ) and time constants ( $\tau_i$ ) show differences (Table 4.3), these are not as dramatic as those observed when varying the mole fraction of POPE (see below). Since  $\tau\alpha$  varies less than 2 folds among the different lipid systems, we conclude that the anionic lipids do not modulate the rate of insertion/refolding of Bcl-xL in a lipid-specific manner.

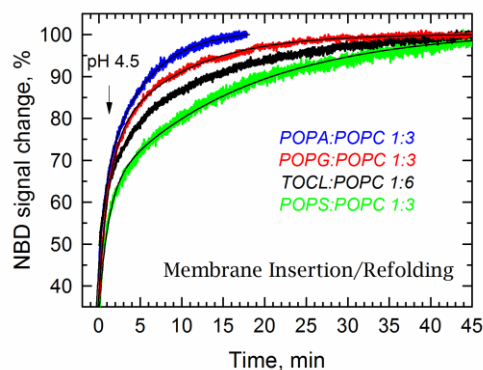


**FIGURE 4.7 Effect of different anionic lipids in the kinetics of insertion/refolding of Bcl-xL into LUV.** The rate of insertion into LUV of low anionic mole fraction was followed by changes in intensity of the environment-sensitive dye NBD selectively attached to a residue in helix  $\alpha_6$  as described in [109]. We chose lipid compositions with anionic lipids of different headgroups but similar membrane surface potential (-67 mV). Solid black lines are fitting curves (see text and methods for details).

Lipid composition	A <sub>0</sub>	A <sub>1</sub>	k <sub>1</sub> , s <sup>-1</sup>	A <sub>2</sub>	k <sub>2</sub> , s <sup>-1</sup>	τ <sub>a</sub> , s
<i>Anionic lipids</i>						
POPG:POPC 1:3	0.37	0.35	1.4 x 10 <sup>-2</sup>	0.28	1.9 x 10 <sup>-3</sup>	1.7 x 10 <sup>2</sup>
TOCL:POPC 1:6	0.51	0.22	0.8 x 10 <sup>-2</sup>	0.27	1.1 x 10 <sup>-3</sup>	2.7 x 10 <sup>2</sup>
POPS:POPC 1:3	0.33	0.29	1.5 x 10 <sup>-2</sup>	0.38	1.0 x 10 <sup>-3</sup>	4.0 x 10 <sup>2</sup>
POPA:POPC 1:3	0.44	0.18	2.1 x 10 <sup>-2</sup>	0.38	3.3 x 10 <sup>-3</sup>	1.3 x 10 <sup>2</sup>
<i>Membrane curvature</i>						
POPE:POPC:POPG 1:2:1	0.36	0.41	1.7 x 10 <sup>-2</sup>	0.23	2.9 x 10 <sup>-3</sup>	1.0 x 10 <sup>2</sup>
POPE:POPG 3:1	0.51	0.35	5.6 x 10 <sup>-2</sup>	0.14	14.3 x 10 <sup>-3</sup>	1.6 x 10 <sup>1</sup>
LysoPC:POPC:POPG 1:2:1	0.33	0.21	1.2 x 10 <sup>-2</sup>	0.46	0.9 x 10 <sup>-3</sup>	5.3 x 10 <sup>2</sup>
<i>Binding</i>						
POPG:POPC 1:3	0.34	0.42	1.2 x 10 <sup>-2</sup>	0.24	1.2 x 10 <sup>-3</sup>	2.4 x 10 <sup>2</sup>
POPG:POPE 1:3	0.94	0.06	14.8 x 10 <sup>-2</sup>	0	-	< 1

**TABLE 4.3 Quantitative analysis of the kinetics of insertion of Bcl-xL into LUV of various lipid compositions.** The kinetic data was fitted to an empirical exponential association (see methods) of two components (k<sub>1</sub> and k<sub>2</sub>) and one fast step (k<sub>0</sub> = 0).

Finally, we tested the effect of the zwitterionic and non-bilayer forming lipid phosphatidylethanolamine (POPE) on the membrane insertion/refolding of Bcl-xL. This lipid, which induces negative curvature stress in biological membranes due to its intrinsic curvature [6, 150], has been reported to act as chaperone for membrane protein folding [148, 149]. In this experiment, we kept a constant mole fraction of POPG as the anionic lipid (as required for membrane binding) and increased the mole fraction of POPE in replacement of POPC. The results (Fig. 4.8) indicate that the rate of insertion becomes faster as the POPE mole fraction increases. This is consistent with POPE chaperoning the refolding of Bcl-xL within the membrane. To determine if POPE effect relates to its intrinsic negative curvature, we replaced a fraction of POPC by lysophosphatidylcholine (LysoPC). In contrast to the case of POPE, LysoPC (dark yellow) slowed down the membrane insertion of Bcl-xL (rate constants presented

in Table 4.3). Our results suggest that membrane curvature modulates the kinetics of membrane insertion/refolding of Bcl-xL.

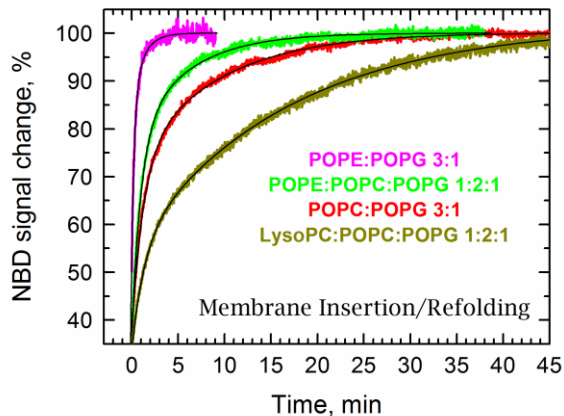


**FIGURE 4.8** Effect of POPE and LysoPC in the insertion of Bcl-xL into the lipid bilayer at pH 4.5. Time-course of insertion of Bcl-xL into LUV composed of 25 mole percent of POPG and various mole fractions of POPC and POPE or LysoPC. POPE and LysoPC cause opposite effects in the insertion kinetics.

## DISCUSSION

In this chapter, we have characterized the effect of various lipids on the membrane interactions of Bcl-xL, an anti-apoptotic member of the Bcl-2 family of proteins. We used a set of fluorescence-based assays to determine how lipids, commonly found in the mitochondrion, modulate the pH-dependence of initial membrane association and refolding of Bcl-xL within the lipid bilayer. Our results suggest that lipids can regulate the membrane interactions of Bcl-xL in multiple ways. The initial membrane association of Bcl-xL is modulated by the membrane surface potential created by any lipid with a negatively-charged headgroup. In contrast to a general electrostatic mechanism, membrane lipids affect the membrane insertion/refolding of Bcl-xL in a lipid-specific manner. In addition, the rate of insertion into the membrane appears to be modulated by the curvature stress induced by non-bilayer forming lipids.

Cardiolipin is suggested to be crucial for the action of the Bcl-2 family of proteins, and multiple biophysical and biochemical studies use this lipid as part of the experimental system to ensure membrane interactions of these proteins [79, 83, 84, 155-157]. However, cardiolipin may be required because of its double negatively charged headgroup or because of some unique property that is important for apoptosis regulation. While we do not rule out that cardiolipin may have unique properties that are important for proper function of the Bcl-2 proteins, our results show that cardiolipin regulates membrane partitioning of Bcl-xL because of its anionic nature (Figs. 4.3-4.5). Indeed, we show that Bcl-xL is responsive to the charge density at the membrane interface, as modulation of the membrane surface potential by changing the mole fractions of other anionic lipids or ionic strength results in a shift on the  $pK_a$  of membrane binding. Our study is in agreement with a previous study that suggested that Bcl-xL association with the

membrane was governed by an electrostatic component [88], although the lipid composition was not explored in that study. This electrostatic component and the effect on the  $pK_a$  of membrane partitioning imply that the role of pH in the membrane partitioning of Bcl-xL depends on the membrane properties, *i.e.* Bcl-xL would partition into the membrane at physiological pH if the interface is negative enough.

For the membrane insertion/refolding of Bcl-xL, our results suggest a different mechanism, where the process appears to be regulated in a lipid specific-manner (Fig. 4.6). While the regulation by cardiolipin and POPA is indistinguishable from that observed in the binding step of Bcl-xL, the dependence of the  $pK_a$  on the membrane surface potential is lost in the case of POPG and POPS. There are three possible explanations for this result: 1) Bcl-xL is trapped in some intermediate state in the presence of POPG or POPS, with the constraint being released upon further acidification; 2) Bcl-xL follows an alternative insertion pathway depending on the lipid composition; or 3) the final transmembrane state has a different topology that is dependent on the lipid composition. Since high resolution structures of Bcl-xL in the membrane are not available, distinguishing between the three alternatives is challenging and requires further structural and functional research. Nonetheless, lipids regulate the final refolding within the membrane in a lipid-specific fashion. It is possible that the size of the headgroup is involved in this regulation. Cardiolipin and POPA have smaller headgroups because, in contrast to POPG and POPS, they do not have a functional group attached to the phosphate group (Fig. 4.2). While the pH-dependence on the surface potential is similar for cardiolipin and POPA, at both membrane binding and insertion events, the membrane insertion into LUV containing POPG or POPS appears to lose pH-dependence on the surface potential.

Interestingly, our experiments with non-bilayer forming lipids show regulation of the membrane interactions of Bcl-xL at the kinetic level (Fig. 4.8). POPE and LysoPC caused opposite effects on the rate of membrane insertion of Bcl-xL without affecting the total magnitude of the change, suggesting that properties at the equilibrium remain the same. While POPE increased the rate of the insertion, LysoPC decreased it. This result correlates with the properties of POPE and LysoPC, which are lipids with opposite intrinsic curvature [150]. Thus, it is possible that the presence of curvature stress at the surface of the membrane controls an energetic barrier that Bcl-xL has to overcome in order adopt its final topology. Previous studies have shown that POPE can act as a chaperone to ensure proper folding of membrane proteins [149, 158, 159].

Previous studies have shown that the Bcl-2 family of proteins plays a regulatory role in apoptosis because they control the permeabilization of the mitochondrial outer membrane, a process that irreversibly leads to cell death [47, 71, 73]. The Embedded Together Model of apoptotic regulation suggests that MOMP can be modulated at four levels: 1) protein-protein interactions in the cytosol, 2) partition of Bcl-2 proteins into the mitochondrial outer membrane, 3) protein-protein interactions at the mitochondrial membrane, and 4) pore formation leading to cell death [82]. Although there is much debate on the exact mechanisms of interaction and regulation of Bcl-2 proteins [75, 76], it is clear that the membrane environment is playing a central role. However, the few studies that address the role of the mitochondrial membrane in apoptosis focus mainly in the levels 3 and 4, *i.e.* protein-protein interactions leading to or preventing cell death (*e.g.* membrane modulating the dissociation constants [84]). Our results provide evidence that the partitioning and refolding of Bcl-xL into the membrane can also be regulated by the properties of the lipid bilayer. Interestingly, recent research has shown that the

lipid composition of the mitochondrial membrane varies before, during and after apoptosis [104]. Thus, regulating the lipid composition may be a mode of controlling the action of Bcl-2 proteins in the cell. Furthermore, our study provides basis for subsequent studies of bilayer modulated protein-protein interactions in apoptotic regulation.

Taken together our results indicate that lipids can modulate the membrane interactions of Bcl-xL in multiple ways, providing an additional regulatory mechanism that ensures proper control of a complex cascade of apoptotic reactions leading to cell death or survival. It will be of interest to test if this holds true for other members of the Bcl-2 family, or if pro- and anti-apoptotic proteins are regulated by the membrane in a different fashion. The latter is also extensive to other proteins that undergo spontaneous membrane insertion (*e.g.* bacterial toxins, antimicrobial peptides), either in a pH-dependent fashion or not, to determine if the lipid composition is a universal mode of regulation for the action of proteins in biological membranes.

## MATERIALS AND METHODS

*Materials:* Palmitoyl-oleoyl-phosphatidylcholine (POPC), palmitoyl-oleoyl-phosphatidylglycerol (POPG), palmitoyl-oleoyl-phosphatidylserine (POPS), palmitoyl-oleoyl-phosphatidic acid (POPA), palmitoyl-oleoyl-phosphatidylethanolamine (POPE), 1,1,2,2-tetraoleoyl-cardiolipin (TOCL), cholesterol (Cho), Lyso-phosphatidylcholine (LysoPC) and Rhodamine-PE were purchased from Avanti Polar Lipids (Alabaster, AL). IANBD-ester and AlexaFluor488-maleimide were obtained from Invitrogen (Carlsbad, CA). Bcl-xL (lacking the C-terminal TM helix and carrying an N-terminal His-tag for purification) mutants C151S/R102C and C151S/N175C were expressed and purified as previously described [109]. Labeling with fluorescent dyes was performed using a standard procedure for thiol-reactive derivatives [109, 129] and the unreacted dye was removed by gel filtration chromatography.

*LUV preparation:* Large unilamellar vesicles containing molar mixtures of POPG:POPC, TOCL:POPC, POPS:POPC, POPA:POPC, POPG:POPE, POPG:POPC:Cho, and POPG:POPC:LysoPC of 0.1  $\mu\text{m}$  diameter were prepared by extrusion as previously described [130, 131]. For the FRET experiments, 2% of Rhodamine-PE was incorporated to the lipid mixture.

*Fluorescence measurements and analysis:* Steady-state fluorescence emission of Alexa488 and NBD labeled protein was measured using a SPEX Fluorolog FL3-22 steady-state fluorescence spectrometer (Jobin Yvon, Edison, NJ) equipped with double-grating excitation and emission monochromators. The measurements were made in a 2x10 mm cuvette oriented perpendicular to the excitation beam and maintained at 25°C using a Peltier device from Quantum Northwest (Spokane, WA) in 1 nm steps. The excitation and emission wavelengths for Alexa488

measurements were 455 and 470-700 nm, respectively, using slits of 2 nm on both monochromators. For NBD measurements, the emission spectra was collected from 490 to 700 nm, and the excitation wavelength was 470 nm, using slits of 5 nm on both monochromators. For each spectrum, we averaged 5 scans after incubating the samples at least 30 min for equilibration. The samples normally contained 0.3 $\mu$ M protein in 50mM phosphate buffer at pH 8.0, unless indicated, and 0.5mM of lipid. The acidification was achieved by the addition of small aliquots of acetic/acetate buffer. The fractions ( $F$ ) of membrane-bound or membrane-inserted states were calculated by normalization of the data to the maximum signal change. The pH-dependencies of these fractions were fitted to the following equation [133]:

$$F = \frac{1}{1 + 10^{n(pH - pKa)}} \quad (\text{Eq. 4.1})$$

where  $pKa$  is a negative logarithm of the dissociation constant, and  $n$  is the Hill coefficient.

The apparent free energy of protonation ( $\Delta G_a$ ) was calculated by rearranging the Gibbs equation:

$$\Delta G_a = 2.3RT(pKa) \quad (\text{Eq. 4.2})$$

where  $R$  and  $T$  are the gas constant and absolute temperature, respectively, and the  $pKa$  is obtained with Eq. 4.1.

*Membrane surface potential calculations:* The calculation of the membrane surface potential was performed using the Gouy-Chapman theory [152]. This model describes the electric potential along the axial plane of the membrane, where the potential at the membrane surface  $\Psi_0$  depends on the surface charge density  $\sigma$  and the concentration of counterions according to:

$$\psi_0 = \frac{2\kappa_B T}{ze} \times \sinh^{-1} \left( \frac{\sigma}{\sqrt{8N\varepsilon_0\varepsilon_r\kappa_B T \times c}} \right) \quad (\text{Eq. 4.3})$$

$\kappa_B$  is the Boltzmann constant ( $1.38 \times 10^{-23}$  J/K),  $T$  is the absolute temperature,  $z$  is the valence of the counterion (+1 in our case),  $e$  is the elementary electric charge ( $-1.602 \times 10^{-19}$  C),  $N$  is the Avogadro number ( $6.022 \times 10^{23}$  mol<sup>-1</sup>),  $\varepsilon_0$  is the permittivity in vacuum ( $8.854 \times 10^{-12}$  C<sup>2</sup>m<sup>-1</sup>/J),  $\varepsilon_r$  is the dielectric constant of water (78.3).  $c$  is the concentration of counterions expressed in mol/m<sup>3</sup>, while  $\sigma$  is the surface charge density expressed in C/m<sup>2</sup>.

The surface charge density was calculated according the following equation:

$$\sigma = \frac{\chi_{AL} \times z_{AL} e}{\chi_{AL} A_{AL} + \chi_{NL} A_{NL}}, \quad (\text{Eq. 4.4})$$

where  $z_{AL}$  is the net charge of the anionic lipid,  $\chi_{AL}$  and  $\chi_{NL}$  are the mole fractions of the anionic and neutral lipid, respectively, and  $A_{AL}$  and  $A_{NL}$  are the area per lipid of the anionic and neutral lipid, respectively, in units of m<sup>2</sup>. For the net charges, we used values of 0 for POPC, -1e for POPG, POPS and POPA, and -2e for TOCL, and further assume that they were constant over the range of pH tested in this study (pH4-8). For the areas per lipid, we used the cross-sectional areas described in the literature for the crystalline phase assuming a cylindrical shape: 64 Å<sup>2</sup> for POPC [160], 66 Å<sup>2</sup> for POPG [161], 63 Å<sup>2</sup> for POPS [13], and 130 Å<sup>2</sup> for TOCL [162]. We also used a value of 68 Å<sup>2</sup> for POPA, which was reported by MD simulations [163] (experimental values range from 42 to 89 Å<sup>2</sup> [164]). We further assume that the area per lipid is not affected by the mixing of different lipids, the presence of the protein, or the concentration of ions.

Finally, the correlation between the free energy of protonation and the membrane surface potential can be described by the equation suggested Fernandez and Fromherz [125]:

$$pK_a = pK_i - \frac{F}{2.3RT} \psi_0 \quad (\text{Eq. 4.5})$$

where  $pK_a$  and  $pK_i$  are the observed apparent  $pK$  and intrinsic  $pK$ , respectively,  $F$  is the Faraday constant,  $R$  is the gas constant and  $T$  the absolute temperature.

Eq. 4.5 can be further combined with Eq. 4.2 to describe the process in terms of free energy:

$$\Delta G_a = \Delta G_i - F\psi_0 \quad (\text{Eq. 4.6})$$

where  $\Delta G_a$  and  $\Delta G_i$  are apparent and intrinsic free energies of protonation, respectively, and  $F$  is the faraday constant ( $0.023\text{kcal mol}^{-1}\text{mV}^{-1}$ ). Eq. 4.6 describes the ideal modulation of free energy by the membrane surface potential.

*Kinetic measurements and analysis:* Time course of membrane insertion were performed using NBD-labeled Bcl-xL. The emission wavelength was fixed at 525 nm and the intensity was recorded in steps of 1 second. The intensity signal ( $I$ ) was fitted to an empirical three-component exponential association equation:

$$I = A_0 + A_1(1 - e^{-k_1 t}) + A_2(1 - e^{-k_2 t}) \quad (\text{Eq. 4.7})$$

where  $A_i$  are the amplitudes of the corresponding kinetic component with apparent rates of  $k_i$  ( $A_0$  corresponds to the amplitude of a fast component with  $k_0=0$ ). The sum of all amplitudes corresponds to the total fraction of inserted state.

## CHAPTER 5 CONCLUSIONS AND FUTURE DIRECTIONS

In this dissertation, we have addressed three different aspects on the pH-triggered membrane insertion of proteins. In chapter 2, we established that there are multiple mechanisms of pH-triggered membrane insertion of proteins. We determine the pH-induced membrane insertion pathway of the anti-apoptotic regulator Bcl-xL and compare it to that of the structurally similar diphtheria toxin T domain. We show differences in their membrane insertion pathways that may be relevant for their physiological action. In chapter 3, we determined the role of histidine protonation upon acidification in the membrane insertion and folding of proteins. We specifically investigate the role of a cluster of histidines located at the C-terminal region of the diphtheria toxin T domain. We show that H322 is critical for proper folding and activity of the N-terminal helices of the T domain in the membrane. Finally, in chapter 4, we studied the role of the physicochemical properties of the membrane itself in regulating the pH-triggered membrane interactions proteins. We found that the charge density at the membrane interface is critical for the initial binding of the Bcl-xL, while additional properties (e.g. membrane curvature stress) regulate the transmembrane insertion.

### *BCL-XL VERSUS T DOMAIN*

The structural similarities between Bcl-xL and the diphtheria toxin T domain had led to hypothesize that they shared common features in their membrane interactions [64, 66]. Here, we tested the validity of this assumption by directly comparing the membrane insertion pathways of both proteins. For a more accurate comparison, we truncated the TM helix of Bcl-xL, which is proposed to anchor the protein to the membrane [85, 86] in a similar fashion as the R domain of the diphtheria toxin. Then, we showed that acidification does not cause a noticeable structural

change in Bcl-xL using measurements of secondary structure and thermal unfolding with CD spectroscopy (Figs. 2.4 and 2.5). In diphtheria toxin T domain, however, mild acidification causes the conversion of a membrane-incompetent into a membrane-competent state. Then, we studied the membrane association of Bcl-xL using a FRET assay, and we found that this association depends on the mole fraction of anionic lipids in the membrane (Figs. 2.6-2.8). This is different from the case of the T domain, which shows no dependence on the lipid composition in the initial membrane binding. Lastly, we compared the transmembrane insertion of Bcl-xL with that of the T domain (Figs. 2.9-2.11), where no major differences were observed. In this case, the membrane interactions of the anti-apoptotic regulator were already regulated by lipids at the binding step, while those of the toxin were regulated at the final step.

The likely reason for the differences observed in the insertion pathways of both proteins is that the membrane-competent states are formed in different places: in solution for the T domain and in the membrane interface for Bcl-xL. This has implications in the regulation of membrane interactions of both proteins because the membrane partitioning of Bcl-xL can be modulated by the lipid composition, while that of the T domain is not. Physiologically, the lack of regulation by lipids is important for the T domain because it ensures robust membrane association regardless of the lipid composition. For Bcl-xL, however, regulation by lipids acts as a rheostat for membrane association because insufficient or excessive association with the membrane disrupts the life/death balance.

The differential regulation of the process for both proteins also suggests a distinct pH-trigger. Since the formation of the membrane-competent form of the T domain is triggered in solution at pH values 6-6.5, histidine protonation plays an important role. Several lines of evidence indicate

that protonation of histidines at the N-terminal cluster is required for proper conformational switching of the T domain in solution and membrane interactions. In contrast, the formation of the membrane-competent form of Bcl-xL occurs at the membrane interface, suggesting that histidine protonation is not necessarily the trigger of the conformational changes. It is suggested that the membrane interface alters the pKa of protonation of amino acid lateral chains. Thus, protonation of acidic residues, rather than histidines, may play a major role for the membrane interactions of Bcl-xL. Although it is a challenge to determine the specific residues involved in the process (Bcl-xL possesses 31 acidic residues), identifying these residues will provide further understanding in the mechanism of pH-triggered membrane insertion of this protein.

The comparison between the T domain and Bcl-xL was initially useful in apoptosis research because it shed light into the functional role of the Bcl-2 family of proteins. However, as described here and in reference [109] (published outcome of chapter 2 of this dissertation), both proteins follow different membrane insertion mechanisms. We suggest that the knowledge built in the membrane interactions of the T domain is not applicable to understand the membrane interactions of Bcl-xL. Bcl-xL and T domain play different roles in the membrane as well: while the T domain forms a channel to allow the passage of a polypeptide during bacterial infection, Bcl-xL prevents the permeabilization of the membrane to polypeptides. Thus, the T domain and Bcl-xL should not be expected to interact with the membrane in a similar fashion. However, we do not rule out that other members of the Bcl-2 family of proteins share mechanistic similarities with the T domain. Future studies should address the case of Bcl-2 proteins whose function is the formation of pores, such as Bak and Bax.

## *HISTIDINES AND FOLDING OF T DOMAIN IN THE MEMBRANE*

In chapter 2, we determined the role of H322 in the membrane folding of the T domain. This residue is part of group of three histidines that are clustered at the top of helices TH8-TH9, which is the membrane insertion unit of the diphtheria toxin T domain. Previously, it was shown that the triple replacement of these histidines to glutamine or arginine caused loss of translocation activity and inability to reach the open-channel state [68]. However, the membrane insertion of TH8-TH9 was not affected, which suggested uncoupling of the membrane insertion of these helices with folding into an open-channel state. Here, we determined that the replacement of H322 alone is sufficient to cause those effects; however, the simultaneous mutation of the three histidines appears to further affect the activity of the T domain (Table 3.1). We also showed that the mutation of H322 alone does not cause misfolding in solution, but leads to the formation of non-productive intermediate states in the membrane, which then misfold and possibly aggregate (Figs. 3.2-35). Similarly, the simultaneous replacement of this and the other histidines enhances the effect of H322 on the membrane folding of the T domain.

Previous research showed that another group of histidines, clustered around the N-terminal helices of the T domain, are important for triggering the initial conformational changes in solution [50, 52]. In the case of the N-terminal histidines, the replacement to arginine and to glutamine cause opposite effects, i.e. the presence of a positive charge triggers the conformational switching in solution and the absence of a charge delays the conformational change. Thus, protonation of the N-terminal histidines would be the signal for the T domain to execute its membrane action. A similar mechanism has been suggested for histidine residues in

other proteins, such as the protective antigen of the anthrax toxin [165] and the influenza hemagglutinin [166, 167].

In the case of the C-terminal histidines, the conformational changes do not appear to respond to mere protonation because the mutation to either lysine or glutamine causes indistinguishable effects. It is possible that the mechanism by which the C-terminal histidines affect T domain's function and folding is their ability to protonate/deprotonate rather than the protonation itself. The membrane interface has been shown to modulate the apparent  $pK_a$  of protonation of titratable peptides [125, 168, 169]. If this is the case, H322 may undergo multiple events of protonation and deprotonation as the T domain refolds into the membrane, where the membrane interface modulates the  $pK_a$ . It is challenging to test this hypothesis experimentally; however, future studies may take advantage of computational tools to visualize whether this may be the case.

The replacement of the C-terminal histidines may prevent the proper membrane insertion of the TH5 helix, which is suggested to become transmembrane along with TH8 and TH9 in the open-channel state [51]. The mutation of the C-terminal histidines causes lack of blue-shifted tryptophan spectra and loss of channel activity. Since tryptophan fluorescence is affected by the polarity of the environment [139], it is possible that one or both tryptophans of the T domain (W206 and W281) do not penetrate the lipid bilayer. W281 is located in the middle of TH5, suggesting that it is possible that TH5 is unable to properly fold into the membrane in the case of the mutants. This would explain not only the lack of blue-shift of the tryptophan emission spectrum, but also the loss of channel formation activity because membrane insertion of TH5 is suggested to be required for such activity [51]. Initial studies to test this hypothesis, where

W281 is the only fluorescence internal probe, confirm that replacement of the C-terminal histidines impedes the membrane insertion of TH5 (unpublished results from Dr. Ghakat and Dr. Ladokhin). Similarly, extended molecular dynamic simulations of the T domain in the membrane will contribute to better visualize the molecular link between the C-terminal histidines and TH5 penetration.

#### *LIPID REGULATION OF MEMBRANE INTERACTIONS OF BCL-XL*

In chapter 3, we have characterized the effect of the membrane lipid composition on the membrane interactions of Bcl-xL. First, we studied the effect of membrane lipids on the initial membrane binding of Bcl-xL by using a FRET assay (Figs. 4.3-4.5 and Table 4.1). Our data showed that the *pKa* of membrane binding can be modulated by varying the mole fraction of anionic lipids, regardless of the type of lipid. This suggested that membrane association of Bcl-xL responded to negatively charged membranes rather than to specific lipids. Varying the ionic strength of the solution also affected the pH-dependence of membrane binding of Bcl-xL, supporting the idea of the charge density at the membrane interface playing a role in the action of Bcl-xL. There was a linear correlation between the *pKas* of membrane binding and the membrane surface potential, regardless of the lipid system or the ionic strength conditions. Thus, we concluded that the initial membrane association of Bcl-xL depends on the charge density of the membrane interface.

Previous research had suggested that the mitochondrial lipid cardiolipin was required for the membrane association of Bid, Bax and Bcl-xL [83, 84, 103, 115]. However, here we show that any lipid with a negatively charged headgroup can replace cardiolipin for the initial membrane association of Bcl-xL. We do not rule out that cardiolipin may play unique roles in modulating

the membrane refolding of Bcl-xL once in the lipid bilayer. Similarly, cardiolipin may play additional roles that can be important for the function of Bcl-xL or other Bcl-2 family proteins *in vivo*. However, for the purposes of *in vitro* studies, it appears that Bcl-xL can be tethered to the membrane by either increasing the mole fraction of anionic lipids or decreasing the ionic strength.

Second, we studied the effects of different lipids on the transmembrane insertion of Bcl-xL. In contrast to the binding event, we found that lipids modulate the transmembrane insertion and refolding of Bcl-xL in the membrane in a lipid-specific manner. The replacement of cardiolipin with other anionic lipids did not cause shifts in the  $pK_a$  in the same degree as cardiolipin does. Since the membrane interactions of Bcl-xL were already regulated at the membrane association step, this lipid-specific regulation suggests that there are additional physicochemical properties of the lipids that modulate Bcl-xL refolding. One possibility is the size of the lipid headgroup, which would affect the size of the interfacial region and therefore the proximity of Bcl-xL to the hydrocarbon core once in the bilayer. In the case of POPA and cardiolipin, the dependence of the  $pK_a$  on the membrane surface potential is similar in both the binding and insertion events (similar slopes in Figs. 4.4 and 4.6). These lipids also have a smaller headgroup because of the lack of a functional group attached to the phosphate group (Fig. 4.2). In the case of POPG and POPS, where the lipid headgroup is larger, the dependence of  $pK_a$  on the membrane surface potential (slopes in Figs. 4.4 and 4.6) is greatly reduced in the insertion event, suggesting that these lipids constrain the membrane insertion of Bcl-xL.

We also observed modulation of the membrane insertion of Bcl-xL by non-bilayer forming lipids. In this case, POPE and LysoPC affected the rate of membrane insertion in opposite ways

(Fig. 4.8). POPE and LysoPC are lipids that induce mechanical stress in lipid bilayers because of their intrinsic curvature (negative and positive curvature, respectively). It is possible that mechanical properties of the membrane are important for modulating the refolding of Bcl-xL within the membrane. Thus, our results are in agreement with previous reports claiming that POPE serves as lipid chaperone for the proper folding of other membrane proteins [148-150].

Research in lipid biology and apoptosis indicates that the lipid composition of the mitochondrial membrane changes before, during and after MOMP [100, 104, 110]. Given our findings, it is possible that Bcl-xL and other Bcl-2 family members can be modulated by the lipid composition *in vivo*. However, our study is the first extensive characterization in the modulation of membrane interactions of Bcl-xL by lipids. Other groups have partially characterized the effect of lipids on the membrane interactions of Bax and Bid, however, those studies focused in few lipids and did not directly address membrane binding and insertion [101, 106]. Thus, to better understand the mechanisms of membrane action of the Bcl-2 family proteins, future research should focus on characterizing the effect of membrane lipids on the membrane-modulated interactions of multiple members of the Bcl-2 family.

## CHAPTER 6 REFERENCES

- [1] L. Fagerberg, K. Jonasson, G. von Heijne, M. Uhlen, L. Berglund, Prediction of the human membrane proteome, *Proteomics*, 10 (2010) 1141-1149.
- [2] M. Uhlén, L. Fagerberg, B.M. Hallström, C. Lindskog, P. Oksvold, A. Mardinoglu, Å. Sivertsson, C. Kampf, E. Sjöstedt, A. Asplund, Tissue-based map of the human proteome, *Science*, 347 (2015) 1260419.
- [3] T.M. Bakheet, A.J. Doig, Properties and identification of human protein drug targets, *Bioinformatics*, 25 (2009) 451-457.
- [4] M.A. Yildirim, K.-I. Goh, M.E. Cusick, A.-L. Barabási, M. Vidal, Drug—target network, *Nature biotechnology*, 25 (2007) 1119-1126.
- [5] S.H. White, The progress of membrane protein structure determination, *Protein Science*, 13 (2004) 1948-1949.
- [6] F.M. Goñi, The basic structure and dynamics of cell membranes: An update of the Singer–Nicolson model, *Biochimica et Biophysica Acta (BBA)-Biomembranes*, 1838 (2014) 1467-1476.
- [7] S.H. White, Biophysical dissection of membrane proteins, *Nature*, 459 (2009) 344-346.
- [8] G. van Meer, D.R. Voelker, G.W. Feigenson, Membrane lipids: where they are and how they behave, *Nat Rev Mol Cell Biol*, 9 (2008) 112-124.
- [9] E. Fahy, D. Cotter, M. Sud, S. Subramaniam, Lipid classification, structures and tools, *Biochimica et Biophysica Acta (BBA)-Molecular and Cell Biology of Lipids*, 1811 (2011) 637-647.

- [10] M. Sud, E. Fahy, D. Cotter, A. Brown, E.A. Dennis, C.K. Glass, A.H. Merrill, R.C. Murphy, C.R. Raetz, D.W. Russell, Lmsd: lipid maps structure database, *Nucleic acids research*, 35 (2007) D527-D532.
- [11] A.S. Reddy, D.T. Warshaviak, M. Chachisvilis, Effect of membrane tension on the physical properties of DOPC lipid bilayer membrane, *Biochimica et Biophysica Acta (BBA)-Biomembranes*, 1818 (2012) 2271-2281.
- [12] M.C. Wiener, S.H. White, Structure of a fluid dioleoylphosphatidylcholine bilayer determined by joint refinement of x-ray and neutron diffraction data. III. Complete structure, *Biophys.J.*, 61 (1992) 434-447.
- [13] J. Pan, X. Cheng, L. Monticelli, F.A. Heberle, N. Kučerka, D.P. Tieleman, J. Katsaras, The molecular structure of a phosphatidylserine bilayer determined by scattering and molecular dynamics simulations, *Soft matter*, 10 (2014) 3716-3725.
- [14] N. Kucerka, Y.F. Liu, N. Chu, H.I. Petrache, S. Tristram-Nagle, J.F. Nagle, Structure of fully hydrated fluid phase DMPC and DLPC lipid bilayers using x-ray scattering from oriented multilamellar arrays and from unilamellar vesicles, *Biophys.J.*, 88 (2005) 2626-2637.
- [15] M. Mihailescu, K. Gawrisch, The structure of polyunsaturated lipid bilayers important for rhodopsin function: a neutron diffraction study, *Biophysical journal*, 90 (2006) L04-06.
- [16] J.F. Nagle, R. Zhang, S. Tristram-Nagle, W. Sun, H.I. Petrache, R.M. Suter, X-ray structure determination of fully hydrated  $L_{\alpha}$  phase dipalmitoylphosphatidylcholine bilayers, *Biophys.J.*, 70 (1996) 1419-1431.

- [17] H.I. Ingólfsson, M.N. Melo, F.J. van Eerden, C. Arnarez, C.A. Lopez, T.A. Wassenaar, X. Periole, A.H. De Vries, D.P. Tieleman, S.J. Marrink, Lipid Organization of the Plasma Membrane, *Journal of the American Chemical Society*, 136 (2014) 14554-14559.
- [18] S.H. White, W.C. Wimley, Membrane protein folding and stability: Physical principles, *Annu.Rev.Biophys.Biomol.Struc.*, 28 (1999) 319-365.
- [19] T.O. Yeates, H. Komiya, D.C. Rees, J.P. Allen, G. Feher, Structure of the reaction center from *Rhodobacter sphaeroides* R-26: Membrane-protein interactions, *Proc.Natl.Acad.Sci.USA*, 84 (1987) 6438-6442.
- [20] K. Murata, K. Mitsuoka, T. Hirai, T. Walz, P. Agre, J.B. Heymann, A. Engel, Y. Fujiyoshi, Structural determinants of water permeation through aquaporin-1, *Nature*, 407 (2000) 599-605.
- [21] L. Song, M.R. Hobaugh, C. Shustak, S. Cheley, H. Bayley, J.E. Gouaux, Structure of staphylococcal  $\alpha$ -hemolysin, a heptameric transmembrane pore, *Science*, 274 (1996) 1859-1866.
- [22] S.H. White, A.S. Ladokhin, S. Jayasinghe, K. Hristova, How membranes shape protein structure, *J.Biol.Chem.*, 276 (2001) 32395-32398.
- [23] D.C. Rees, L. De Antonio, D. Eisenberg, Hydrophobic organization of membrane proteins, *Science*, 245 (1989) 510-513.
- [24] A. Oberai, Y. Ihm, S. Kim, J.U. Bowie, A limited universe of membrane protein families and folds, *Protein science*, 15 (2006) 1723-1734.

- [25] S.H. White, Translocons, thermodynamics, and the folding of membrane proteins, *FEBS Lett.*, 555 (2003) 116-121.
- [26] J.-L. Popot, S.-E. Gerchman, D.M. Engelman, Refolding of bacteriorhodopsin in lipid bilayers. A thermodynamically controlled two-stage process, *J.Mol.Biol.*, 198 (1987) 655-676.
- [27] N. Ben-Tal, A. Ben-Shaul, A. Nicholls, B. Honig, Free-energy determinants of  $\alpha$ -helix insertion into lipid bilayers, *Biophys.J.*, 70 (1996) 1803-1812.
- [28] N. Ben-Tal, D. Sitkoff, I.A. Topol, A.-S. Yang, S.K. Burt, B. Honig, Free energy of amide hydrogen bond formation in vacuum, in water, and in liquid alkane solution, *J.Phys.Chem.B*, 101 (1997) 450-457.
- [29] P.F. Almeida, A.S. Ladokhin, S.H. White, Hydrogen-bond energetics drive helix formation in membrane interfaces, *Biochimica et biophysica acta*, (2011).
- [30] D. Deng, C. Xu, P. Sun, J. Wu, C. Yan, M. Hu, N. Yan, Crystal structure of the human glucose transporter GLUT1, *Nature*, (2014).
- [31] M. Bayrhuber, T. Meins, M. Habeck, S. Becker, K. Giller, S. Villinger, C. Vornrhein, C. Griesinger, M. Zweckstetter, K. Zeth, Structure of the human voltage-dependent anion channel, *Proceedings of the National Academy of Sciences*, 105 (2008) 15370-15375.
- [32] T.C. Terwilliger, D. Eisenberg, The structure of melittin. I. Structure determination and partial refinement, *J.Biol.Chem.*, 257 (1982) 6010-6015.
- [33] M. Higy, T. Junne, M. Spiess, Topogenesis of membrane proteins at the endoplasmic reticulum, *Biochemistry*, 43 (2004) 12716-12722.

- [34] S.H. White, G. von Heijne, The machinery of membrane protein assembly, *Curr.Opin.Struct.Biol.*, 14 (2004) 397-404.
- [35] K.H. Kim, S. Aulakh, M. Paetzel, The bacterial outer membrane  $\beta$ -barrel assembly machinery, *Protein Science*, 21 (2012) 751-768.
- [36] L.K. Tamm, A. Arora, J.H. Kleinschmidt, Structure and assembly of  $\beta$ -barrel membrane proteins, *J.Biol.Chem.*, 276 (2001) 32399-32402.
- [37] F. Cymer, G. von Heijne, S.H. White, Mechanisms of Integral Membrane Protein Insertion and Folding, *Journal of molecular biology*, (2014).
- [38] F. Duong, W. Wickner, Sec-dependent membrane protein biogenesis: SecYEG, preprotein hydrophobicity and translocation kinetics control the stop-transfer function, *EMBO Journal*, 17 (1998) 696-705.
- [39] T.H. Meyer, J.-F. Ménétre, R. Breitling, K.R. Miller, C.W. Akey, T.A. Rapoport, The bacterial SecY/E translocation complex forms channel-like structures similar to those of the eukaryotic Sec61p complex, *J.Mol.Biol.*, 285 (1999) 1789-1800.
- [40] J. Oliver, B. Jungnickel, D. Görlich, T. Rapoport, S. High, The Sec61 complex is essential for the insertion of proteins into the membrane of the endoplasmic reticulum, *FEBS Lett.*, 362 (1995) 126-130.
- [41] T. Hessa, N.M. Meindl-Beinker, A. Bernsel, H. Kim, Y. Sato, M. Lerch-Bader, I. Nilsson, S.H. White, G. von Heijne, Molecular code for transmembrane-helix recognition by the Sec61 translocon, *Nature*, 450 (2007) 1026-1030.

[42] J.R. Murphy, Mechanism of diphtheria toxin catalytic domain delivery to the eukaryotic cell cytosol and the cellular factors that directly participate in the process, *Toxins*, 3 (2011) 294-308.

[43] A.S. Ladokhin, pH-triggered conformational switching along the membrane insertion pathway of the diphtheria toxin T-domain, *Toxins*, 5 (2013) 1362-1380.

[44] J.A. Young, R.J. Collier, Anthrax Toxin: Receptor Binding, Internalization, Pore Formation, and Translocation, *Annu Rev Biochem*, 76 (2007) 243-265.

[45] W.A. Cramer, J.B. Heymann, S.L. Schendel, B.N. Deriy, F.S. Cohen, P.A. Elkins, C.V. Stauffacher, Structure-function of the channel-forming colicins, *Annu.Rev.Biophys.Biomol.Struc.*, 24 (1995) 611-641.

[46] V. Gerke, S.E. Moss, Annexins: From structure to function, *Physiological Reviews*, 82 (2002) 331-371.

[47] R.J. Youle, A. Strasser, The BCL-2 protein family: opposing activities that mediate cell death, *Nat Rev Mol Cell Biol*, 9 (2008) 47-59.

[48] R.M. Voorhees, I.S. Fernández, S.H. Scheres, R.S. Hegde, Structure of the mammalian ribosome-Sec61 complex to 3.4 Å resolution, *Cell*, 157 (2014) 1632-1643.

[49] M.J. Bennett, D. Eisenberg, Refined structure of monomeric diphtheria toxin at 2.3 Å resolution, *Protein Sci.*, 3 (1994) 1464-1475.

[50] I.V. Kurnikov, A. Kyrychenko, J.C. Flores-Canales, M.V. Rodnin, N. Simakov, M. Vargas-Uribe, Y.O. Posokhov, M. Kurnikova, A.S. Ladokhin, pH-Triggered Conformational

Switching of the Diphtheria Toxin T-Domain: The Roles of N-Terminal Histidines, *J Mol Biol*, 425 (2013) 2752-2764.

[51] L. Senzel, M. Gordon, R.O. Blaustein, K.J. Oh, R.J. Collier, A. Finkelstein, Topography of diphtheria toxin's T domain in the open channel state, *J.Gen.Physiol.*, 115 (2000) 421-434.

[52] M.V. Rodnin, A. Kyrychenko, P. Kienker, O. Sharma, Y.O. Posokhov, R.J. Collier, A. Finkelstein, A.S. Ladokhin, Conformational switching of the diphtheria toxin T domain, *J Mol Biol*, 402 (2010) 1-7.

[53] A. Kyrychenko, Y.O. Posokhov, M.V. Rodnin, A.S. Ladokhin, Kinetic intermediate reveals staggered pH-dependent transitions along the membrane insertion pathway of the diphtheria toxin T-domain, *Biochemistry*, 48 (2009) 7584-7594.

[54] J. Huotari, A. Helenius, Endosome maturation, *The EMBO journal*, 30 (2011) 3481-3500.

[55] R.W. van Dyke, Acidification of lysosomes and endosomes, *Subcellular Biochem.*, 27 (1996) 331-360.

[56] R.F. Murphy, S. Powers, C.R. Cantor, Endosome pH measured in single cells by dual fluorescence flow cytometry: rapid acidification of insulin to pH 6, *The Journal of cell biology*, 98 (1984) 1757-1762.

[57] K.J. Oh, H. Zhan, C. Cui, K. Hideg, R.J. Collier, W.L. Hubbell, Organization of diphtheria toxin T domain in bilayers: A site-directed spin labeling study, *Science*, 273 (1996) 810-812.

[58] K.J. Oh, H. Zhan, C. Cui, C. Altenbach, W.L. Hubbell, R.J. Collier, Conformation of the diphtheria toxin T domain in membranes: A site-directed spin-labeling study of the TH8 helix and TL5 loop, *Biochemistry*, 38 (1999) 10336-10343.

[59] M.P. Rosconi, G. Zhao, E. London, Analyzing topography of membrane-inserted diphtheria toxin T domain using BODIPY-streptavidin: At low pH, helices 8 and 9 form a transmembrane hairpin but helices 5-7 form stable nonclassical inserted segments on the cis side of the bilayer, *Biochemistry*, 43 (2004) 9127-9139.

[60] Y. Wang, S.E. Malenbaum, K. Kachel, H.J. Zhan, R.J. Collier, E. London, Identification of shallow and deep membrane-penetrating forms of diphtheria toxin T domain that are regulated by protein concentration and bilayer width, *J.Biol.Chem.*, 272 (1997) 25091-25098.

[61] P.K. Kienker, Z. Wu, A. Finkelstein, Mapping the membrane topography of the TH6–TH7 segment of the diphtheria toxin T-domain channel, *The Journal of general physiology*, (2015) jgp. 201411326.

[62] M.P. Rosconi, E. London, Topography of helices 5-7 in membrane-inserted diphtheria toxin T domain: identification and insertion boundaries of two hydrophobic sequences that do not form a stable transmembrane hairpin, *The Journal of biological chemistry*, 277 (2002) 16517-16527.

[63] M. Vargas-Uribe, M.V. Rodnin, K. Ojemalm, A. Holgado, A. Kyrychenko, I. Nilsson, Y.O. Posokhov, G. Makhatadze, G. von Heijne, A.S. Ladokhin, Thermodynamics of Membrane Insertion and Refolding of the Diphtheria Toxin T-Domain, *The Journal of membrane biology*, (2014).

- [64] A. Antignani, R.J. Youle, How do Bax and Bak lead to permeabilization of the outer mitochondrial membrane?, *Current opinion in cell biology*, 18 (2006) 685-689.
- [65] A.J. Minn, P. Velez, S.L. Schendel, H. Liang, S.W. Muchmore, S.W. Fesik, M. Fill, C.B. Thompson, Bcl-x(L) forms an ion channel in synthetic lipid membranes, *Nature*, 385 (1997) 353-357.
- [66] S.W. Muchmore, M. Sattler, H. Liang, R.P. Meadows, J.E. Harlan, H.S. Yoon, D. Nettlesheim, B.S. Chang, C.B. Thompson, S.L. Wong, S.L. Ng, S.W. Fesik, X-ray and NMR structure of human Bcl-xL, an inhibitor of programmed cell death, *Nature*, 381 (1996) 335-341.
- [67] A. Perier, A. Chassaing, S. Raffestin, S. Pichard, M. Masella, A. Menez, V. Forge, A. Chenal, D. Gillet, Concerted protonation of key histidines triggers membrane interaction of the diphtheria toxin T domain, *The Journal of biological chemistry*, 282 (2007) 24239-24245.
- [68] M.V. Rodnin, A. Kyrychenko, P. Kienker, O. Sharma, M. Vargas-Uribe, R.J. Collier, A. Finkelstein, A.S. Ladokhin, Replacement of C-terminal histidines uncouples membrane insertion and translocation in diphtheria toxin T-domain, *Biophysical journal*, 101 (2011) L41-43.
- [69] J.F. Kerr, A.H. Wyllie, A.R. Currie, Apoptosis: a basic biological phenomenon with wide-ranging implications in tissue kinetics, *British journal of cancer*, 26 (1972) 239.
- [70] A. Strasser, S. Cory, J.M. Adams, Deciphering the rules of programmed cell death to improve therapy of cancer and other diseases, *The EMBO journal*, 30 (2011) 3667-3683.
- [71] S.W. Tait, D.R. Green, Mitochondria and cell death: outer membrane permeabilization and beyond, *Nat Rev Mol Cell Biol*, 11 (2010) 621-632.

[72] A.H. Wyllie, "Where, o death, is thy sting?" a brief review of apoptosis biology, *Mol Neurobiol*, 42 (2010) 4-9.

[73] C. Wang, R.J. Youle, The role of mitochondria in apoptosis\*, *Annual review of genetics*, 43 (2009) 95-118.

[74] J.M. Hardwick, R.J. Youle, SnapShot: BCL-2 proteins, *Cell*, 138 (2009) 404, 404 e401.

[75] A.J. Garcia-Saez, The secrets of the Bcl-2 family, *Cell Death Differ*, 19 (2012) 1733-1740.

[76] A. Shamas-Din, J. Kale, B. Leber, D.W. Andrews, Mechanisms of action of bcl-2 family proteins, *Cold Spring Harb Perspect Biol*, 5 (2013).

[77] Y.T. Hsu, K.G. Wolter, R.J. Youle, Cytosol-to-membrane redistribution of Bax and Bcl-X(L) during apoptosis, *Proceedings of the National Academy of Sciences of the United States of America*, 94 (1997) 3668-3672.

[78] K.G. Wolter, Y.T. Hsu, C.L. Smith, A. Nechushtan, X.G. Xi, R.J. Youle, Movement of Bax from the cytosol to mitochondria during apoptosis, *The Journal of cell biology*, 139 (1997) 1281-1292.

[79] J.F. Lovell, L.P. Billen, S. Bindner, A. Shamas-Din, C. Fradin, B. Leber, D.W. Andrews, Membrane binding by tBid initiates an ordered series of events culminating in membrane permeabilization by Bax, *Cell*, 135 (2008) 1074-1084.

- [80] F. Edlich, S. Banerjee, M. Suzuki, M.M. Cleland, D. Arnoult, C. Wang, A. Neutzner, N. Tjandra, R.J. Youle, Bcl-x(L) retrotranslocates Bax from the mitochondria into the cytosol, *Cell*, 145 (2011) 104-116.
- [81] M.E. Soriano, L. Scorrano, Traveling Bax and forth from mitochondria to control apoptosis, *Cell*, 145 (2011) 15-17.
- [82] C. Bogner, B. Leber, D.W. Andrews, Apoptosis: embedded in membranes, *Current opinion in cell biology*, 22 (2010) 845-851.
- [83] L.P. Billen, C.L. Kokoski, J.F. Lovell, B. Leber, D.W. Andrews, Bcl-XL inhibits membrane permeabilization by competing with Bax, *PLoS biology*, 6 (2008) e147.
- [84] A.J. Garcia-Saez, J. Ries, M. Orzaez, E. Perez-Paya, P. Schwille, Membrane promotes tBID interaction with BCL(XL), *Nat Struct Mol Biol*, 16 (2009) 1178-1185.
- [85] A.J. García-Sáez, I. Mingarro, E. Pérez-Payá, J. Salgado, Membrane-insertion fragments of Bcl-XL, Bax, and Bid, *Biochemistry*, 43 (2004) 10930-10943.
- [86] Y. Yao, L.M. Fujimoto, N. Hirshman, A.A. Bobkov, A. Antignani, R.J. Youle, F.M. Marassi, Conformation of BCL-XL upon membrane-integration, *Journal of Molecular Biology*, (2015).
- [87] F. Todt, Z. Cakir, F. Reichenbach, R.J. Youle, F. Edlich, The C-terminal helix of Bcl-x(L) mediates Bax retrotranslocation from the mitochondria, *Cell Death Differ*, 20 (2013) 333-342.

[88] G.R. Thuduppathy, J.W. Craig, V. Kholodenko, A. Schon, R.B. Hill, Evidence that membrane insertion of the cytosolic domain of Bcl-xL is governed by an electrostatic mechanism, *J Mol Biol*, 359 (2006) 1045-1058.

[89] G.R. Thuduppathy, R.B. Hill, Acid destabilization of the solution conformation of Bcl-xL does not drive its pH-dependent insertion into membranes, *Protein science : a publication of the Protein Society*, 15 (2006) 248-257.

[90] G.R. Thuduppathy, O. Terrones, J.W. Craig, G. Basanez, R.B. Hill, The N-terminal domain of Bcl-xL reversibly binds membranes in a pH-dependent manner, *Biochemistry*, 45 (2006) 14533-14542.

[91] J.J. Donovan, M.I. Simon, R.K. Draper, M. Montal, Diphtheria toxin forms transmembrane channels in planar lipid bilayers, *Proc.Natl.Acad.Sci.USA*, 78 (1981) 172-176.

[92] M.G. Blewitt, L.A. Chung, E. London, Effect of pH on the conformation of diphtheria toxin and its implications for membrane penetration, *Biochemistry*, 24 (1985) 5458-5464.

[93] M. Suzuki, R.J. Youle, N. Tjandra, Structure of Bax: coregulation of dimer formation and intracellular localization, *Cell*, 103 (2000) 645-654.

[94] S.L. Schendel, Z. Xie, M.O. Montal, S. Matsuyama, M. Montal, J.C. Reed, Channel formation by antiapoptotic protein Bcl-2, *Proceedings of the National Academy of Sciences*, 94 (1997) 5113-5118.

[95] R.F. Epand, J.-C. Martinou, S. Montessuit, R.M. Epand, C.M. Yip, Direct evidence for membrane pore formation by the apoptotic protein Bax, *Biochemical and biophysical research communications*, 298 (2002) 744-749.

[96] C.M. Franzin, J. Choi, D. Zhai, J.C. Reed, F.M. Marassi, Structural studies of apoptosis and ion transport regulatory proteins in membranes, *Magn Reson Chem*, 42 (2004) 172-179.

[97] K. Kachel, J.H. Ren, R.J. Collier, E. London, Identifying transmembrane states and defining the membrane insertion boundaries of hydrophobic helices in membrane-inserted diphtheria toxin T domain, *J.Biol.Chem.*, 273 (1998) 22950-22956.

[98] M. Gordon, A. Finkelstein, The number of subunits comprising the channel formed by the T domain of diphtheria toxin, *J Gen Physiol*, 118 (2001) 471-480.

[99] S.S. Palchevskyy, Y.O. Posokhov, B. Olivier, J.L. Popot, B. Pucci, A.S. Ladokhin, Chaperoning of Insertion of Membrane Proteins into Lipid Bilayers by Hemifluorinated Surfactants: Application to Diphtheria Toxin, *Biochemistry*, 45 (2006) 2629-2635.

[100] I.M. Cristea, M. Degli Esposti, Membrane lipids and cell death: an overview, *Chem Phys Lipids*, 129 (2004) 133-160.

[101] E. Martínez-Abundis, N. Garcia, F. Correa, M. Franco, C. Zazueta, Changes in specific lipids regulate BAX-induced mitochondrial permeability transition, *Febs Journal*, 274 (2007) 6500-6510.

[102] S. Lucken-Ardjomande, S. Montessuit, J.-C. Martinou, Contributions to Bax insertion and oligomerization of lipids of the mitochondrial outer membrane, *Cell Death & Differentiation*, 15 (2008) 929-937.

[103] Z.T. Schug, E. Gottlieb, Cardiolipin acts as a mitochondrial signalling platform to launch apoptosis, *Biochimica et Biophysica Acta (BBA)-Biomembranes*, 1788 (2009) 2022-2031.

- [104] M. Crimi, M.D. Esposti, Apoptosis-induced changes in mitochondrial lipids, *Biochimica et biophysica acta*, 1813 (2011) 551-557.
- [105] K. Zhao, H. Zhou, X. Zhao, D.W. Wolff, Y. Tu, H. Liu, T. Wei, F. Yang, Phosphatidic acid mediates the targeting of tBid to induce lysosomal membrane permeabilization and apoptosis, *Journal of lipid research*, 53 (2012) 2102-2114.
- [106] E.Y. Cho, C.-H. Yun, T. Ahn, Effects of phospholipids on the functional regulation of tBID in membranes, *Molecular and cellular biochemistry*, 363 (2012) 395-408.
- [107] V. Mignard, L. Lalier, F. Paris, F. Vallette, Bioactive lipids and the control of Bax pro-apoptotic activity, *Cell death & disease*, 5 (2013) e1266-e1266.
- [108] T. Zhang, A. Saghatelian, Emerging roles of lipids in BCL-2 family-regulated apoptosis, *Biochimica et Biophysica Acta (BBA)-Molecular and Cell Biology of Lipids*, 1831 (2013) 1542-1554.
- [109] M. Vargas-Uribe, M.V. Rodnin, A.S. Ladokhin, Comparison of membrane insertion pathways of the apoptotic regulator Bcl-xL and the diphtheria toxin translocation domain, *Biochemistry*, 52 (2013) 7901-7909.
- [110] K. Cosentino, A.J. García-Sáez, Mitochondrial alterations in apoptosis, *Chemistry and physics of lipids*, (2014).
- [111] M.D. Esposti, Lipids, cardiolipin and apoptosis: a greasy licence to kill, *Cell death and differentiation*, 9 (2002) 234.

- [112] G. Olofsson, E. Sparr, Ionization constants pKa of cardiolipin, PloS one, 8 (2013) e73040.
- [113] D. Marsh, CRC Handbook of Lipid Bilayers, CRC Press, Boca Raton, 1990.
- [114] F. Jiang, M.T. Ryan, M. Schlame, M. Zhao, Z. Gu, M. Klingenberg, N. Pfanner, M.L. Greenberg, Absence of cardiolipin in the *crd1* null mutant results in decreased mitochondrial membrane potential and reduced mitochondrial function, Journal of Biological Chemistry, 275 (2000) 22387-22394.
- [115] J.B. McMillin, W. Dowhan, Cardiolipin and apoptosis, Biochimica et biophysica acta, 1585 (2002) 97-107.
- [116] S.-D. Aisha, B. Scott, C. Xiaoke, L. Brian, W.A. David, F. Cecile, Distinct lipid effects on tBid and Bim activation of membrane permeabilization by pro-apoptotic Bax, Biochemical Journal, (2015).
- [117] J. Ren, K. Kachel, H. Kim, S.E. Malenbaum, R.J. Collier, E. London, Interaction of diphtheria toxin T domain with molten globule-like proteins and its implications for translocation, Science, 284 (1999) 955-957.
- [118] L. Senzel, P.D. Huynh, K.S. Jakes, R.J. Collier, A. Finkelstein, The diphtheria toxin channel-forming T domain translocates its own NH<sub>2</sub>-terminal region across planar bilayers, J.Gen.Physiol., 112 (1998) 317-324.
- [119] M.V. Rodnin, A.S. Ladokhin, Membrane translocation assay based on proteolytic cleavage: Application to diphtheria toxin T domain, Biochimica et biophysica acta, (2014).

[120] A.S. Ladokhin, R. Legmann, R.J. Collier, S.H. White, Reversible refolding of the diphtheria toxin T-domain on lipid membranes, *Biochemistry*, 43 (2004) 7451-7458.

[121] M.V. Rodnin, Y.O. Posokhov, C. Contino-Pepin, J. Brettmann, A. Kyrychenko, S.S. Palchevskyy, B. Pucci, A.S. Ladokhin, Interactions of fluorinated surfactants with diphtheria toxin T-domain: testing new media for studies of membrane proteins, *Biophysical journal*, 94 (2008) 4348-4357.

[122] A. Kyrychenko, M.V. Rodnin, M. Vargas-Urbe, S.K. Sharma, G. Durand, B. Pucci, J.L. Popot, A.S. Ladokhin, Folding of diphtheria toxin T-domain in the presence of amphipols and fluorinated surfactants: Toward thermodynamic measurements of membrane protein folding, *Biochimica et biophysica acta*, 1818 (2012) 1006-1012.

[123] A. Chenal, P. Savarin, P. Nizard, F. Guillain, D. Gillet, V. Forge, Membrane protein insertion regulated by bringing electrostatic and hydrophobic interactions into play. A case study with the translocation domain of the diphtheria toxin, *J.Biol.Chem.*, 277 (2002) 43425-43432.

[124] M. Vargas-Urbe, M.V. Rodnin, P. Kienker, A. Finkelstein, A.S. Ladokhin, Crucial Role of H322 in Folding of the Diphtheria Toxin T-Domain into the Open-Channel State, *Biochemistry*, 52 (2013) 3457–3463.

[125] M.S. Fernandez, P. Fromherz, Lipoid pH indicators as probes of electrical potential and polarity in micelles, *J.Phys.Chem.*, 81 (1977) 1755-1761.

[126] Y.O. Posokhov, M.V. Rodnin, L. Lu, A.S. Ladokhin, Membrane insertion pathway of annexin B12: thermodynamic and kinetic characterization by fluorescence correlation spectroscopy and fluorescence quenching, *Biochemistry*, 47 (2008) 5078-5087.

[127] J.S. Brooke, J.H. Cha, L. Eidels, Diphtheria toxin:receptor interaction: association, dissociation, and effect of pH, *Biochem Biophys Res Commun*, 248 (1998) 297-302.

[128] H. Zhan, K.J. Oh, Y.-K. Shin, W.L. Hubbell, R.J. Collier, Interaction of the isolated transmembrane domain of diphtheria toxin with membranes, *Biochemistry*, 34 (1995) 4856-4863.

[129] R.P. Haugland, *Handbook of Fluorescent Probes and Research Chemicals*, 6th ed., Molecular Probes, Inc., Eugene, OR, 1996.

[130] M.J. Hope, M.B. Bally, L.D. Mayer, A.S. Janoff, P.R. Cullis, Generation of multilamellar and unilamellar phospholipid vesicles, *Chem.Phys.Lipids*, 40 (1986) 89-107.

[131] L.D. Mayer, M.J. Hope, P.R. Cullis, Vesicles of variable sizes produced by a rapid extrusion procedure, *Biochim.Biophys.Acta*, 858 (1986) 161-168.

[132] Y.O. Posokhov, A.S. Ladokhin, Lifetime fluorescence method for determining membrane topology of proteins, *Anal Biochem*, 348 (2006) 87-93.

[133] A.S. Ladokhin, Fluorescence spectroscopy in thermodynamic and kinetic analysis of pH-dependent membrane protein insertion, *Methods Enzymol.*, 466 (2009) 19-42.

[134] L.K. Koriazova, M. Montal, Translocation of botulinum neurotoxin light chain protease through the heavy chain channel, *Nature Struct.Biol.*, 10 (2003) 13-18.

[135] R.J. Collier, J.A. Young, Anthrax toxin, *Annu Rev Cell Dev Biol*, 19 (2003) 45-70.

- [136] D.H. Hoch, M. Romero-Mira, B.E. Ehrlich, A. Finkelstein, B.R. DasGupta, L.L. Simpson, Channels formed by botulinum, tetanus, and diphtheria toxins in planar lipid bilayers: Relevance to translocation of proteins, *Proc.Natl.Acad.Sci.USA*, 82 (1985) 1692-1696.
- [137] Y. Wang, K. Kachel, L. Pablo, E. London, Use of Trp mutations to evaluate the conformational behavior and membrane insertion of A and B chains in whole diphtheria toxin, *Biochemistry*, 36 (1997) 16300-16308.
- [138] P.K. Kienker, K.S. Jakes, A. Finkelstein, Protein translocation across planar bilayers by the colicin Ia channel-forming domain: where will it end?, *J Gen Physiol*, 116 (2000) 587-597.
- [139] A.S. Ladokhin, S. Jayasinghe, S.H. White, How to measure and analyze tryptophan fluorescence in membranes properly, and why bother?, *Anal.Biochem.*, 285 (2000) 235-245.
- [140] B.A. Wallace, C.L. Teeters, Differential absorption flattening optical effects are significant in the circular dichroism spectra of large membrane fragments, *Biochemistry*, 26 (1987) 65-70.
- [141] R.M. Glaeser, B.K. Jap, Absorption flattening in the circular dichroism spectra of small membrane fragments, *Biochemistry*, 24 (1985) 6398-6401.
- [142] A.S. Ladokhin, Insertion intermediate of annexin B12 is prone to aggregation on membrane interfaces, *Biopolymers and Cell*, 24 (2008) 101-104.
- [143] A.S. Ladokhin, M. Fernandez-Vidal, S.H. White, CD spectroscopy of peptides and proteins bound to large unilamellar vesicles, *The Journal of membrane biology*, 236 (2010) 247-253.

[144] M.R. Eftink, The use of fluorescence methods to monitor unfolding transitions in proteins, *Biophys.J.*, 66 (1994) 482-501.

[145] C. Borner, D. Andrews, The apoptotic pore on mitochondria: are we breaking through or still stuck?, *Cell Death Differ*, 21 (2014) 187-191.

[146] F. Llambi, T. Moldoveanu, S.W. Tait, L. Bouchier-Hayes, J. Temirov, L.L. McCormick, C.P. Dillon, D.R. Green, A unified model of mammalian BCL-2 protein family interactions at the mitochondria, *Mol Cell*, 44 (2011) 517-531.

[147] S.E. Horvath, G. Daum, Lipids of mitochondria, *Progress in lipid research*, 52 (2013) 590-614.

[148] T. Becker, S.E. Horvath, L. Böttinger, N. Gebert, G. Daum, N. Pfanner, Role of phosphatidylethanolamine in the biogenesis of mitochondrial outer membrane proteins, *Journal of Biological Chemistry*, 288 (2013) 16451-16459.

[149] M. Bogdanov, W. Dowhan, Lipid-assisted protein folding, *J.Biol.Chem.*, 274 (1999) 36827-36830.

[150] S.M. Gruner, Intrinsic curvature hypothesis for biomembrane lipid composition: A role for nonbilayer lipids, *Proc.Natl.Acad.Sci.USA*, 82 (1985) 3665-3669.

[151] G. Daum, Lipids of mitochondria, *Biochimica et Biophysica Acta (BBA)-Reviews on Biomembranes*, 822 (1985) 1-42.

[152] S. McLaughlin, The electrostatic properties of membranes, *Annual review of biophysics and biophysical chemistry*, 18 (1989) 113-136.

[153] M. Eisenberg, T. Gresalfi, T. Riccio, S. McLaughlin, Adsorption of monovalent cations to bilayer membranes containing negative phospholipids, *Biochemistry*, 18 (1979) 5213-5223.

[154] A.P. Winiski, A.C. McLaughlin, R.V. McDaniel, M. Eisenberg, S. McLaughlin, An experimental test of the discreteness-of-charge effect in positive and negative lipid bilayers, *Biochemistry*, 25 (1986) 8206-8214.

[155] A. Shamas-Din, S. Bindner, W. Zhu, Y. Zaltsman, C. Campbell, A. Gross, B. Leber, D.W. Andrews, C. Fradin, tBid undergoes multiple conformational changes at the membrane required for Bax activation, *Journal of Biological Chemistry*, 288 (2013) 22111-22127.

[156] S. Shivakumar, M. Kurylowicz, N. Hirmiz, Y. Manan, O. Friaa, A. Shamas-Din, P. Masoudian, B. Leber, D.W. Andrews, C. Fradin, The proapoptotic protein tBid forms both superficially bound and membrane-inserted oligomers, *Biophysical journal*, 106 (2014) 2085-2095.

[157] S. Bleicken, C. Wagner, A.J. Garcia-Saez, Mechanistic Differences in the Membrane Activity of Bax and Bcl-xL Correlate with Their Opposing Roles in Apoptosis, *Biophysical journal*, 104 (2013) 421-431.

[158] M. Bogdanov, W. Dowhan, Phospholipid-assisted protein folding: Phosphatidylethanolamine is required at a late step of the conformational maturation of the polytopic membrane protein lactose permease, *EMBO Journal*, 17 (1998) 5255-5264.

[159] D.C. Mitchell, Progress in understanding the role of lipids in membrane protein folding, *Biochimica et Biophysica Acta (BBA)-Biomembranes*, 1818 (2012) 951-956.

[160] N. Kučerka, M.-P. Nieh, J. Katsaras, Fluid phase lipid areas and bilayer thicknesses of commonly used phosphatidylcholines as a function of temperature, *Biochimica et Biophysica Acta (BBA)-Biomembranes*, 1808 (2011) 2761-2771.

[161] J. Pan, F.A. Heberle, S. Tristram-Nagle, M. Szymanski, M. Koepfinger, J. Katsaras, N. Kučerka, Molecular structures of fluid phase phosphatidylglycerol bilayers as determined by small angle neutron and X-ray scattering, *Biochimica et Biophysica Acta (BBA)-Biomembranes*, 1818 (2012) 2135-2148.

[162] J. Pan, X. Cheng, M. Sharp, C.-S. Ho, N. Khadka, J. Katsaras, Structural and mechanical properties of cardiolipin lipid bilayers determined using neutron spin echo, small angle neutron and X-ray scattering, and molecular dynamics simulations, *Soft matter*, 11 (2015) 130-138.

[163] M.H. Cheng, L.T. Liu, A.C. Saladino, Y. Xu, P. Tang, Molecular dynamics simulations of ternary membrane mixture: phosphatidylcholine, phosphatidic acid, and cholesterol, *The Journal of Physical Chemistry B*, 111 (2007) 14186-14192.

[164] G.S. Patil, N.J. Dorman, D.G. Cornwell, Effects of ionization and counterion binding on the surface areas of phosphatidic acids in monolayers, *Journal of lipid research*, 20 (1979) 663-668.

[165] D.S. Wimalasena, J.C. Cramer, B.E. Janowiak, S.J. Juris, R.A. Melnyk, D.E. Anderson, K.L. Kirk, R.J. Collier, J.G. Bann, Effect of 2-fluorohistidine labeling of the anthrax protective antigen on stability, pore formation, and translocation, *Biochemistry*, 46 (2007) 14928-14936.

[166] M.R. Kalani, A. Moradi, M. Moradi, E. Tajkhorshid, Characterizing a histidine switch controlling pH-dependent conformational changes of the influenza virus hemagglutinin, *Biophysical journal*, 105 (2013) 993-1003.

[167] M.L. Reed, H.-L. Yen, R.M. DuBois, O.A. Bridges, R. Salomon, R.G. Webster, C.J. Russell, Amino acid residues in the fusion peptide pocket regulate the pH of activation of the H5N1 influenza virus hemagglutinin protein, *Journal of virology*, 83 (2009) 3568-3580.

[168] M. Mosior, S. McLaughlin, Binding of Basic Peptides to Acidic Lipids in Membranes - Effects of Inserting Alanine(s) Between the Basic Residues, *Biochemistry*, 31 (1992) 1767-1773.

[169] A. Kyrychenko, V. Vasquez-Montes, M.B. Ulmschneider, A.S. Ladokhin, Lipid Headgroups Modulate Membrane Insertion of pHLIP Peptide, *Biophysical journal*, 108 (2015) 791-794.